EXPERIMENTAL STUDIES ON FRACTURE OF NOTCHED WHITE SPRUCE BEAMS

by

WILSON W.S. LAU

B.A.Sc University of Windsor, 1984

A THESIS SUBMITTED IN PARTIAL FULFILMENT OF

THE REQUIREMENTS FOR THE DEGREE OF

MASTER OF APPLIED SCIENCE

in

FACULTY OF GRADUATE STUDIES

DEPARTMENT OF CIVIL ENGINEERING

We accept this thesis as conforming

to the required standard

THE UNIVERSITY OF BRITISH COLUMBIA

April, 1987

In presenting this thesis in partial fulfilment of the requirements for an advanced degree at the University of British Columbia, I agree that the Library shall make it freely available for reference and study. I further agree that permission for extensive copying of this thesis for scholarly purposes may be granted by the head of my department or by his or her representatives. It is understood that copying or publication of this thesis for financial gain shall not be allowed without my written permission.

Department of Civil Engineering

The University of British Columbia
1956 Main Mall
Vancouver, Canada
V6T 1Y3

Date April, 1987

ABSTRACT

The fracture problem due to the singular stresses arising from the sudden change of geometric properties around cracks and notches was studied both analytically and experimentally.

The failure models of the cracked and the notched specimens were derived by using linear elastic fracture mechanics methodology, which led to the determination of the critical stress intensity factors. Experiments were conducted to determine fracture toughness for different modes as well as the effect of variations in the crack-front width, specimen size and moisture content. Subsequently, failure surfaces for cracks and notches were developed based on the experiments undertaken, describing in each case the interaction between mode I and mode II fracture toughness. To verify the reliability of these experiments, the results obtained were compared with the published literature.

As an application, design curves for a 90 degrees-cracked beam and a 90 degrees-notched beam are presented. These curves allow the prediction of the failure loads due to the rapid crack propagation under different loading conditions.

Table of Contents

LIST OF TABLES

LIST OF FIGURES

LIST OF FIGURES - Cont'd

LIST OF FIGURES - Cont'd

LIST OF FIGURES - Cont'd

ACKNOWLEDGEMENTS

The author would like to express his sincere gratitude to Dr. R.O. Foschi and Dr. J.D. Barrett for their guidance and invaluable advice in the preparation of this thesis.

The author would also like to thank Conroy Lum for his assistance in using the finite element program NOTCH, Mr. D. Postgate and Mr. B. Merkli for their helpful suggestions and assistance in the manufacture of the apparatus, and also the Departments of Civil Engineering and Wood Science and Harvesting of the University of British Columbia for the use of their laboratories and equipment.

1. INTRODUCTION

1.1 THE PROBLEM

In practical situations wood is sawn, chopped, chipped, sliced, dried, drilled, flaked, and fastened. Flaws or defects unavoidably occur as a result of each of these processes. In other cases, gaps between ends of boards in laminated timber (which are usually denoted by the term "butt-joint"), notches formed by a sawcut, re-entrant notches occurring at open butt or lap joints in laminated beams lead to a sudden change in geometry and stress concentrations. All of these cases result in a stress singularity formed at the notch root which can not be analyzed by ordinary stress formulae. The Timber Design Manual, as well as the governing Canadian design code, CAN3-086-M84: Code for Engineering Design in Wood, use a reduced net depth to account for the present of a notch in a beam, without consideration of the intense stress concentration at the notch corner. Furthermore, the code does not cover splited specimens.

Obviously, a theoretical understanding of these singularities in wood should be of practical importance.

Application of fracture mechanics to wood is concerned with structural failure by catastrophic crack propagation. In many applications, fracture mechanics techniques are used to eliminate such failures by special material control tests or by defining maximum crack or flaw sizes that can be

tolerated in the structure. As mentioned above, flaws in a wood structure cannot be totally controlled, so fracture mechanics methods must be used to assess the allowable load on the structure.

Near the vicinity of a notch root or a crack tip, the stress at every point in this region is subjected to plane stress or strain conditions which can be expressed in terms of the stress intensity factors. Therefore, the determination of the allowable load is the same as obtaining the critical values of the stress intensity factors.

Depending on the mode of crack tip deformation, the stress intensity factors K are designated with a subscript I, II, III for the cracked specimen (zero notch angle cracks) which corresponds to the opening, forward shear and tranverse shear modes of deformation. For notches, the subscript A, B are used to define the stress intensity factors for the primary and the secondary stress fields respectively.

Critical values for the pure mode I and mode II for a cracked specimen have been studied and published for different species of wood. There is, however, a lack of information about the critical values for the mixed mode failure of a cracked specimen.

1.2 PREVIOUS RESEARCH

Studies of the cracks or notches were initiated by Inglis (1913) who made the stress analysis of an elliptical hole in a uniformly stressed elastic plate. A crack can be represented by an infinitesimally narrow ellipse. Based on Inglis' theory, Griffith (1921) formulated his well known energy criterion for brittle fracture which was extended by Irwin (1948) and Orowan (1955) to apply to metallic solids where plastic deformation takes place at crack tips. Later, Savin (1961), using his photoelastic method, analyzed the stress at re-entrant corners. Up to that moment, the study of cracks and notches was mainly based on the energy method or individual experiment results to determine the stress concentration factors for specific geometries.

Linear elastic fracture mechanics (LEFM) is based on the elastic solution of the crack tip stress field where the yielding has been highly localized at the crack front. Williams (1957) has solved the problem of a cracked plate, expressing the stresses σ_{ij}, the strains ϵ_{ij}, and the displacements u_{ij} in terms of infinite series of singular and regular terms of r and θ, where r and θ are polar coordinates, with the crack tip at the origin. Later, Irwin (1957) found that the first singular term always dominate in the stress formulae and expressed the stress and strain equations introducing the K_I stress intensity factor.

A comprehensive analysis of crack tip elastic stresses, strains and displacements, using the stress intensity factor

method, was studied by Liu (1965&1966). For the case of small scale yielding, SSY, Liu has shown that K is capable of characterizing the crack tip stresses, strains and displacements within the elastic field zone which forms the fundamental basis of the linear elastic fracture mechanics.

The application of linear elastic fracture mechanics (LEFM), to cracked material using the stress intensity factors has been shown to be an effective method by Knott (1973), Broek (1982), Hellan (1984) but restricted to isotropic material. The extension of LEFM to orthotropic body was first made by Sih et at (1965) who derived formulae for the stresses in a small region surrounding a crack tip in an orthotropic body.

In the application of LEFM to the strength of structures, it is not only the form of singularity but also the magnitude of the stresses near the root of the fractured surface what is needed. This requires the computation of the so-called stress intensity factors for the singularity. And except for some simple geometry and boundary conditions, the solutions always require a numerical method. Walsh (1971,1972,1974) introduced a calibrated finite element method to compute the stress intensity factors using LEFM, which incorporated the singular terms in the displacement field. This method also satisfies the equilibrium and compatibility conditions at the interface between the conventional finite elements and the modified elements. This method was extended to apply to orthotropic materials and

right angle notches. However, the method does not account for compatibility at the elements interfaces, which enhances monotonic convergence.

A method suggested by Benzley (1974), using a compatible displacement formulation for a finite element, with singular 'enrichment' terms, solves this problem thoroughly. The method has been shown to be efficient and reliable.

This conformable displacement model was extended by Foschi and Barrett (1976) for the anisotropic case and used by Gifford and Hilton (1978) to analyze cracks in isotropic bodies with 12-node isoparametric elements and a coarser mesh.

The application of LEFM to the analysis of the stress field at the root of a sharp notch of arbitrary notch angle was first proposed by Leicester (1971). He introduced the stress intensity factors for notches, K_A and K_B, which correspond respectively to the primary and the secondary stress field of the eigenfields governing the notch tip stress distribution. However, the terms "opening mode" and "sliding mode" which are commonly used in connection with sharp cracks are applicable to notches only if the notches are symmetrical with respect to the axes of elastic symmetry. These factors were incorporated in the finite element method to analyze notches in Leicester's paper with Walsh (1982). The V-notch, which is a special case of notches, has been studied by Gross and Mendelson (1972)

using the boundary collocation procedure and also by Lin and Tong (1980) using the singular finite element method.

According to the linear fracture mechanics model, fracture is assumed to occur when the stress intensity factor attains a critical value -- the critical stress intensity factor. This factor is material dependent and has to be determined experimentally for different species of wood. Schniewind and Centeno (1971) presented K_{IC} values for the six principal systems of propagation for Douglas-fir wood; using the end-split beam method, Barrett and Foschi (1971) found the K_{IIC} values for Hemlock. Hunt and Croager (1982) also established the mode II fracture toughness for baltic redwood by a mixed mode test method assuming an interation curve existed between mode I and mode II. The studies on the interaction curve for isotropic and orthotropic materials has been restricted to cracked elements due to the fact that the notch root can have different types of singularities, whereas the sharp cracks always have a $1/\sqrt{r}$ singularity. A method suggested by Lum (1986), which incorporates the eigenvalue λ as a failure parameter, has proved to be a reasonable approach to specify the critical notch root stress conditions and may be used to describe interaction curves for notches as well as for cracks.

Studies on the crack-front width effect have shown that it influences the prediction of the failure load for large structures. Barrett (1976) found a size effect due to

crack-front width on K_{IC} for cracks using the Weibull's theory whereas Ewing (1979), has also shown the existence of this effect based on his stress-state model. Leicester (1969,1973) has studied the magnitude of a size effect on notches by considering a size coefficient implied on the nominal stress.

The moisture content effect was studied by Ewing & Williams (1979) on compact tension specimen and by Dolan & Madsen (1985) on the shear strength.

1.3 OBJECTIVE

The objective of this thesis is to investigate the fracture behavior of white spruce under the mode I, mode II and the combined mixed mode loading conditions. The effects such as the variation of the moisture content and the crack-front width will also be studied.

1.4 SCOPE

1.4.1 INTRODUCTION

In order to develop a design procedure for cracks and notches under loading, experiments were carried out to establish the critical values for the stress intensity factors and results were compared with published ones. In particular, the experiments were designed to examine the following features.

1.4.2 MODE I FRACTURE TOUGHNESS

To determine experimentally the critical value of the opening mode stress intensity factor for white spruce using a compact tension specimen and a double cantilever beam specimen. Effect of crack orientation with respect to the grain was also considered.

1.4.3 MODE II FRACTURE TOUGHNESS

To determine experimentally the critical value of the sliding mode stress intensity factor for White Spruce by the end-split beam method. Effect of the crack orientation was also considered for cracks propagating along the grain.

1.4.4 SPECIMEN SIZE EFFECT

The strength of complex structures are frequently assessed from laboratory tests on scaled models. This is most simply done by use of the assumption that a scale model and a full-size structure will fail at the same nominal stress level. However, for structures containing singular stress fields, this may not be the real case. Experiments were carried out to study the dependence of the mode I stress intensity factor on the size of the specimen and also to study the applicability of the crack-front width theory developed by Barrett (1976) on the mode I stress intensity factor.

1.4.5 MOISTURE CONTENT EFFECT

Many published papers have shown that the fracture toughness of wood depends on the moisture content as well as the temperature, but design formula are lacking to account for this effect. Experiments were conducted to study the moisture content effect on the mode I critical stress intensity factor and a model is proposed in terms of residual stresses.

1.4.6 INTERACTION CURVES FOR MIXED MODE LOADING

Since wood is often subjected to combined loading producing both opening and sliding deformation modes, interaction curves are necessary to predict the failure strength of the structures. Experiments were carried out to establish the interaction curves for both cracks and notches.

1.5 SUMMARY OF OBJECTIVES

1. To determine the mode I critical stress intensity factor for white spruce.
2. To determine the mode II critical stress intensity factor for white spruce.
3. To study the specimen size effect on the mode I fracture toughness.
4. To study the moisture content effect on the fracture toughness of the white spruce.
5. To establish the family of mixed mode failure

interaction curves for cracks and notches of white spruce.

6. To discuss the results, their application to design practice and suggested directions for further research.

2. THEORY

2.1 INTRODUCTION

This chapter explains the basic theory of linear elastic fracture mechanics as applied to cracked (zero angle notch) and notched wood specimens. The theory requires the computation of the stress intensity factors, which are associated with the singular stresses near the crack tip or notch root.

For simplicity, the theory will be introduced starting from a sharp crack in an isotropic and orthotropic specimen. This will be extended to the more general cases of notches. This information, combined with the experimentally determined critical stress intensity factors, makes the prediction of the ultimate strength of fracture structures possible.

The size and the moisture content of the specimen had been proven to have pronounced effect on the strength of the specimen and will be discussed in the following sections. This chapter will end with the theory of interaction curves of stress intensity factor.

2.2 APPLICATION OF LEFM ON WOOD STRUCTURES

The concept of linear elastic fracture mechanics for determining the fracture failure mode and strength in wood have received a abundant amount of attention in the past several years. Fracture mechanics is concerned with

structural failure by catastrophic crack propagation at average stress below the normal failure stress level. In many applications, fracture techniques are used to eliminate this kind of failure by controlling the flaw size or in the cases that these defects are unavoidable, by considering the effect of the flaw on the allowable load on the structures.

Complete studies of fracture behavior cover both the stress analysis aspects and the resistance of the material to the stress imposed. In this chapter, the purpose is to develop the significant stress analysis details and relevant parameters, which will govern the failure strength of structures containing cracks or notches.

The redistribution of stress in a body due to the existence of a crack or a notch will be analyzed by the LEFM method. The greatest attention should be paid to the high elevation of stresses at the vicinity of the crack tip which will usually be accompanied by at least some plasticity and other non-linear effects. The surfaces of a crack or a notch dominate the distribution of stresses near or around the crack tip since they are stress-free boundaries of the body. Other remote boundaries and loading forces affect only the intensity of the local stress field at the tip.

The stress fields near a crack or a notch tip can be divided into three basic types, each associated with a local mode of deformation as illustrated in Figure 1.

In mode I propagation, the crack surfaces open normal to themselves; in mode II the surfaces slide tangential to

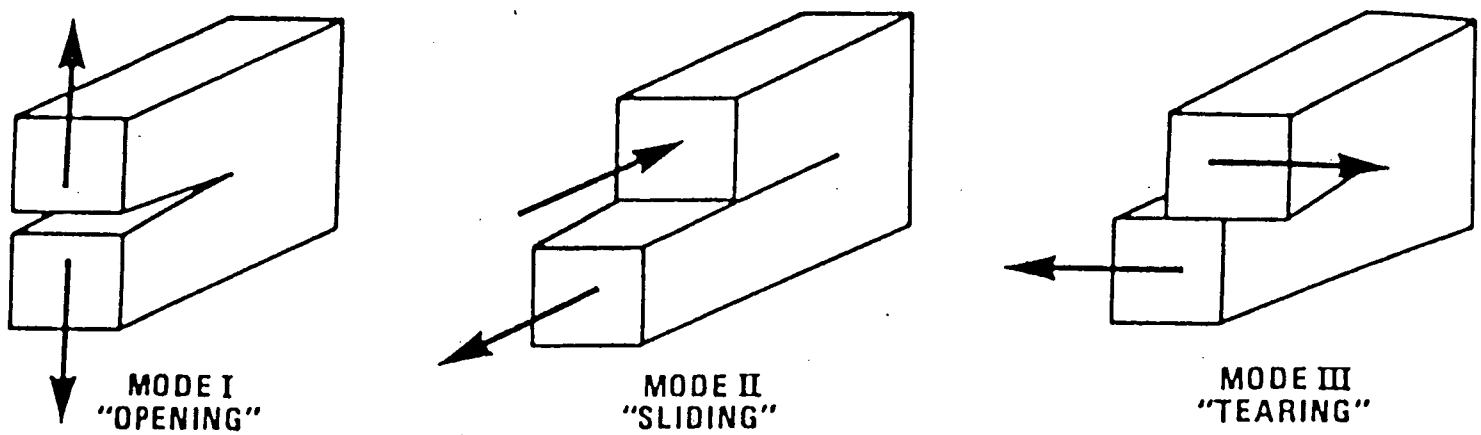

Figure 1 - Three basic modes of crack surface displacement

themselves longitudinally; and in mode III the surfaces slide tangential to themselves and perpendicular to the propagation direction in a tearing fashion. The superposition of these three modes is sufficient to describe the most general 3-dimensional case of local crack-tip deformation and the associated stress fields. As we know, wood is a highly anisotropic, heterogeneous and porous material with varying mechanical properties in different directions. The longitudinal-radial and the longitudinal-tangential planes are natural cleavage planes. For specimen surface free of checks, crack propagation usually occurs along the grain. Due to the high orthotropy, a system specifying the principal crack propagation directions within the orthotropic planes of symmetry will be necessary. For each of the three modes of propagation, six principal systems of propagation exists as shown in Figure 2. A system of propagation is identified with a pair of letters, the first refers to the direction normal to the fracture surface, and the second refers to the direction in which the crack plane propagates.

The solutions of the isotropic crack problem require the computation of stress intensity factors. A variety of solutions are available for sharp cracks, particularly for symmetrically placed cracks in isotropic materials, and many of these solutions have been summarized by Paris and Sih (1957).

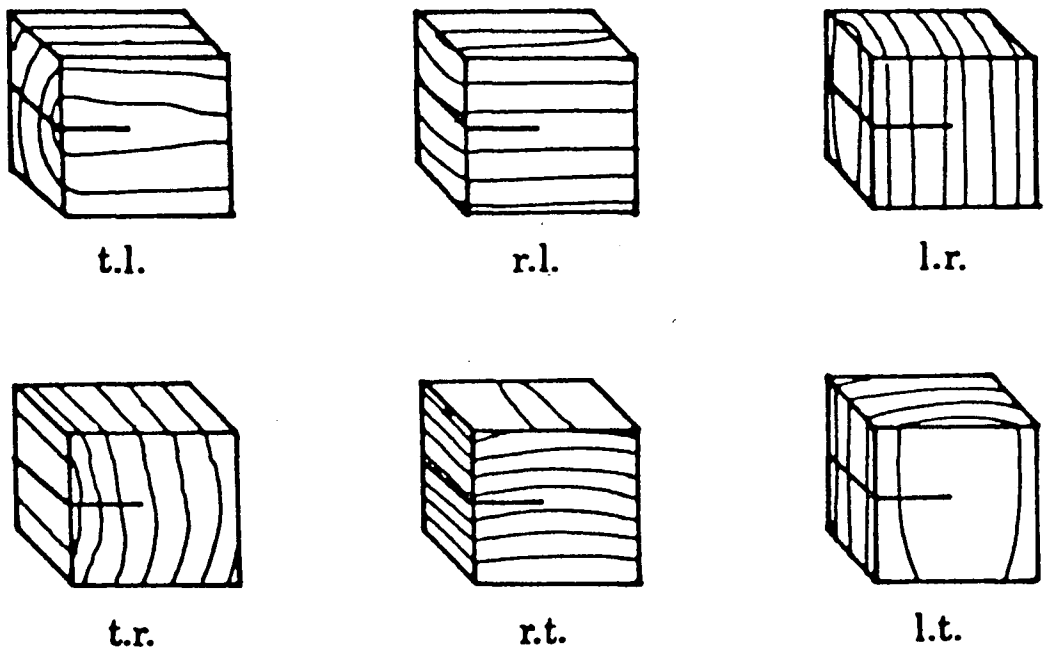

Figure 2 - Three-letter system for designing orientation relations in wood, according to A.P. Schniewind and R.A. Pozniak

Since the formulation of this fracture theory is based on continuum mechanics where material differences are not considered, it is expected that fracture mechanics should be equally applicable to orthotropic materials such as wood. Similar formulation of stress intensity factors in anisotropic materials has also been proposed by Paris and Sih (1965). Walsh (1972) had investigated the effect of orthotropy on computed stress intensity factors for several geometry and concluded that for rectangular specimen of sufficient length, orthotropic and isotropic results agree closely. However, it would appear only for the case of symmetrical and skew-symmetrical self-equilibrating loading on cracked infinite plates. Thus, to apply LEFM on wood products, one must aware the dependence of stress intensity factor on the material properties of the specimen.

Another assumption that is necessary to apply LEFM is the condition of small scale yielding (SSY) around the crack tip. Under this condition, K can characterize the crack tip stresses and strains even within the plastic zone. This is equivalent to the plastic zone radius (r_p) being much smaller that the radius of elastic field zone (r_e). Since r_e is proportional to the specimen size, in principle, the SSY condition can always be satisfied, if one uses a large enough specimen. The ASTM recommended size requirements for valid K_C measurements are:

$$\frac{a}{L} > 2.5 \left(\frac{K_C}{\sigma_y}\right)^2 \qquad (2.1)$$

where a is the length of the crack, L is the distance ahead of the crack front, σ_Y is the yielding stress or that stress that results in gross deformation. The condition of $r_e >> r_p$ is a sufficient but not necessary condition for the validity of the LEFM. The condition could be unduly restrictive in terms of specimen size requirements. The necessary condition for the validity of the LEFM is that K would be able to characterize the crack tip stress or strain component at the location of the defined fracture process.

The zero notch root assumption will be imperative for applying LEFM on notch problem. In order to have SSY at the notch root, the notch radius should be small compare to other dimensions, so that variation of the notch radius does not influence the surrounding stress and strain fields.

Ewing and Williams (1979) had studied the importance of the sharpness of the initial notch on the fracture toughness of Scots Pine and found that the mode I fracture toughness tends to increase as the radius increases.

2.3 FORMULATION OF THE STRESS INTENSITY FACTORS FOR CRACKS

The formulation of the solution of the stress and displacement fields associated with each mode using the LEFM methodology follows in the manner of Irwin (1957) based on the method of Westergaard (1939). Mode I and II can be analyzed as two-dimensional plane problems with the symmetric and skew-symmetric stress fields with respect to the crack plane. Mode III can be treated as a pure shear

problem. From the cracks handbook by Hiroshi Tada (1973), the resulting stress and displacement fields for the isotropic case are given as follows with the notation referred to Figure 3.

Mode I :

$$\sigma_x = \frac{K_I}{(2\pi r)^{1/2}} \cos\frac{\theta}{2}\left[1 - \sin\frac{\theta}{2}\sin\frac{3\theta}{2}\right] + \sigma_{xo} + O(r^{1/2}) \qquad (2.2a)$$

$$\sigma_y = \frac{K_I}{(2\pi r)^{1/2}} \cos\frac{\theta}{2}\left[1 + \sin\frac{\theta}{2}\sin\frac{3\theta}{2}\right] + 0\ (r^{1/2}) \qquad (2.2b)$$

$$\tau_{xy} = \frac{K_I}{(2\pi r)^{1/2}} \sin\frac{\theta}{2}\cos\frac{\theta}{2}\cos\frac{3\theta}{2} + O(r^{1/2}) \qquad (2.2c)$$

and for plane strain (with higher order terms omitted)

$$\sigma_z = \nu(\sigma_x + \sigma_y) \qquad (2.2d)$$

$$\tau_{xy} = \tau_{yz} = 0 \qquad (2.2e)$$

The corresponding displacements are:

$$u = \frac{K_I}{G}\left[r/(2\pi)\right]^{1/2} \cos\frac{\theta}{2}\left[1 - 2\nu + \sin\frac{2\theta}{2}\right] \qquad (2.2f)$$

$$v = \frac{K_I}{G}\left[r/(2\pi)\right]^{1/2} \sin\frac{\theta}{2}\left[2 - 2\nu - \cos\frac{2\theta}{2}\right] \qquad (2.2g)$$

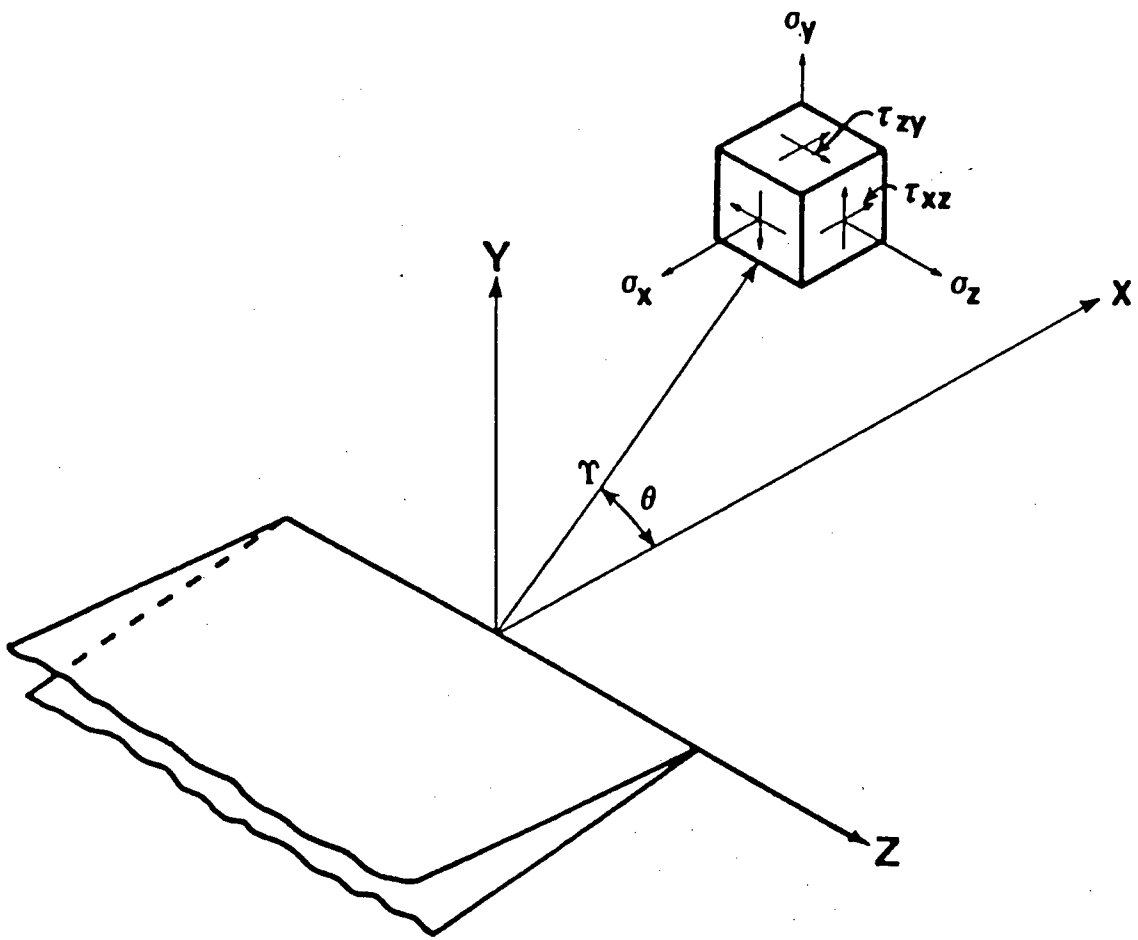

Figure 3 - Coordinate system used for describing the stresses ahead of a crack. From P.C. Paris and G.C. Sih

$$w = 0 \tag{2.2h}$$

Mode II :

$$\sigma_x = -\frac{K_{II}}{(2\pi r)^{1/2}} \sin\frac{\theta}{2}\left[2 + \cos\frac{\theta}{2}\cos\frac{3\theta}{2}\right] + \sigma_{xo} + O(r^{1/2}) \tag{2.3a}$$

$$\sigma_y = \frac{K_{II}}{(2\pi r)^{1/2}} \sin\frac{\theta}{2}\cos\frac{\theta}{2}\cos\frac{3\theta}{2} + O(r^{1/2}) \tag{2.3b}$$

$$\tau_{xy} = \frac{K_{II}}{(2\pi r)^{1/2}} \cos\frac{\theta}{2}\left[1 - \sin\frac{\theta}{2}\sin\frac{3\theta}{2}\right] + O(r^{1/2}) \tag{2.3c}$$

and for plane strain (with higher order terms omitted)

$$\sigma_z = \nu(\sigma_x + \sigma_y) \tag{2.3d}$$

$$\tau_{xz} = \tau_{yz} = 0 \tag{2.3e}$$

with dispalcements:

$$u = \frac{K_{II}}{G}\left[r/(2\pi)\right]^{1/2} \sin\frac{\theta}{2}\left[2 - 2\nu + \cos\frac{2\theta}{2}\right] \tag{2.3f}$$

$$v = \frac{K_{II}}{G}\left[r/(2\pi)\right]^{1/2} \cos\frac{\theta}{2}\left[-1 + 2\nu + \sin\frac{2\theta}{2}\right] \tag{2.3g}$$

$$w = 0 \tag{2.3h}$$

Mode III :

$$\tau_{xz} = -\frac{K_{III}}{(2\pi r)^{1/2}} \sin\frac{\theta}{2} + \tau_{xzo} + O(r^{1/2}) \tag{2.4a}$$

$$\tau_{yz} = \frac{K_{III}}{(2\pi r)^{1/2}} \cos\frac{\theta}{2} + O(r^{1/2}) \tag{2.4b}$$

$$\sigma_x = \sigma_y = \sigma_z = \tau_{xy} = 0 \tag{2.4c}$$

$$w = \frac{K_{III}}{G}\left[(2r)/\pi\right]^{1/2} \sin\frac{\theta}{2} \tag{2.4d}$$

$$u = v = 0 \tag{2.4e}$$

Equations (2.2) and (2.3) have been written for the case of plane strain, but can be changed to plane stress by taking $\sigma_z = 0$ and replace ν by $\nu/(1+\nu)$.

As seen from equations (2.2) and (2.3), the formulae include higher order terms such as uniform stresses parallel to cracks, σ_{xo} and τ_{xzo}, and terms of the order of square root of r, $O(r^{1/2})$. But these terms can be neglected since as the value of r approaches 0, (i.e. close to the crack tip), the singular term $1/\sqrt{r}$ becomes the governing term in the equations.

The parameters K_I, K_{II}, K_{III} in these equations are called the stress intensity factors for the three modes respectively, as shown in Fig 1. It is found that these parameters are coordinate-independent, so they can be thought of as the magnitude of the stress fields surrounding the crack tip. The parameters, K, are determined by the other boundaries conditions and the imposed loads. Consequently, formulae for their evaluation come from a complete stress analysis for the specimen configuration and loading.

A crack stress field for certain loading and geometry is represented by a unique combination of the three stress intensity factors. Since they are correlated parameters , the failure criterion will depends on all three.

From the Equations (2.2), (2.3) and (2.4), we observe that the stress intensity factors have units of $(\text{Force})\text{x}(\text{Length})^{-3/2}$. Since they are linear factors in a linear elastic stress solution, the stress intensity factors are linearly related to the applied loads.

Sih et al (1965) derived formulae for the stresses in a small region surrounding a crack tip of <u>orthotropic</u> material using a complex variable formulation for the LEFM method.

Their results for a crack parallel to a material axis and coincident with the negative x-axis (Figure 3) are :

Symmetric (about x-axis) plane loading,

$$\sigma_x = \frac{K_I}{\sqrt{2\pi r}} \text{Re} \left[\frac{-\beta_1\beta_2}{\beta_1-\beta_2} \left(\frac{\beta_2}{B_2} - \frac{\beta_1}{B_1}\right)\right] \tag{2.5a}$$

$$\sigma_y = \frac{K_I}{\sqrt{2\pi r}} \text{Re} \left[\frac{1}{\beta_1-\beta_2} \left(\frac{\beta_1}{B_2} - \frac{\beta_2}{B_1}\right)\right] \tag{2.5b}$$

$$\tau_{xy} = \frac{K_I}{\sqrt{2\pi r}} \text{Re} \left[\frac{-\beta_1\beta_2}{i(\beta_1-\beta_2)} \left(\frac{1}{B_1} - \frac{1}{B_2}\right)\right] \tag{2.5c}$$

and

Skew-symmetric (about x-axis) plane loading,

$$\sigma_x = \frac{K_{II}}{\sqrt{2\pi r}} \text{Re} \left[\frac{1}{i(\beta_1-\beta_2)} \left(\frac{\beta_1^2}{B_1} - \frac{\beta_2^2}{B_2}\right)\right] \tag{2.6a}$$

$$\sigma_y = \frac{K_{II}}{\sqrt{2\pi r}} \text{Re} \left[\frac{1}{i(\beta_1-\beta_2)} \left(\frac{1}{B_1} \quad \frac{1}{B_2}\right)\right] \tag{2.6b}$$

$$\tau_{xy} = \frac{K_{II}}{\sqrt{2\pi r}} \text{Re} \left[\frac{1}{\beta_1-\beta_2} \left(\frac{\beta_1}{B_1} - \frac{\beta_2}{B_2}\right)\right] \tag{2.6c}$$

where

$$B_j = \sqrt{\cos\theta + i\beta_j \sin\theta} \qquad j = 1,2 \tag{2.6d}$$

$$i = \sqrt{-1} \tag{2.6e}$$

$$\text{Re} = \text{real part} \tag{2.6f}$$

$$\beta_1^2 = \varepsilon^2 \left[\kappa + (\kappa^2-1)^{1/2}\right]^{-1} \tag{2.6g}$$

$$\beta_2^2 = \varepsilon^2 \left[\kappa - (\kappa^2-1)^{1/2}\right]^{-1} \tag{2.6h}$$

$$\left.\begin{aligned} \varepsilon^4 &= \frac{E_x}{E_y} \\ \kappa &= \frac{\varepsilon^2}{2}\left(\frac{E_y}{G_{xy}} - 2\nu_{yx}\right) \end{aligned}\right\} \quad \text{for plane stress} \tag{2.6i}$$

And directly ahead of the crack the stresses are :

$$\sigma_y = \frac{K_I}{\sqrt{2\pi x}} \qquad \tau_{xy} = \frac{K_{II}}{\sqrt{2\pi x}} \tag{2.7}$$

where the K's values are dependent on remote boundaries conditions, highly dependent on geometry, and slightly dependent on orthotropic parameters (for finite bodies).

Some typical symmetric and skew-symmetric stress fields are shown in Figure 4 and Figure 5. The stresses in polar co-ordinates are obtained by doing the transformation as follows :

$$\sigma_r = \sigma_x \cos^2\theta + \sigma_y \sin^2\theta + 2\sigma_{xy} \cos\theta \sin\theta \tag{2.8a}$$

$$\sigma_\theta = \sigma_x \sin^2\theta + \sigma_y \cos^2\theta - 2\sigma_{xy} \cos\theta \sin\theta \tag{2.8b}$$

$$\sigma_{r\theta} = (\sigma_y - \sigma_x) \cos\theta \sin\theta + \sigma_{xy}(\cos^2\theta - \sin^2\theta) \tag{2.8c}$$

The symmetric and skew-symmetric stress fields will only exist if the crack is parallel to an axis of elastic material symmetry. Then, the stresses around the crack tip

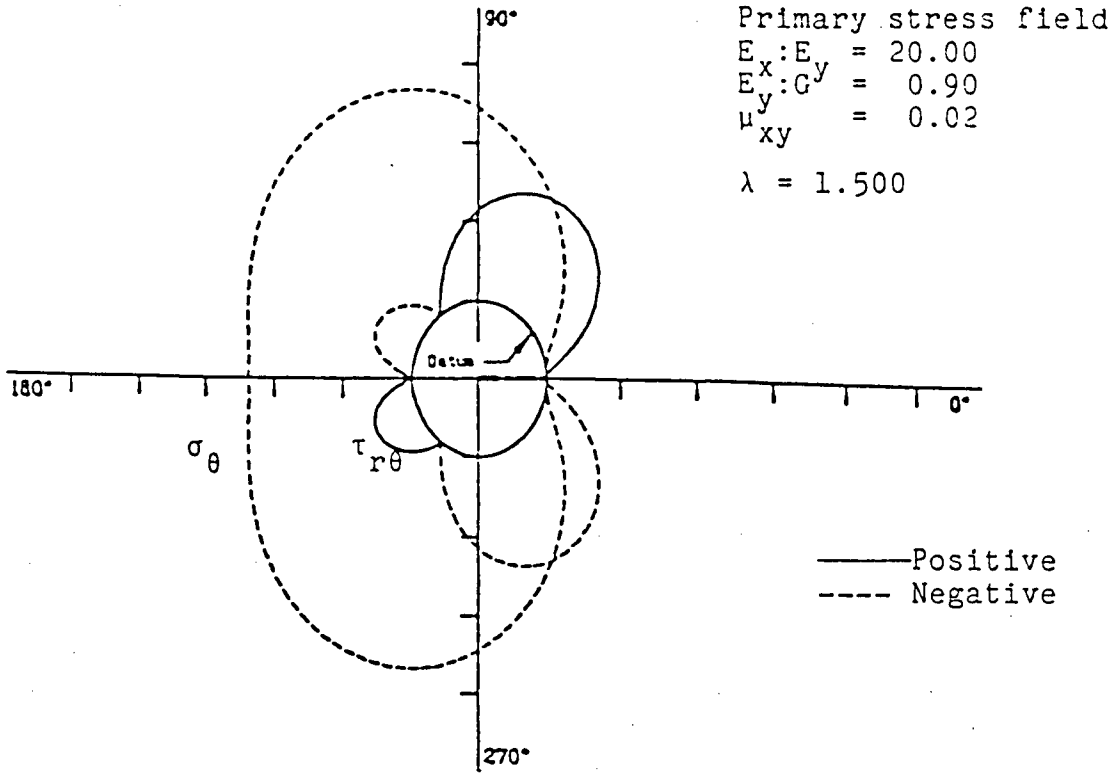

Figure 4 - First primary singular stress field for a 0° crack

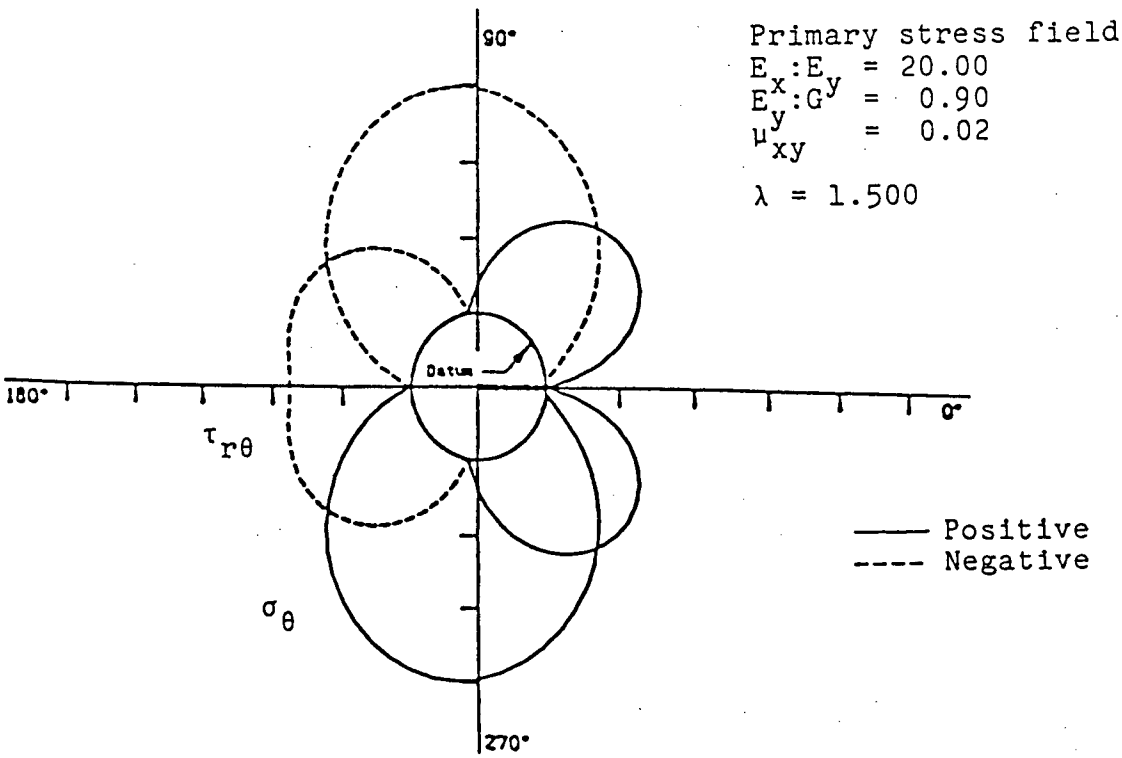

Figure 5 - Second primary singular stress field for a 0° crack

will be the superposition of some linear combination of these two fields.

2.4 STRESS INTENSITY FACTORS FOR SHARP NOTCHES

2.4.1 INTRODUCTION

The stress intensity factors have been shown to characterize the stress fields surrounding the fracture plane. However, the literature on stress intensity factors is mostly concerned with sharp cracks. Although there are few papers on notches, the method was based on the nominal fracture stress combined with limited experimental results. Leicester(1971) has presented a new method for the analysis of the stress fields at the root of a mathematically sharp notch of arbitrary notch angle. The application of this method indicates that in general there are two stress singularities of stress at the roots of notches in typical orthotropic structural materials. The magnitude of these stress fields are noted as the stress intensity factors for notch angle. He used the indices of A and B referring to the two stress fields and these two stress fields are different from the symmetry and skew-symmetry stress fields in most cases.

The significance of the stress intensity factors lies in the fact that a criterion for crack propagation from the notch root may be formulated as follows:

$$f(K_A/K_{AC},\ K_B/K_{BC}) = 1 \qquad (2.9)$$

where K_{AC} and K_{BC}, the critical stress intensity factors, and the interaction equation (2.9) are determined by direct measurement. For the specific case of a zero angle notch, i.e., a crack, the notation K_I , K_{IC}, K_{II} and K_{IIC} will replace the notation K_A , K_{AC}, K_B and K_{BC}.

2.4.2 FORMULATION OF THE PROBLEM FOR NOTCHES

The formulation of the problem follows the method proposed by Lum (1986).

The equations of equilibrium under zero body forces, in cartesian co-ordinates, are:

$$\frac{\partial \sigma_x}{\partial x} + \frac{\partial \sigma_{xy}}{\partial y} = 0 \qquad (2.10a)$$

$$\frac{\partial \sigma_y}{\partial y} + \frac{\partial \sigma_{xy}}{\partial x} = 0 \qquad (2.10b)$$

The strain-displacement kinematic relationships are:

$$\varepsilon_x = \frac{\partial u}{\partial x} \qquad (2.11a)$$

$$\varepsilon_y = \frac{\partial v}{\partial y} \qquad (2.11b)$$

$$\varepsilon_{xy} = \frac{\partial u}{\partial y} + \frac{\partial v}{\partial x} \qquad (2.11c)$$

and the stress-strain equations for an orthotropic material with plane stress condition are :

$$\varepsilon_x = \frac{\sigma_x}{E_x} - \frac{\mu_{yx}}{E_y}\sigma_y \tag{2.12a}$$

$$\varepsilon_y = \frac{\sigma_y}{E_y} - \frac{\mu_{xy}}{E_x}\sigma_x \tag{2.12b}$$

$$\varepsilon_{xy} = \frac{\sigma_{xy}}{G_{xy}} \tag{2.12c}$$

From strain-energy considerations it is known that :

$$\frac{\mu_{xy}}{E_x} = \frac{\mu_{yx}}{E_y} \tag{2.13}$$

Equations (2.11a,b,c) may be shown to result in the following equation of compatibility :

$$\frac{\partial^2 \varepsilon_{xy}}{\partial x \partial y} = \frac{\partial^2 \varepsilon_x}{\partial y^2} + \frac{\partial^2 \varepsilon_y}{\partial x^2} \tag{2.14}$$

Equations (2.10a,b) are satisfied when the stress components are expressed by Airy's stress function ϕ through

$$\frac{\partial^2 \phi}{\partial x^2} = \sigma_y \tag{2.15a}$$

$$\frac{\partial^2\phi}{\partial y^2} = \sigma_x \tag{2.15b}$$

$$\frac{\partial^2\phi}{\partial x \partial y} = -\sigma_{xy} \tag{2.15c}$$

Substitude (2.15a,b,c) into (2.12a,b,c) we get the expressions for strains in term of Airy's stress functions :

$$\varepsilon_x = \frac{\partial^2\phi}{\partial y^2}\left(\frac{1}{E_x}\right) - \frac{\mu_{xy}}{E_y}\left(\frac{\partial^2\phi}{\partial x^2}\right) \tag{2.16a}$$

$$\varepsilon_y = \frac{\partial^2\phi}{\partial x^2}\left(\frac{1}{E_y}\right) - \frac{\mu_{xy}}{E_x}\left(\frac{\partial^2\phi}{\partial y^2}\right) \tag{2.16b}$$

$$\varepsilon_{xy} = -\frac{\partial^2\phi}{\partial x \partial y}\left(\frac{1}{G_{xy}}\right) \tag{2.16c}$$

Substituding (2.16a,b,c) into the equation of compatibility (2.14), one finally obtains :

$$\frac{\partial^4\phi}{\partial x^4} + \frac{2\kappa}{\varepsilon^2} \cdot \frac{\partial^4\phi}{\partial x^2 \partial y^2} + \frac{1}{\varepsilon^4}\frac{\partial^4\phi}{\partial y^4} = 0 \tag{2.17a}$$

where

$$\epsilon^4 = \frac{E_x}{E_y}$$

$$\kappa = \frac{1}{2}(E_x E_y)^{1/2}\left[(1/G_{xy}) - (\mu_{xy}/E_x) - (\mu_{yx}/E_y)\right] \qquad (2.17b)$$

In order to solve equation (2.17a), it may also be written as :

$$\left[\frac{\partial^2}{\partial x^2} + \alpha_I \frac{\partial^2}{\partial y^2}\right]\left[\frac{\partial^2}{\partial x^2} + \alpha_{II} \frac{\partial^2}{\partial y^2}\right]\phi = 0 \qquad (2.18a)$$

where

$$\alpha_I = \frac{1}{\epsilon^2}\left[\kappa + (\kappa^2-1)^{1/2}\right] \qquad (2.18b)$$

$$\alpha_{II} = \frac{1}{\epsilon^2}\left[\kappa - (\kappa^2-1)^{1/2}\right] \qquad (2.18c)$$

Since equation (2.18a) was derived from the equilibrium, stress-strain and compatibility equations, the solution of this equation will satisfy all the governing equations. Also, the parameters that govern the solution of the notch root stress fields will be the constants ϵ and κ defined as (2.17a,b). These two parameters are material dependent and have values between 0.1 and 10. For isotropic materials, $\epsilon=\kappa=1.0$ and for White Spruce, $\epsilon=2.13$ $\kappa=1.60$ with axes in the longitudinal-tangential plane, and $\epsilon=1.87$ $\kappa=1.98$

with axes in the longitudinal-radial plane.

The representative range for the elastic properties of structural materials published by Leicester (1971) is shown in Table 1.

The solution of the field equation with subscripts I and II indicates that two further transformed co-ordinates may be defined. These are

$$x = x_I = x_{II} \tag{2.19a}$$

$$y = \alpha_I y_I = \alpha_{II} y_{II} \tag{2.19b}$$

and shown in Figure 6.

The field equation (2.18), written in the new co-ordinates, is :

$$\left[\frac{\partial^2}{\partial x_I^2} + \frac{\partial^2}{\partial y_I^2}\right]\left[\frac{\partial^2}{\partial x_{II}^2} + \frac{\partial^2}{\partial y_{II}^2}\right] \phi = 0 \tag{2.20}$$

For the case $\alpha_I = \alpha_{II}$, equation (2.20) reduces to a biharmonic equation, and in terms of polar co-ordinates :

$$\nabla^2\left(\nabla^2(\phi)\right) = 0 \tag{2.21}$$

where the operator ∇^2 is :

$$\nabla^2 \equiv \frac{\partial^2}{\partial r^2} + \frac{1}{r}\frac{\partial}{\partial r} + \frac{1}{r}\frac{\partial^2}{\partial \theta^2} \tag{2.22}$$

Table 1

Elastic Properties of Structural Materials

Type of Material	ε	κ
Isotropic solid	1.0	1.0
Typical Wood (LR & LT planes)	2.0	2.0
Typical plywood of balanced condition	1.0	4.0
Typical fibre-reinforced plastic	2.0	4.0

From R.H. Leicester (1971)

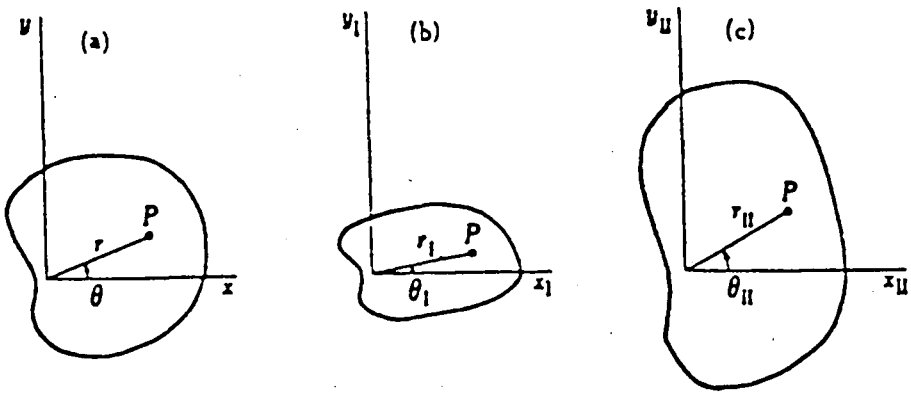

Figure 6 Notation for real space and transformed coordinates.(a) Coordinates of real space. (b) Coordinates system I.(c) Coordinate system II. From R.H. Leicester (1971)

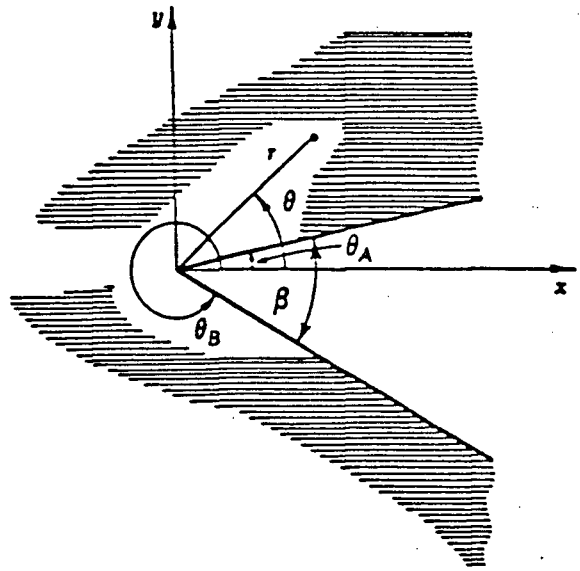

Figure 7 Notation and coordinates for notch roots. From R.H. Leicester (1971)

In general, for the orthotropic materials $a_I \neq a_{II}$, and the solution may be written as

$$\phi = \phi_I + \phi_{II} \tag{2.23}$$

where ϕ_I and ϕ_{II} are harmonic functions of the co-ordinates systems I and II respectively.

The solution to equation (2.22) may be sought in the product form :

$$\phi_i = r_i^\lambda f(\theta_i) \qquad i = I,II \tag{2.24}$$

where λ is a constant.

A suitable pair of harmonic functions for the solutions is the following :

$$\phi_I = A_1 r_I^\lambda \cos(\lambda\theta_I) + A_2 r_I^\lambda \sin(\lambda\theta_I) \tag{2.25a}$$

$$\phi_{II} = A_3 r_{II}^\lambda \cos(\lambda\theta_{II}) + A_4 r_{II}^\lambda \sin(\lambda\theta_{II}) \tag{2.25b}$$

where A_1 to A_4 are arbitrary constants.

Substituting (2.25) into (2.15a,b,c) leads to the following :

$$\sigma_x = \lambda(\lambda-1) r_I^{\lambda-2} (1/\alpha_I^2)[-A_1\cos(\lambda\theta_I - 2\theta_I) - A_2\sin(\lambda\theta_I - 2\theta_I)]$$

$$+ \lambda(\lambda-1) r_{II}^{\lambda-2} (1/\alpha_{II}^2)[-A_3\cos(\lambda\theta_{II} - 2\theta_{II}) - A_4\sin(\lambda\theta_{II} - 2\theta_{II})] \tag{2.26a}$$

$$\sigma_y = \lambda(\lambda-1)r_I^{\lambda-2}\left[A_1\cos(\lambda\theta_I-2\theta_I) + A_2\sin(\lambda\theta_I-2\theta_I)\right]$$

$$+ \lambda(\lambda-1)r_{II}^{\lambda-2}\left[A_3\cos(\lambda\theta_{II}-2\theta_{II}) + A_4\sin(\lambda\theta_{II}-2\theta_{II})\right] \qquad (2.26b)$$

$$\sigma_{xy} = \lambda(\lambda-1)r_I^{\lambda-2}(1/\alpha_I)\left[A_1\sin(\lambda\theta_I-2\theta_I) - A_2\cos(\lambda\theta_I-2\theta_I)\right]$$

$$+ \lambda(\lambda-1)r_{II}^{\lambda-2}(1/\alpha_{II})\left[A_3\sin(\lambda\theta_{II}-2\theta_{II}) - A_4\cos(\lambda\theta_{II}-2\theta_{II})\right] \qquad (2.26c)$$

The constants A_1 to A_4 are obtained by substitution of eqnations (2.26a,b,c) in the boundary conditions $\sigma_\theta = \sigma_{r\theta} = 0$ at the notch edges along $\theta=\theta_A$ and $\theta=\theta_B$, as shown in Figure 7. These four conditions lead to a matrix equation :

$$\begin{pmatrix} a_{11} & a_{12} & a_{13} & a_{14} \\ a_{21} & a_{22} & a_{23} & a_{24} \\ a_{31} & a_{32} & a_{33} & a_{34} \\ a_{41} & a_{42} & a_{43} & a_{44} \end{pmatrix} \begin{pmatrix} A_1 \\ A_2 \\ A_3 \\ A_4 \end{pmatrix} = 0 \qquad (2.27)$$

For any particular notch, the eigenequation (2.27) is satisfied when a value of λ has been found such that the determinant $|a_{mn}|$ is zero. Figure 8 is a plot of this determinant for a notch in Douglas fir.

It can be shown that the eigenvalues of a singular eigenfield are limited to the range $1 < \lambda < 2$. Within this

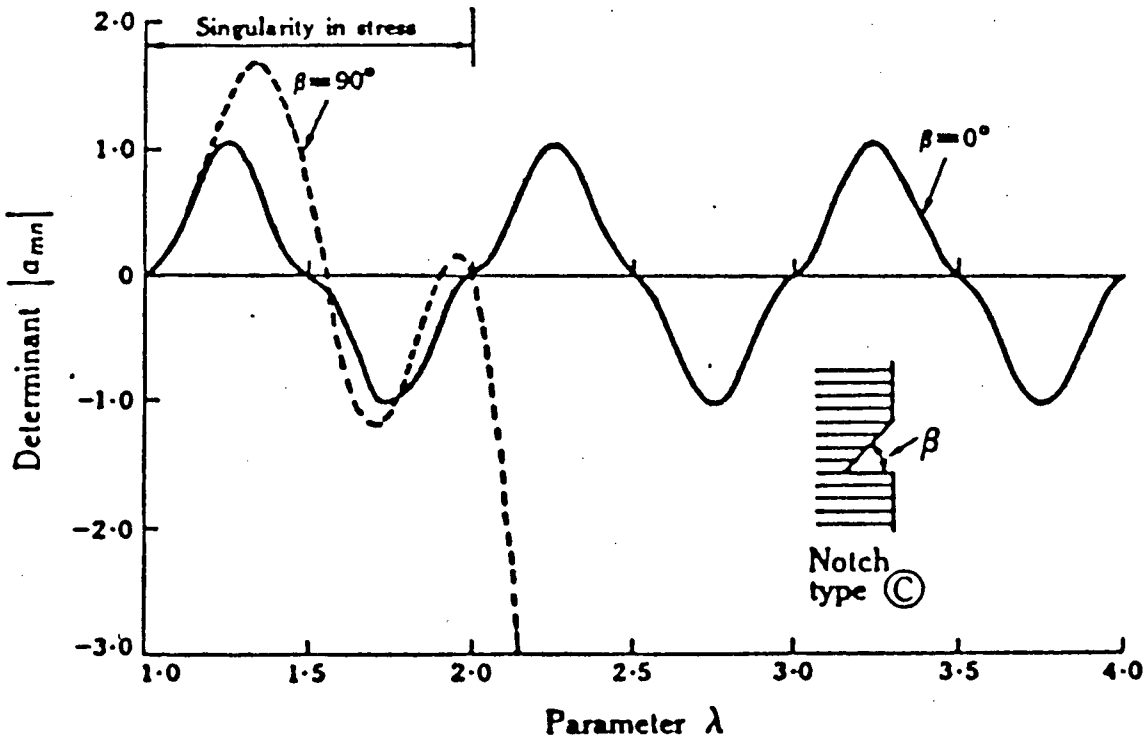

Figure 8 - Determinant of eigenequation for notch in Douglas fir.
From R.H. Leicester (1971)

range it is found that there is always at least one eigenvalue, and if the notch angle is small there will be two eigenvalues.

Denote these two eigenvalues, λ_A and λ_B with $\lambda_A < \lambda_B$. The eigenfields associated with these eigenvalues will be defined as 'primary' and 'secondary' eigenfields respectively. In general, the primary eigenfield will dominate at the notch root as r approaches 0 except in pure shear mode where the secondary eigenfield will govern.

Since equation (2.27) is a homogeneous equation, an additional constraint must be applied besides the four boundary conditions. The magnitude of the stress fields will fulfil this requirement. The stress intensity factors corresponding to the primary and the secondary stress fields will be denoted by K_A and K_B respectively. The definitions of K_A and K_B are quite arbitrary but in most cases of orthotropic material, they are defined as follows :

$$\sigma_\theta(\theta=\Omega) = K_A/(2\pi r)^{2-\lambda_A} \qquad (2.28a)$$

$$\sigma_{r\theta}(\theta=\Omega) = K_B/(2\pi r)^{2-\lambda_B} \qquad (2.28b)$$

where Ω is the angle of crack propagation and is usually the grain angle in the wood.

For the special case of a sharp crack, $K_A = K_I$ and $K_B = K_{II}$. However, the terms "opening mode" and "sliding mode",

which are usually associated with a sharp crack, are applicable to notches only if the notches are symmetrical with respect to the axes of elastic symmetry.

The failure criterion characterizing the onset of propagation of a crack from a sharp notch corresponds to these two stress intensity factors, K_A and K_B, reaching some critical values K_{AC} and K_{BC} respectively.

From the equations of stress fields, we can derive the equations of strain and displacement field in terms of the stress intensity factors. The method for obtaining these factors is discussed in the next section.

2.4.3 IMPLEMENTATION IN A FINITE ELEMENT PROGRAM

A singular finite element method is manipulated to compute the stress intensity factors. The finite element mesh consists of three regions --the elements around the notch tip, the elements remote from the notch tip, and the transitional elements in between to assure the compatibility of the elements.

Around the notch tip, the quadratic displacement field is enriched by the singular terms as follows :

$$u_i = a_1 + a_2\zeta + a_3\eta + a_4\zeta^2 + a_5\zeta\eta + a_6\eta^2 + a_7\zeta^2\eta + a_8\zeta\eta^2 + K_A f_i(\zeta,\eta) + K_B g_i(\zeta,\eta) \qquad (2.29)$$

where ζ and η are natural co-ordinates.

Substituting the nodal displacements in equation (2.29), we get :

$$\{u_i\} = [M]\{a\} + K_A\{f_i\} + K_B\{g_i\} \tag{2.30}$$

or

$$\{a\} = [M]^{-1}[\{u_i\} - K_A\{f_i\} - K_B\{g_i\}] \tag{2.31}$$

Substituting back into equation (2.29),

$$\begin{aligned} u_i(\zeta,\eta) = {} & [N(\zeta,\eta)]\{u_i\} \\ & + K_A\left[f_i(\zeta,\eta) - [N(\zeta,\eta)]\{f_i\}\right] \\ & + K_B\left[g_i(\zeta,\eta) - [N(\zeta,\eta)]\{g_i\}\right] \end{aligned} \tag{2.32}$$

Using the virtual work principle results in

$$\int_V \delta^T\{\delta\}[B]^T\left[[D][B]\{\delta\} + \{K\}^T[D]\{\Omega\}\right]dV = \delta^T\{\delta\}\{R\} \tag{2.33}$$

for a virtual change in $\{\delta\}$, and

$$\int_V \delta^T \{K\}\{\Omega\}^T \left[[D][B]\{\delta\} + \{K\}^T[D]\{\Omega\}\right]dV = \delta^T \{K\}\{R_k\} \qquad (2.34)$$

for a virtual change in {K}. Combining equations (2.33) and (2.34), we get :

$$\begin{bmatrix} [S] & \{P_1\} & \{P_2\} \\ \{P_1\}^T & [C_{11}] & [C_{21}] \\ \{P_2\}^T & [C_{12}] & [C_{22}] \end{bmatrix} \begin{Bmatrix} \{\delta\} \\ \{K\} \end{Bmatrix} = \begin{Bmatrix} \{R\} \\ \{R_k\} \end{Bmatrix} \qquad (2.35)$$

where

$$[S] = \int_V [B]^T [D][B]dV \qquad (2.36)$$

$$\{P_n\} = \int_V [B]^T [D]\{\Omega_n\}dV \qquad (2.37)$$

$$[C_{ij}] = \int_V \{\Omega_i\}^T [D]\{\Omega_j\}dV \qquad (2.38)$$

The element stiffness matrix can be assembled to form the global stiffness matrix, and the element load vector, the global load vector. The elements far from the notch tip will be ordinary quadratic, regular elements, whereas the transitional elements are introduced in a transition zone between fully singular and regular elements.

The displacement field of the transitional elements will be :

$$u_i(\zeta,\eta) = [N(\zeta,\eta)]\{u_i\} + R(\zeta,\eta)\{K_A[f_i(\zeta,\eta) - [N(\zeta,\eta)\{f_i\}] + K_B\,[g_i(\zeta,\eta) - [N(\zeta,\eta)]\{g_i\}]\} \tag{2.39}$$

where $R(\zeta,\eta)$ is bilinear transition function with R=1 at singular-singular boundary and is equal to 0 at singular-regular boundary. The use of the bilinear transitional elements ensures conformity between elements.

After forming the stiffness matrix, the solution method will be the same as for an ordinary finite element problem. From the calculated K_A and K_B values, which indicate the magnitude of the eigenfields, we can get the K_I and K_{II} stress intensity factors by assigning the amounts of opening and shear-sliding in each eigenfields.

Thus, for a direction of crack propagation ψ,

$$K_I = \sqrt{2\pi}\ \lim_{r\to 0}\ (r^{2-\lambda_A}\ \sigma_\theta(r,\theta=\psi)$$

$$= \sqrt{2\pi}\ \lim_{r\to 0}\ (K_A f_A(\theta=\psi) + K_B\ r^{\lambda_B-\lambda_A}\ f_B(\theta=\psi) + \ldots \tag{2.40}$$

$$K_{II} = \sqrt{2\pi} \lim_{r\to 0} (r^{2-\lambda_A} \tau_{r\theta}(r,\theta=\psi)$$

$$= \sqrt{2\pi} \lim_{r\to 0} (K_A g_A(\theta=\psi) + K_B r^{\lambda_B-\lambda_A} g_B(\theta=\psi) + \ldots \qquad (2.41)$$

then

$$K_I = \sqrt{2\pi}\, K_A f_A(\theta=\psi) \qquad \text{for } \lambda_A < \lambda_B \qquad (2.42a)$$

$$K_I = \sqrt{2\pi}\, [K_A f_A(\theta=\psi) + K_B f_B(\theta=\psi)] \qquad \text{for } \lambda_A = \lambda_B \qquad (2.42b)$$

and

$$K_{II} = \sqrt{2\pi}\, K_A g_A(\theta=\psi) \qquad \text{for } \lambda_A < \lambda_B \qquad (2.43a)$$

$$K_{II} = \sqrt{2\pi}\, [K_A g_A(\theta=\psi) + K_B g_B(\theta=\psi)] \qquad \text{for } \lambda_A = \lambda_B \qquad (2.43b)$$

For notches, the primary eigenfield will always dominate the stress and strain fields around the notch root except loading in pure shear-sliding mode.

Lum (1986) has developed the program NOTCH, which utilized this method and has shown good results in comparison with the collocation method used by Gandhi (1972).

From equation (2.28) we can observe that the dimension of K_A and K_B is (Force)x(Length)$^{2-\lambda_A}$ which depends on the material elastic properties and grain angle. Therefore, for different angle of notches, we have different dimensions of stress intensity factors. Thus, in order to derive a failure criterion for sharp notches, we must include the parameter λ in our criterion.

2.5 EFFECT OF SPECIMEN SIZE ON STRESS INTENSITY FACTORS

In predicting the strength of large structures, experiments were usually done by using the scale models. This employs an assumption that a scale model and a full-size structure will fail at the same nominal stress. However, failure of large structures at a lower nominal stress indicates that there may be a specimen size effect.

Most of the previous literature has applied a statistical model based on the weakest link principle to account for the strength of reduction. Such a theory assumes that failure of a single volume element leads to the failure of the whole specimen. This has an obvious analogy with the strength of a chain in which weakest link govern the strength.

2.5.1 EFFECT OF MATERIAL HETEROGENEITY

Barrett (1976) has applied this method to compare Mode I fracture toughness data obtained from specimens of differing thickness as multiple crack-fronts. Using the

Weibull analogy, Barrett defined the cumulative distribution function for critical stress intensity factor with total crack-front width B assuming all cracks have the same nominal stress intensity factor :

$$F(K_{IC}) = 1 - \exp[-(K_{IC}/m)^{k} B] \qquad (2.44)$$

where k and m are the shape and scale parameters respectively.

An expression relating the fracture toughness of two specimens with the crack-front widths, B and B*,is :

$$\frac{K_{IC}}{K^{*}_{IC}} = (\frac{B^{*}}{B})^{1/k} \qquad (2.45)$$

Obviously, if we plot K_{IC} against specimen width on a log-log scale, the slope of the regression line should be -1/k.

2.5.2 EFFECT OF THE CHANGE OF THE STRESS STATE

Another model to explain the crack-front width effect is proposed by Ewing (1979) based on the stress state in the specimen, and in particular the residual stresses induced by the drying which increases the toughness and constraint stresses which cause a decrease.

A useful model for describing plane stress-plane strain effects has been used in other materials and has some utility here. Figure 9 shows a cross section diagram of a specimen, the region near the surface within the area H is in a plane stress condition. The region in the middle is in the plane strain stress condition. Let denote K_{C1} and K_{C2} be the critical fracture toughness for the plane strain and plane stress condition respectively. Then the average critical stress intensity factor K'_C for $D \geq 2H$ will be :

$$DK'_c = 2HK_{C2} + (D-2H)\, K_{C1} \tag{2.46a}$$

$$K'_c = K_{C1} + \frac{2H}{D}(K_{C2} - K_{C1}) \tag{2.46b}$$

Usually $K_{C1} < K_{C2}$ so that we'll have a positive slope if we plot K'_C versus inverse thickness and an intercept of K_{C1} at $D^{-1}=0$. The depth of the value H of the plane stress region can be computed from :

$$H = \frac{1}{2\pi}\frac{K_{C2}^2}{\sigma_C^2} \tag{2.47}$$

where σ_C is the yield stress or the stress which results in gross deformation. The plane strain condition can only exists as long as there is enough thickness to provide the constraint and in general :

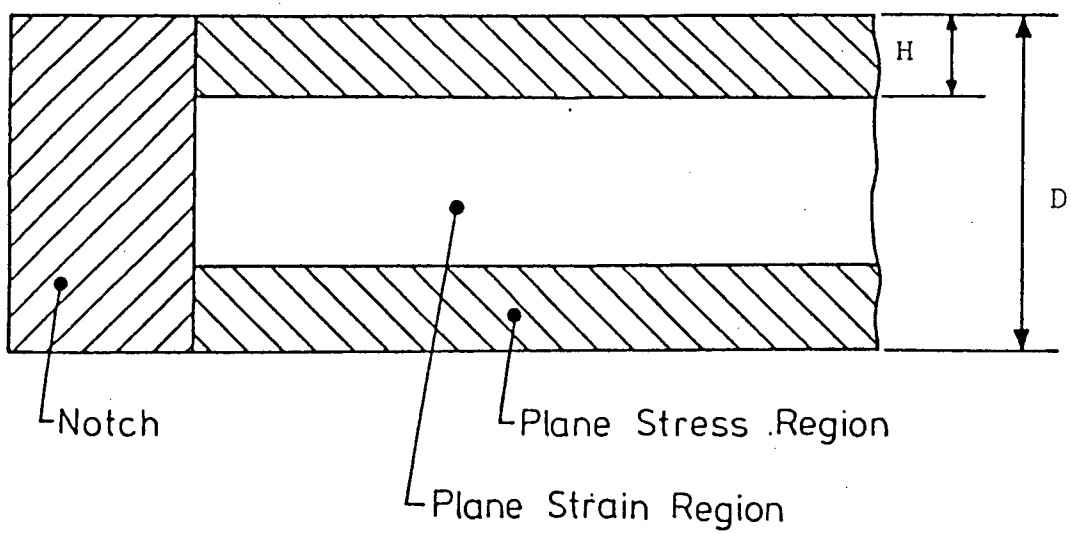

Figure 9 - Stress state in specimen

$D > 4H$ (2.48)

In general cases, if D<2H, then we'll have a complete plane stress condition and $K'_C = K_{C2}$. For D>2H, then plane strain condition will result in the middle that decrease the average stress intensity factor.

For the notched specimen, there is a similar size effect on the critical stress intensity factor proposed by Leicester (1973). From equations (2.26a,b,c), we can rewrite it for the plane stress at failure due to the primary stress singularity field as follows :

$$\sigma_{ij} r^s = A_f \tag{2.49}$$

where σ_{ij} is the stress component around the notch root and A_f is a constant that depends on the notch root angle, material and detail of the notch root.

From the dimensional analysis, we get :

$$\frac{\sigma_{ij}}{\sigma_o} \left(\frac{r}{L}\right)^s = B \tag{2.50}$$

where

σ is the normal stress,

L is a characteristic length denoting the size of the element,

B is a dimensionless constant depends on the geometry and loading.

Hence for a structural element of specific shape and loading, we can write :

$$\sigma_{of} = A_1/L^s \qquad s > 0 \tag{2.51}$$

where σ_{of} is the value of σ_o at failure and A_1 is a constant.

Similarily for the secondary stress field :

$$\sigma_{of}L^q = A_2 \qquad q > 0 \tag{2.52}$$

where A_2 is another constant.

Since s>q it follow that (2.51) always predominates provided the structural element is sufficiently large.

We can also write (2.51) for two similar specimen with different size :

$$\frac{\sigma_{f1}}{\sigma_{f2}} = (\frac{L_2}{L_2})^s \tag{2.53}$$

where σ_{f1} and σ_{f2} are the nominal stress at failure and L_1 and L_2 are the corresponding characteristic lengths respectively.

There are also two conditions required to apply the size coefficient factor on two different specimens. Firstly, the detail of the notch roots must be identical (not scaled) and secondly, the predicted fracture stress must be less than about 70% of the nominal proportional limit stress for unnotched members.

Based on the experimental results, the values of s follow a trend with the variation of the notch angle.

2.6 EFFECT OF MOISTURE CONTENT ON FRACTURE TOUGHNESS

Fracture toughness values show thickness variation in the kiln dried state, but the toughness also varies with moisture content. In green timber, water is contained within the cell lumens and cell walls, and drying to the fibre saturation point (approximately 27%) removes free water from the cell lumens. Below this value, water is removed from the cell walls, resulting in shrinkage and significant property changes. It was expected that strength would increase with decreasing moisture content below 27%. Since the drying process increases strength, then it is reasonable to propose that the residual stresses will increase K'_C providing no cupping and consequential cracking occurs.

Debaise, Porter, and Pentoney (1966) found that G_{ITLC} of Western white pine varied according to :

$$G_{ITLC} = 1.28 + 0.1125\ (\theta - 243)(1 - e^{-M/6}) \qquad (2.54)$$

where

θ = temperature (0°K)

M = moisture content (% ovendry weight)

G_{ITLC} = critical strain energy release rate for the TL system

We can relate G_{ITLC} to K_{IC} for TL system by :

$$G_{ITLC} = K_I^2 \sqrt{\frac{a_{11}\ a_{12}}{2}} \cdot \phi \tag{2.55}$$

where

$$\phi = \left[\sqrt{\frac{a_{22}}{a_{11}}} + \frac{2a_{12}+a_{66}}{2a_{11}}\right]^{1/2} \tag{2.56}$$

and a_{11}, a_{22}, etc., are the usual anisotropic compliances.

Substituting into (2.54) for critical value :

$$K_{ITL_C^2} = C[1.28 + 0.1125(\theta-243)(1-e^{-M/6})] \tag{2.57}$$

where

$$C = 1/\sqrt{\frac{a_{11}a_{22}}{2}} \cdot \phi \tag{2.58}$$

A similar equation can be derived for the critical fracture toughness of white spruce along the TL system.

2.7 MIXED MODE FRACTURE IN WHITE SPRUCE

In recent years, attention has been dedicated to the fracture of wood in the opening mode (mode I). It has been shown that fracture toughness, K_{IC}, is a geometry independent material property of wood characterizing the stress field around cracks, which govern the initiation of a crack propagation. The fracture failure of wood for sliding mode, mode II, has also been investigated by Barrett and Foschi (1977). However,wood structural members are often subjected to complex loading condition that result in mixed mode fracture. Available information under this mixed mode is limited, and will be discussed briefly in the following.

The mixed mode fracture in wood was first studied by Wu (1967). He carried out mixed mode loading tests on balsa wood and proposed the first interation curve for the mixed mode fracture in the form:

$$\frac{K_I}{K_{IC}} + \left(\frac{K_{II}}{K_{IIC}}\right)^2 = 1 \qquad (2.59)$$

Similar experiments had been conducted by Leicester (1974) on pine and an interaction curve for K_I and K_{II} stress intensity factors is in the form :

$$\frac{K_I}{K_{IC}} + \frac{K_{II}}{K_{IIC}} = 1 \qquad (2.60)$$

Although most of the investigators favor the idea that an interaction relation exists, Williams and Birch (1976), based on their experiments on Scots pine, concluded that there is no effect on the opening mode failure due to the sliding mode caused by the shear stress. Their proposed failure criterion is :

$$\frac{K_I}{K_{IC}} = 1 \qquad (K_{II} > 0) \qquad (2.61)$$

Recently, Woo and Chow (1979) investigated the mixed mode fracture in Kapur and Gagil using the single-edge notch and center-crack specimen. Their results has shown that there is some interaction relation between the mode I and mode II stress intensity factors under combined loading conditions.

More recently, Mall and Murphy (1983) have studied the mixed mode fracture failure of eastern red spruce by means of single-edge notch and center-crack specimen with various crack inclinations in the TL system. Their results have shown that the criterion for the mixed mode fracture failure of red spruce is same as equation (2.59).

A more general form for the interaction curve for mixed mode fracture may be proposed :

$$\frac{K_I}{K_{IC}} + \left(\frac{K_{II}}{K_{IIC}}\right)^{\alpha} = 1 \qquad (2.62)$$

where constants a is determined experimentally.

The interaction phenomenon will also be valid for mixed mode loading of sharp notches. As we know, the dimension of the critical stress intensity factor for sharp notches depends on the parameter λ, which is material and geometry dependent. In order to generate the interaction curve for notches, we need to have the same dimensions. A rational method is to generate a family of interaction curves each with a different λ, where λ has a range of 1.5 to 2.0. Then each curve will apply to all the mixed mode cases in the same dimension. For the special case of sharp crack, λ=1.5. To describe mixed mode fracture of each species of wood for both cracks and notches, we need to generate the interaction curve for intermediate values, for example, λ =1.5, 1.6, 1.7, 1.8, 1.9 and 2.0. For specific geometry and loading condition, the value of λ is determined and the appropriate curve to estimate the K_I and K_{II} values at failure.

3. EXPERIMENT PARAMETERS

3.1 INTRODUCTION

The aim of carrying out experiments is to verify the applicability of the theories to real practice. Different experiments were designed to study the validity of critical stress intensity factors methodology in predicting the failure mode and strength of the real structures. This chapter outlines the important considerations with regard to the selection of a fracture geometry, mode of failure, specimen preparation, and some guidelines on the experiment procedure and measurements.

3.2 CRACK ORIENTATION AND PROPAGATION

Since wood is a typical orthotropic material, one must specify the mode of crack propagation so as to describe the initial crack surface orientation (see sec.2.2). Within a plane, the crack may propagate in different directions and in a combination of the three different fundamental modes (see Figure 1). Therefore, in preparing the specimen for the experiments, attention must be paid to the crack orientation. Also, due to the large number of possibilities of fracture orientation, a set of appropiate experiments must be designed in order to simulate the fracture behavior in real structures.

First of all, the determination of mode I fracture toughness may lead to six different sets of experiments for

each different crack orientation, namely TL,RL,LT,LR,RT or TR, where the first letter refers to the direction perpendicular to the crack surface and the second letter refers to the crack propagation direction. However, the fracture toughness results of Schniewind and Centeno (1973) have shown that the fracture strength for the plane in longitudinal direction has values approximately one-tenth the values where propagation is across the grain. This implies that the fracture would always occur in the weakest natural cleavage plane, i.e., either the tangential-radial plane or the radial-longitudinal plane.

In addition, in order to obtain the best design of the experiment, the correct choice between two alternative failure planes need to be made. On a macroscopic level, most of the commercial boards under bending are observed to fail in the radial longitudinal plane. However, a closer look at the crack initiation will reveal that the failure has been initiated in the tangential-longitudinal plane. Therefore it was decided to conduct the experiments with specimen in this category and it is postulated that it would be representative of the initiation of failure in commercial material.

In addition, some of the specimens with different orientation such as RL system were tested in order to study the effect of orthotropy on the opening mode and the sliding mode fracture toughness.

3.3 MATERIALS

Thirty two kiln-dried nominal 2-in by 8-in White Spruce (Picea glauca) boards were purchased from one sawmill. For studies of between board variation of K_{IC}, 115 compact tension specimens, 125mm by 120mm by 38mm, were cut randomly from 10 different boards. From another eleven board, sixty two one-metre long end-split beam specimens were used to study the K_{IC}, K_{IIC} and mixed mode loading. Sixty-six one-metre mid-crack specimens were cut to study the mid-cracked beams under the condition of mixed mode loading and another twenty-four one-metre long specimens were cut and used for the study of between board variations of notched beams. Twenty of the one-metre long specimen were tested for the average modulus of elasticity (MOE) by stressing them under three-point loading and measuring the displacement. Due to the high bearing stresses induced at the supports, the specimens were tested about their weak axis -- on the flat -- to eliminate the bearing effect. The average MOE obtained was approximately 9000 MPa. Since obtaining local modulus of elasticity and Poisson ratios is difficult, published values of these constants were used in the analysis. (E_L =10163 MPa, E_T=494 MPa, E_R=830 MPa, G_{LT}=663 MPa, G_{LR}=700 MPa, ν_{LR}=0.337, ν_{LT}=0.40, ν_{RL}=0.0275, ν_{TL}= 0.0194). These elastic parameters were computed from regression equations as proposed by Bodig and Goodman (1973). All the specimens had been previously kiln-dried and were stored for a period of at least one month in a

temperature and humidity controlled room of 70°C which maintained a nominal 9% (±1%) equilibrium moisture content. These boards were straight-grained with the dominant system of propagation being TL.

3.4 SPECIMEN PREPARATION

In order to maintain similar samples, the specimens were cut in a mass production pattern to ensure uniform dimensions of the testing specimens. The cracks were first cut by a bandsaw which produced a kerf of about 1/8" so as to have enough room to accomodate the crack starter (see Figure 10) and the smooth plastic plate for the mode II fracture toughness testing. Then just prior to testing, the bandsawn notch was sharpened with the crack starter to extend the sawn notch approximately 0.1 in.

An importance consideration of the specimens prepared is the sharpness of the initial crack. As we assumed a zero notch root hypothesis, we need to have some control of the crack sharpness. Leicester (1974) has shown that the influence of root diameter on the fracture strength of drilled notches is less than 10% for notch roots below 5 mm in diameter. Thus a single point crack starter with an included angle of approximately 10° and a tip radius of less than 0.5μm was used. It is postulated that this would give the same result as the cracks made by a razor blade.

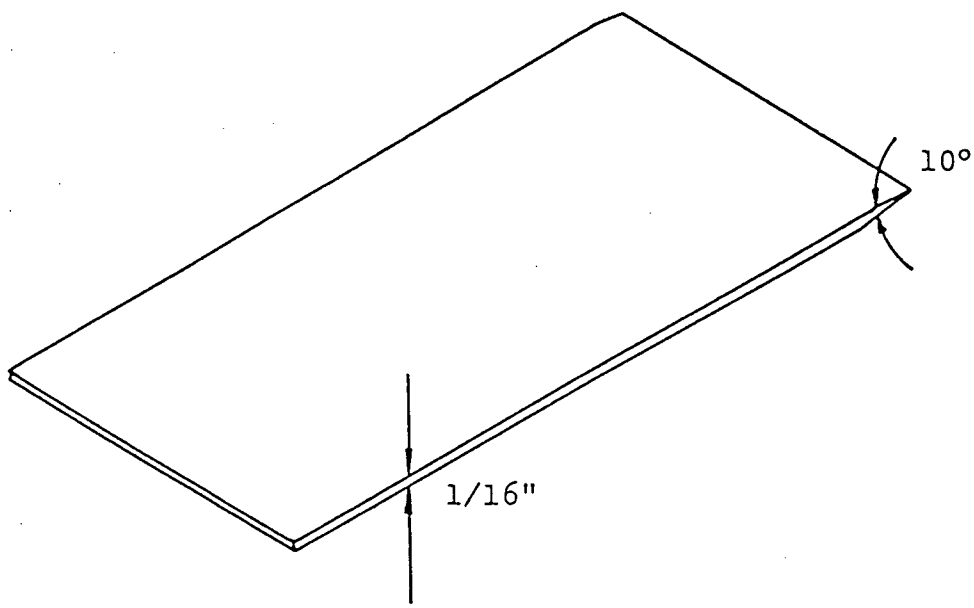

Figure 10 A steel crack starter with crack tip radius less than 0.5μm

3.5 EXPERIMENTAL MEASUREMENT OF LOAD AND DISPLACEMENT

In the experiments, centerline deflection was measured using a linear variable differential transducer (LVDT) in all cases (see Figure 11), while a modified LVDT (as shown in Figure 12) was used to measure the crack opening displacement (COD) and the relative longitudinal displacement of the crack in a cracked beam.

In obtaining the critical stress intensity factors, some criterion was employed to determine the critical failure load during the testings. Load-deflection plots were generated at the time of testing on an X-Y recorder. Since these curves were similar to those encountered in the ASTM fracture tests, a similar method was adopted to check the validity of the results. Small amounts of slow crack growth are allowed in the ASTM test, but growth is limited to approximately 5% of initial crack length in a valid K_{IC} test. Three different curves were encountered during the experiments (as shown in Figure 13), and the load P_Q corresponding to a 5% offset from the initial slope was used to compute the critical stress intensity factors.

The compact tension specimens were done in the humidity room with an Instron universal testing machine which provided autographic recordings of the load and displacement. Cross head speed of 0.5 mm/min was selected which produced failures in about 1 minute.

All the beam tests were done at room temperature (approx. 20°C) with a Satec testing machine which provided

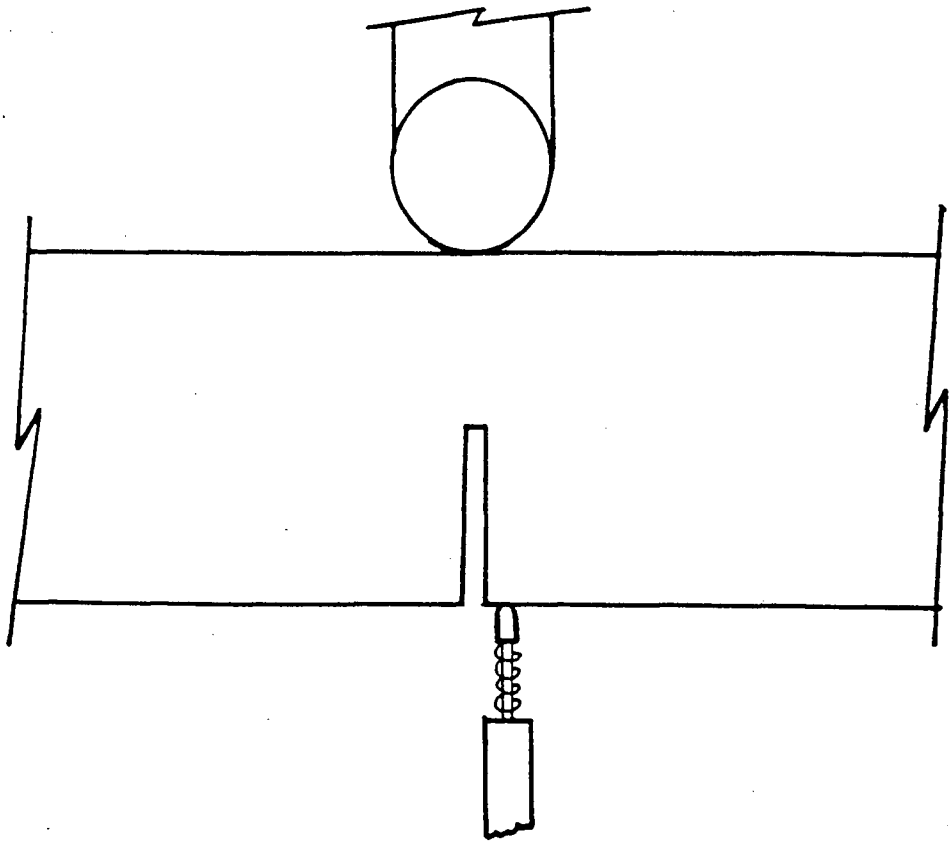

Figure 11 - LVDT gage for centerline deflection measurement

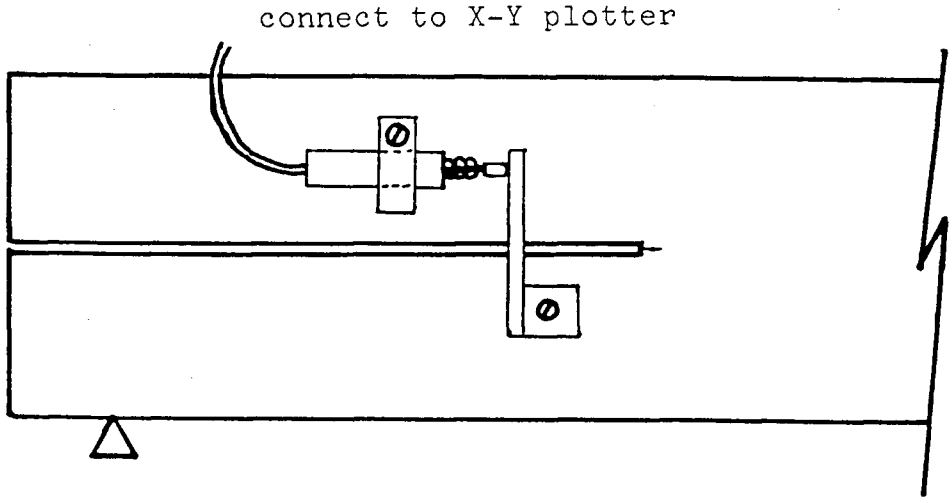

Figure 12 - Modified LVDT gage for measuring longitudinal sliding displacement

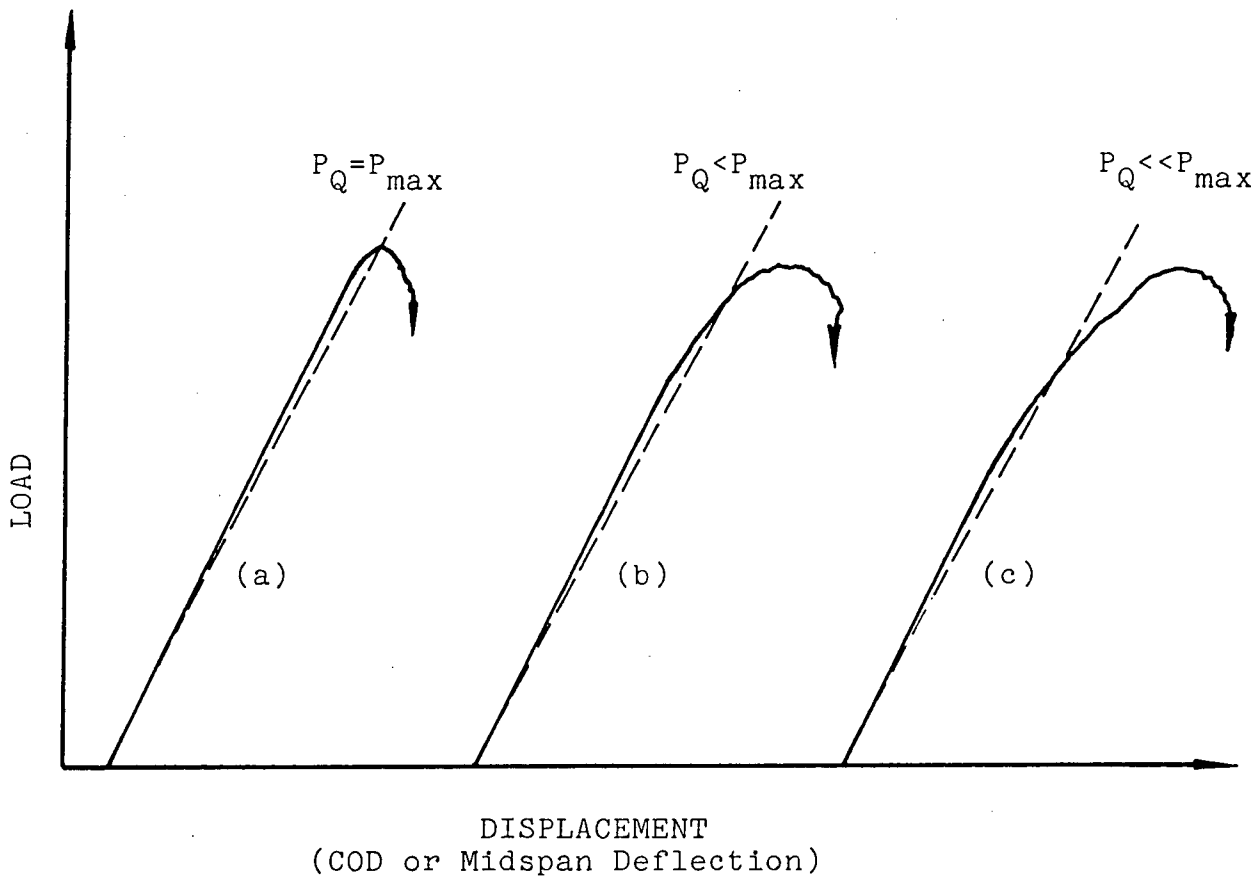

Figure 13 - Typical Load Vs Displacement Curves: (a)$P_Q=P_{max}$(acceptable); (b) $1.2P_Q \geq P_{max}$(acceptable);(c) $1.2P_Q<P_{max}$(unacceptable)

plotting of the load and displacement. Cross head speed was controlled so as to produce failures at about 2-4 minutes.

The moisture content at the time of testing and the specific gravity were determined for all specimens tested.

3.6 TREATMENT OF DATA

An average failure load as well as the variance were calculated for each experiment. Moisture content data were also collected to assure that all the specimens were tested under uniform conditions and provide a basis for adjusting data as required.

The values of the deflection is not significant in these experiments except that the load deflection curve is used for determining the failure loads. As mentioned earlier, the stress intensity factor is linearly related to the applied load in a linear elastic material, so the failure loads were used to compute the critical stress intensity factors by the following equation :

$$K_{ic} = \frac{P_Q}{P^*} K_i^* \qquad i = 1,2 \tag{3.1}$$

where P_Q is the failure load; P* is the arbitrary load entered into the finite element computer program to compute the corresponding stress intensity factor K_I^*, and K_{IC} is the critical stress intensity factor for the specific specimen geometry and loading.

Calculated stress intensity factors were collected and used to generate the interaction curves for cracks and notches. The curves were expected to have a form similar to a quadrant of an ellipse as proposed by many investigators as shown in Figure 14. In order to verify the equation or derive a new empirical formula, we need to have evenly spreaded failure points on the curves. Different experiments were designed to generate the curves as well as to study the moisture constant effect and the specimen size effect.

The details of each experiment as well as the results will be described in the next chapter.

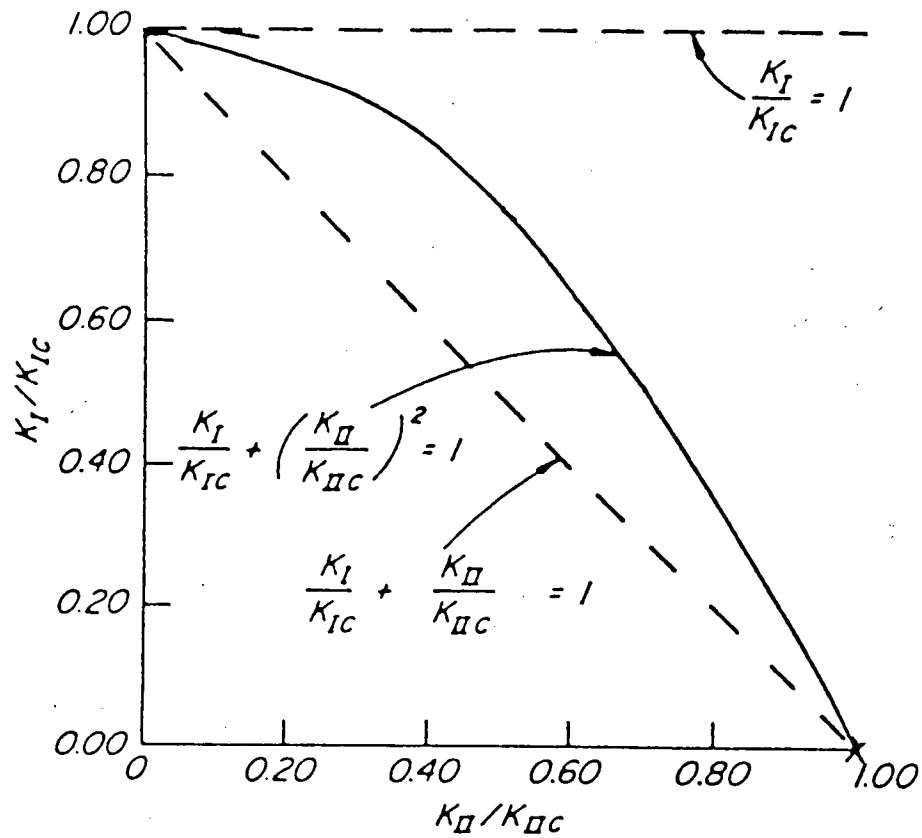

Figure 14 - Relations between K_I/K_{IC} and K_{II}/K_{IIC}

4. EXPERIMENT DESCRIPTIONS AND RESULTS

4.1 INTRODUCTION

This chapter gives a full description of the procedures and results of the experiments. The eight experiments conducted will be discussed in separate sections, namely No.1 to No.8.

Emphasis was put on studies of mode I critical stress intensity factors which tend to dominates in wood fracture failure. Effects of variation of the moisture content and crack-front width on the mode I fracture toughness was also studied. At the beginning of this thesis, it was expected that the critical stress intensity factors would be a constant for specific geometry, material and crack orientation. However, as the experiments progressed, it was found that K_{IC} may also depends on the actual size of the specimen. Experiments were conducted to study the effect of the variation of the uncracked length in front of the crack on the mode I fracture toughness.

4.2 EXPERIMENT NO.1, MODE I FRACTURE TOUGHNESS

4.2.1 EXPERIMENTAL DESIGN AND PROCEDURE

Experiment No.1 was designed to determine the mode I fracture toughness for white spruce. Effects of the grain orientation and specific gravity were also investigated. Two type of specimens were used to study the fracture toughness --the ASTM compact tension specimen (CTS) and the double

cantilever beam specimen (DCB) as shown in Figure 15 and 16.

The length to width ratio of the compact tension specimen was as recommended by the ASTM Standard with thickness of 38 mm. A total of 75 specimens were machined from two 20ft boards with the dominant system of propagation being TL. The CTS is also designed to study the effect of the grain orientation on the mode I fracture toughness as well as the between board variation of K_{IC}. The crack opening displacement (COD) was measured by the modified LVDT and all the testing was done with an Instron Testing Machine in a humidity room at 70°F and 50 per cent relative humidity. Crosshead speed was maintained at 0.5mm/min which produced failures in about 1 minute. The experiment setup is shown in Figure 17.

For the double cantilever beam test, a total of 18 specimens were cut from three 20ft kiln-dried boards and were previously conditioned to approximately 10 per cent moisture content.

The tests were carried out at room temperature with the Satec Testing Machine at a rate of 0.2mm/min which caused failure in about 2 minutes.

4.2.2 RESULTS

In order to determine the mode I fracture toughness, we need to compute the geometrical correction factors for both the CTS as well as the DCB specimens. This was accomplished with the finite element program NOTCH, using quadratic

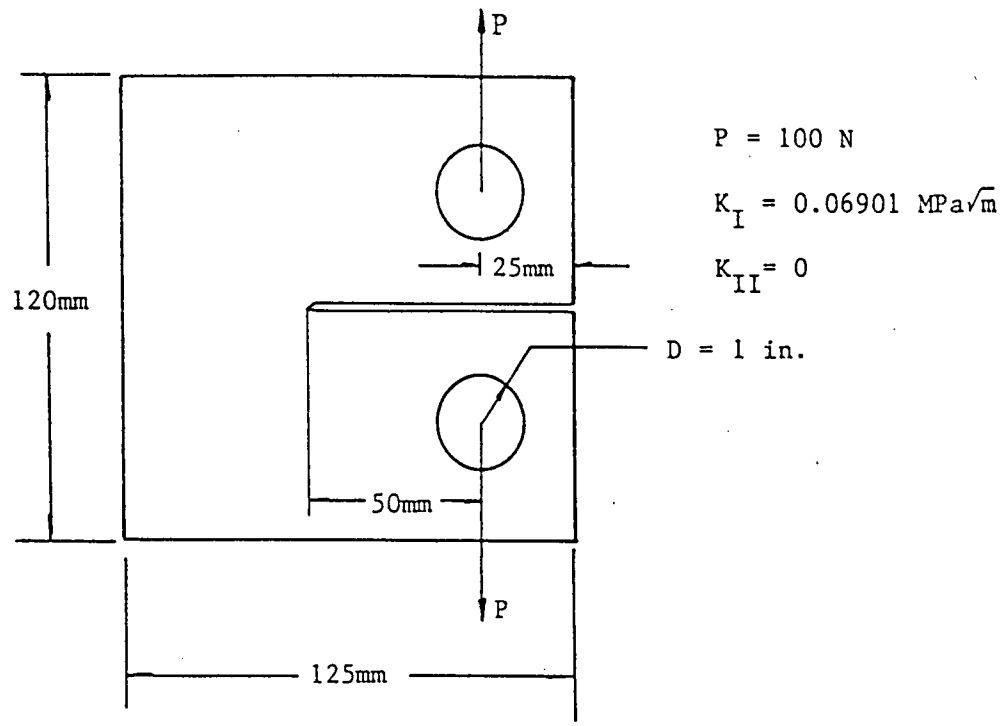

Figure 15 Configuration of Compact Tension Specimen (CTS)

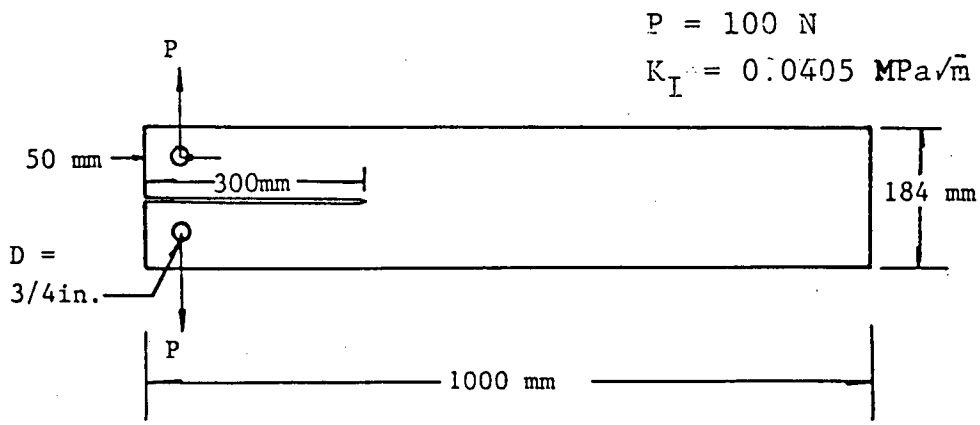

Figure 16 Configuration of Double Cantilever Beam specimen (DCB)

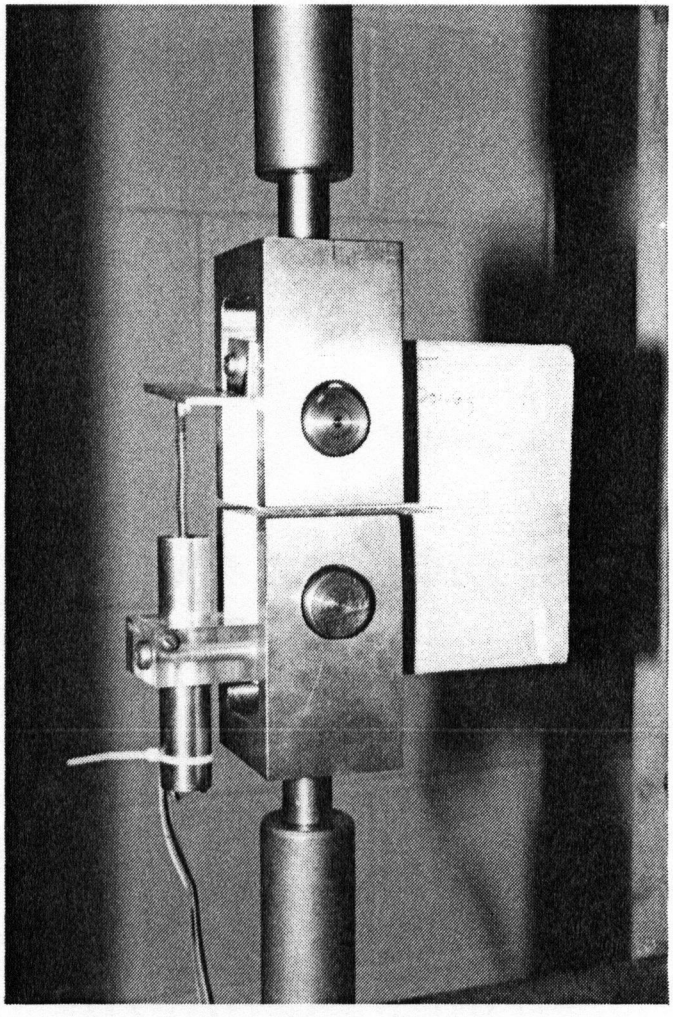

Figure 17 The experimental setup of the compact tension specimen.

isoparametric, singular-enriched elements. An arbitrary load of 100 N was selected in obtaining the stress intensity factors and the critical fracture toughness were easily obtained by eqn. (3.1). The finite elements mesh for the CTS and the DCB specimens are shown respectively in Figure 18 and Figure 19.

Table 2 summarizes results for both cases for different grain orientations. A trend of decreasing mode I fracture toughness from TL system to RL system is apparent. A plot of K_{IC} versus annual rings angle is shown in Figure 20 and a line was fitted by least-squares to the data. Thus,

$$K_{IC} = 0.3933 - 2.1323 \times 10^{-3}\ \theta \qquad (4.1)$$

where K_{IC} is the mode I fracture toughness, MPa$\sqrt{m}$; θ is the angle between the crack and the growth ring angle as defined in Figure 20.

Figure 21 and Figure 22 shows the cumulative distribution functions of the K_{IC} for the CTS and DCB specimens. They were best-fitted by the Weibull distribution curves which are often used to model the strength distribution of wood products.

From Table 2, it is obvious that the K_{IC} values for the CTS is lower than the DCB specimens. This implies there is some relationship between the K_{IC} and the specimen size, and this was investigated in the later phase of the experiments.

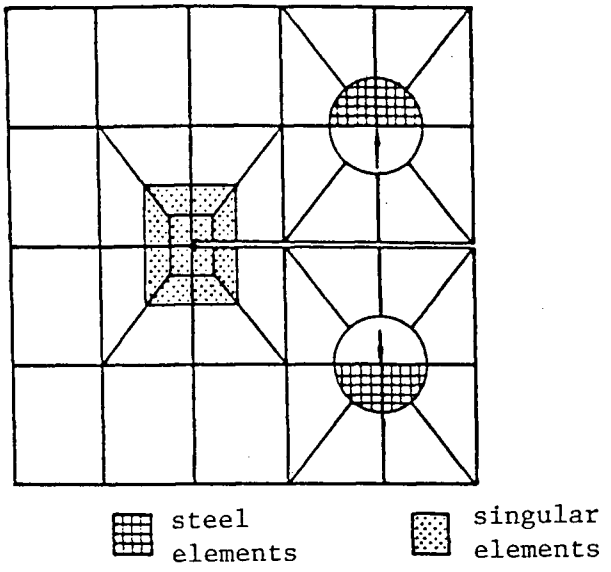

Figure 18 Finite Element Mesh for the CTS

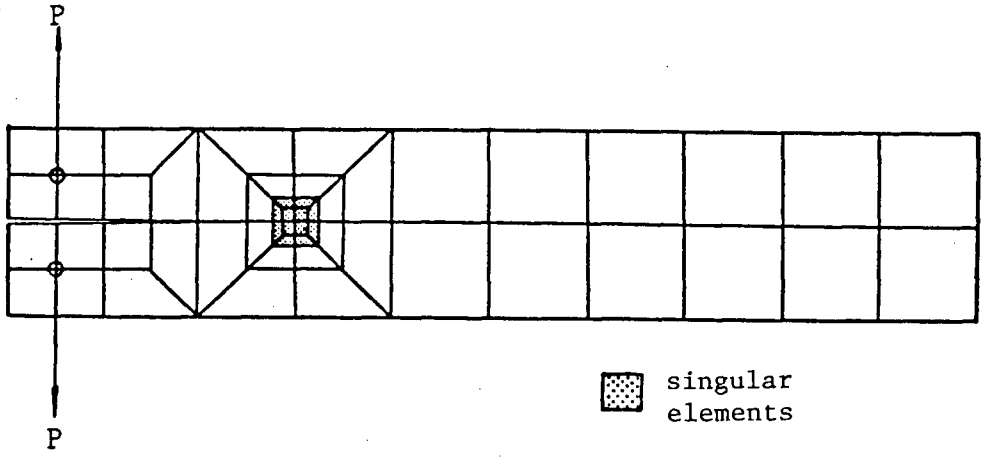

Figure 19 Finite Element Mesh for the DCB specimens

Table 2

Effect of the Annual Rings Angle on K_{IC}

Specimen Type	Angle to RL(deg)	sample no.	M.C. (%)	S.G.	P_{max}/P_Q	K_{IC} (MPa$\sqrt{m}$)	K_{IC} (psi$\sqrt{in}$)
CTS	0 - 10	6	9.54	0.349	1.02	0.3872	352.31
	11 - 20	4	9.40	0.354	1.04	0.3650	332.17
	21 - 30	1	10.00	0.336	1.06	0.3666	333.60
	31 - 40	5	8.44	0.374	1.05	0.3153	286.96
	41 - 50	12	8.49	0.386	1.03	0.2972	270.44
	51 - 60	8	8.96	0.380	1.03	0.2822	256.80
	61 - 70	1	9.00	0.400	1.05	0.3061	278.55
	71 - 80	3	9.00	0.393	1.03	0.2245	204.30
	81 - 90	33	9.33	0.388	1.05	0.2051	228.41
DCB	90	17	9.43	0.370	1.05	0.3879	352.99

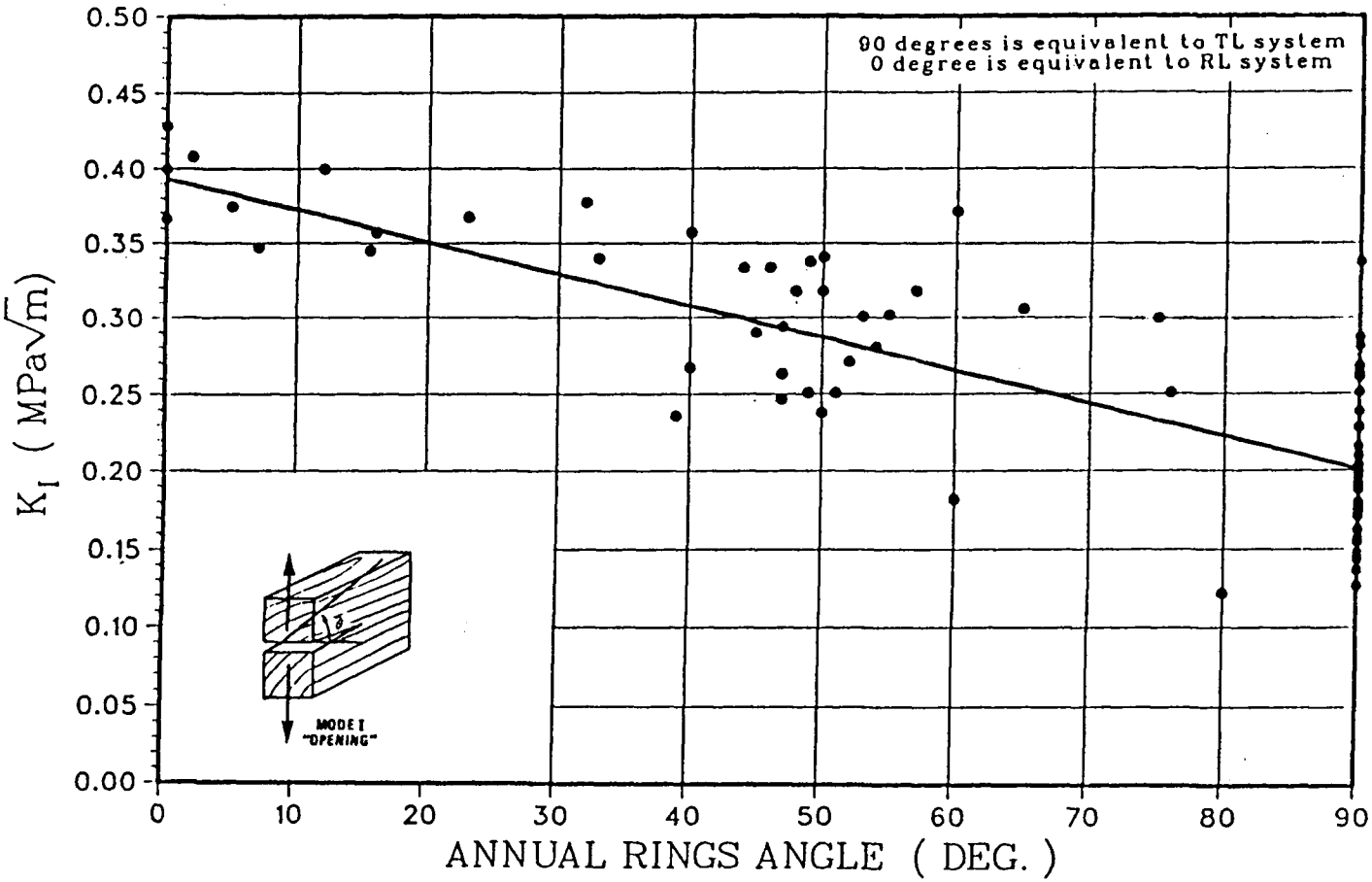

Figure 20 Mode I Fracture Toughness Variation with Annual Rings Angle

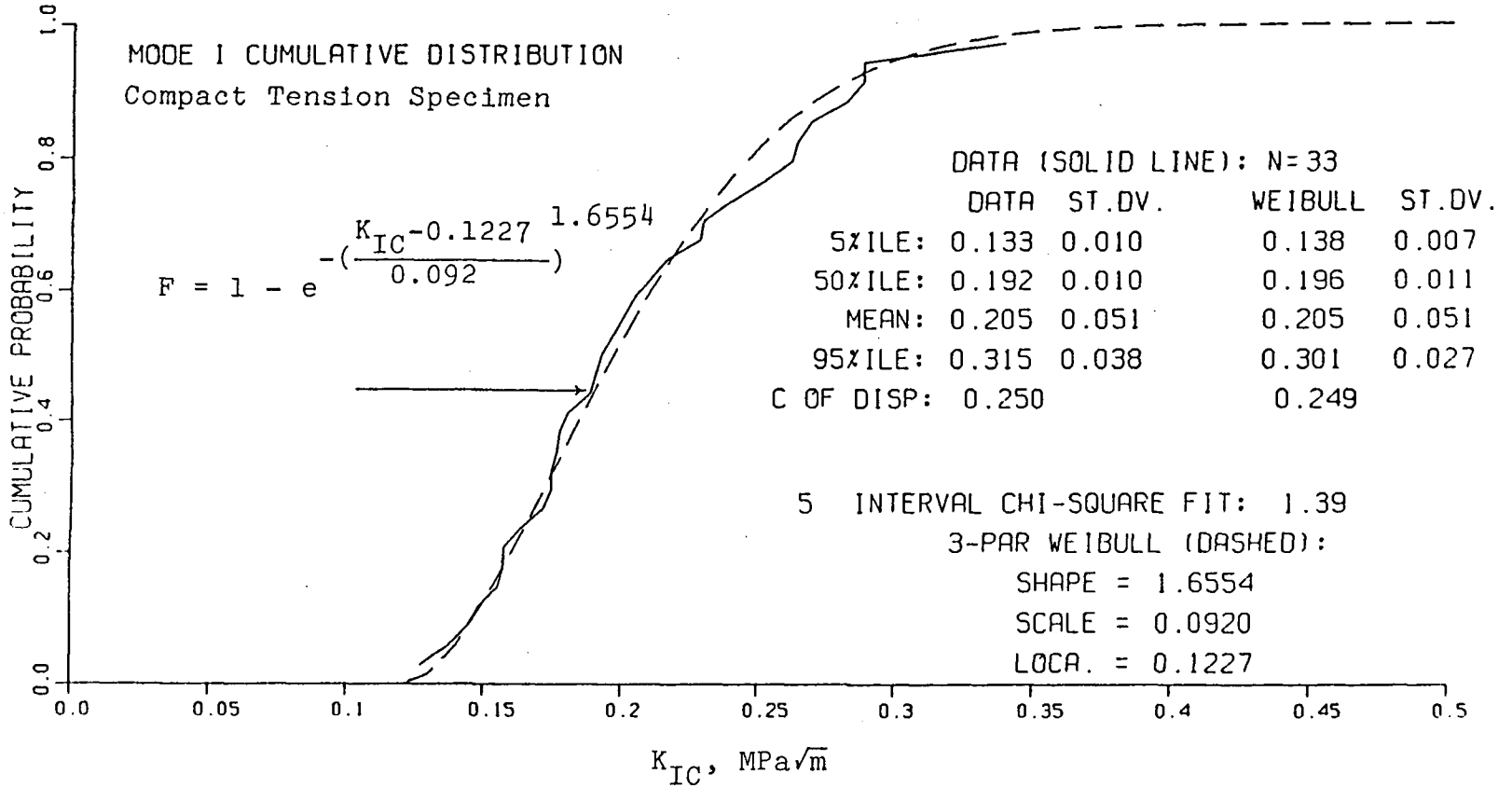

Figure 21 Cumulative Distribution Curve of the Compact Tension Specimen.

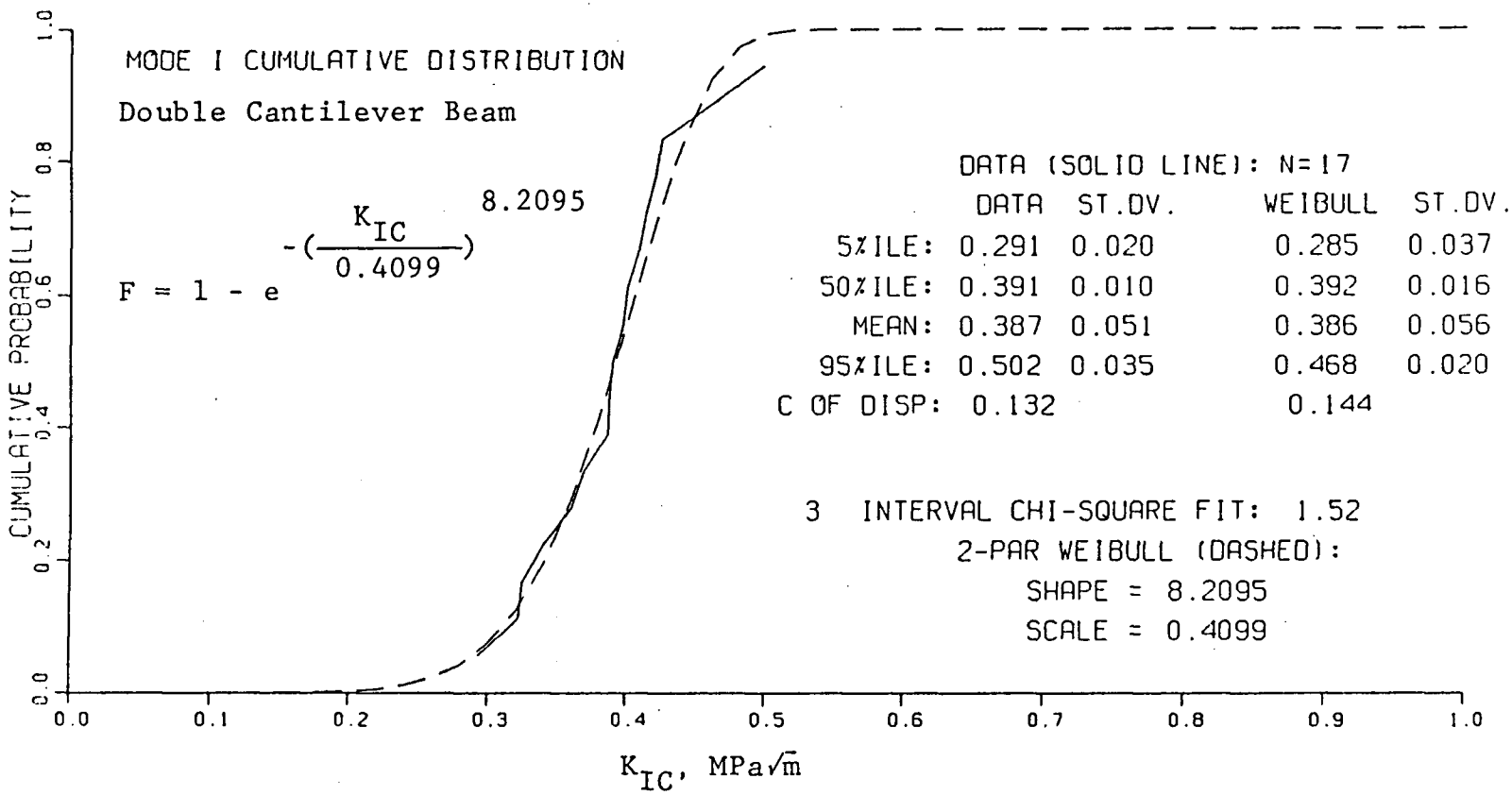

Figure 22 Cumulative Distribution Curve of the Double Cantilever Beam.

The critical mode I stress intensity factor, K_{IC} , for the CTS of white spruce in the TL and RL system of crack propagation were 0.205 MPa$\sqrt{m}$ and 0.387 MPa$\sqrt{m}$ respectively. (see Table 2) This species of wood has not been previously tested for this fracture mechanics parameters. However, present values of K_{IC} are comparable with their counterparts obtained for other species; K_{IC} for the TL mode of western white pine is about 0.190 MPa$\sqrt{m}$ and for western red cedar is about 0.185 MPa$\sqrt{m}$ obtained by Johnson (1973).

The mode I fracture toughness for the DCB spscimens in the TL system of crack propagation is approximately 0.387 MPa$\sqrt{m}$.

Average moisture content recorded for all tested specimens is 9.1% and average specific gravity is 0.38, based on the ovendry weight-ovendry volume. An example of the dependence of K_{IC} on specific gravity is shown in Figure 23 for the CTS and it is apparent that there is no corelation between the specific gravity and the K_{IC} .

4.3 EXPERIMENT NO.2 CRACK-FRONT WIDTH EFFECT ON FRACTURE TOUGHNESS

4.3.1 EXPERIMENT DESIGN AND PROCEDURE

Experiment No.2 was designed to study the effect of the variation of the crack-front width on the mode I fracture toughness. A total of thirty-eight CTSs were cut into five different widths, nominally B = 7,15,21,29,38 mm and mostly

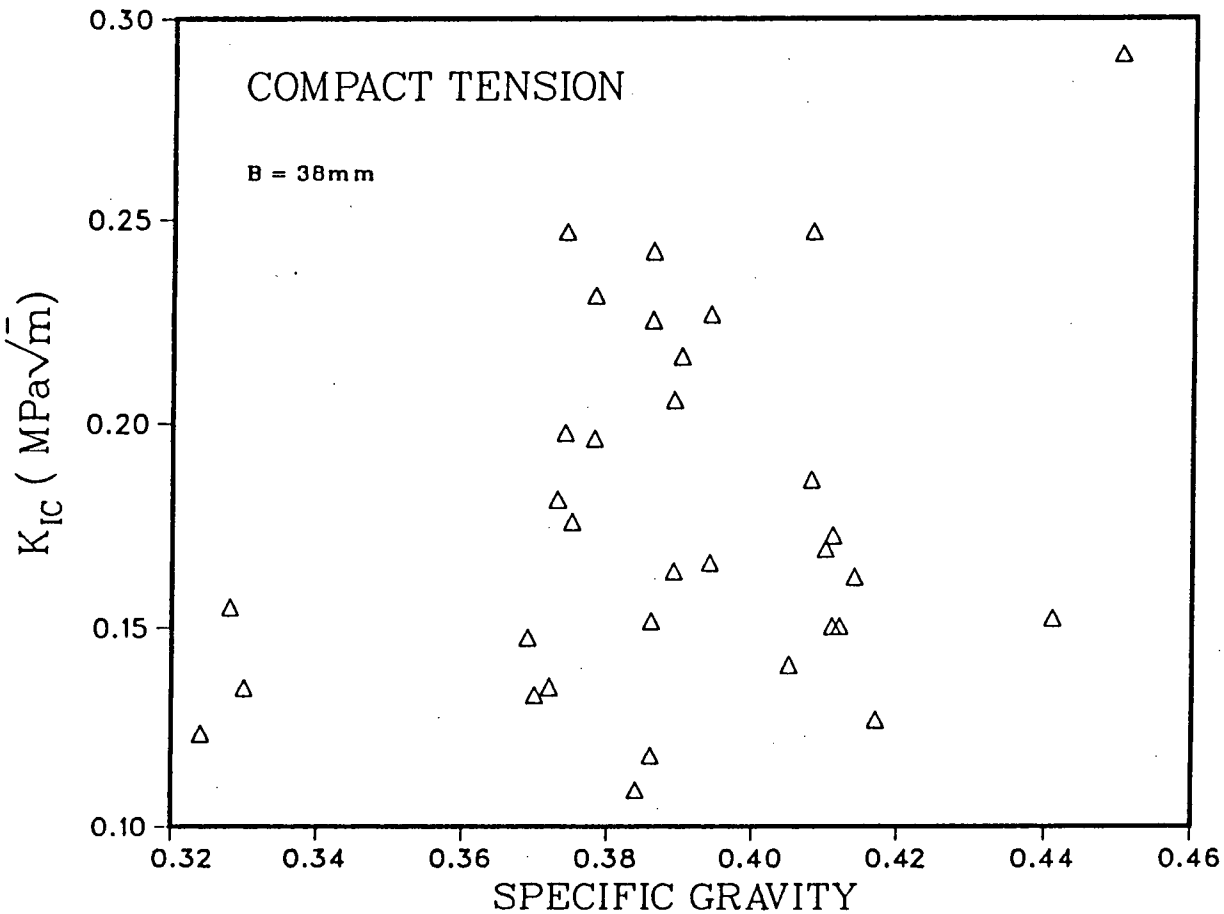

Figure 23 Effect of Specific Gravity on Mode I Fracture Toughness.

in the TL system. The specimen geometry and the loading procedure was same as used in Experiment No.1. It is expected that the stress intensity factor is inversely proportional to the width of the specimen, so if we double the width of the specimen, the stress intensity factor will be half of before. All the specimens were tested in the temperature and humidity controlled room with the Instron Testing Machine.

4.3.2 RESULTS

The critical stress intensity factors obtained for each width are given in Table 3. Shown are the average values of critical stress intensity factors, K_{IC} , coefficient of variation (COV) i.e., ratio of standard deviation to average values, sample size as well as the shape (k) and scale (m) parameters for a 2-parameters Weibull model. The large variation of the k and m values can be explained by the limited tests for each case.

The influence of crack-front width on the fracture toughness can be derived by the Weibull weakest link model. The crack-front width, B ,mm, is also incorporated in the derivation and the relationship obtained is:

$$F(K_{IC}) = 1 - \exp[-(K_{IC}/m)^{k}B] \qquad (4.2)$$

where k and m are the shape and scale paramters respectively.

Table 3

Effect of crack-front width on K_{IC} for compact-tension specimens of white spruce for longitudinal propagation

Width, B mm	Sample size	Specific gravity	P_{max}/P_Q	Average K_{IC} MPa$\sqrt{m}$	C.V. %	Shape parameter k	Scale parameter m
7	5	0.335	1.08	0.2570	2.15	47.98	0.2598
15	7	0.378	1.05	0.2282	9.33	10.95	0.2384
21	6	0.395	1.03	0.2435	6.18	22.31	0.2501
29	7	0.375	1.04	0.1805	10.87	12.93	0.1887
38	10	0.389	1.05	0.1768	27.15	4.23	0.1940

Considering two different width, B and B*, the effect of variation of B on median values of K_{IC} can be derived by evaluating equation (4.2) at F = 0.5. Then, we get :

$$\frac{K_{IC}}{K^*_{IC}} = \left(\frac{B^*}{B}\right)^{1/k} \qquad (4.3)$$

If we plotted K_{IC} values against specimen width B on a log-log plot, the slope of the regression line will be -1/k. The least-squares method was used to fit the regression line to the data. The relationship between K_{IC} and crack-front width obtained is :

$$\log K_{IC} = -0.3795 - 1/4.423 \log_{10} B \qquad R^2 = 0.735 \qquad (4.4)$$

where B is the crack front width,mm; K_{IC} is the critical stress intensity factor, $MPa\sqrt{m}$.

A plot of this relationship is shown in Figure 24 and results obtained by Barrett (1976) for Douglas fir is also presented in the graph. The parameters k and m obtained by Barrett (1976) are 7.41 and 0.41 respectively. The discrepany between the two curves is due to the difference in the elastic properties of two species of wood.

From equation (4.2) we get the cumulative distribution for K_{IC} :

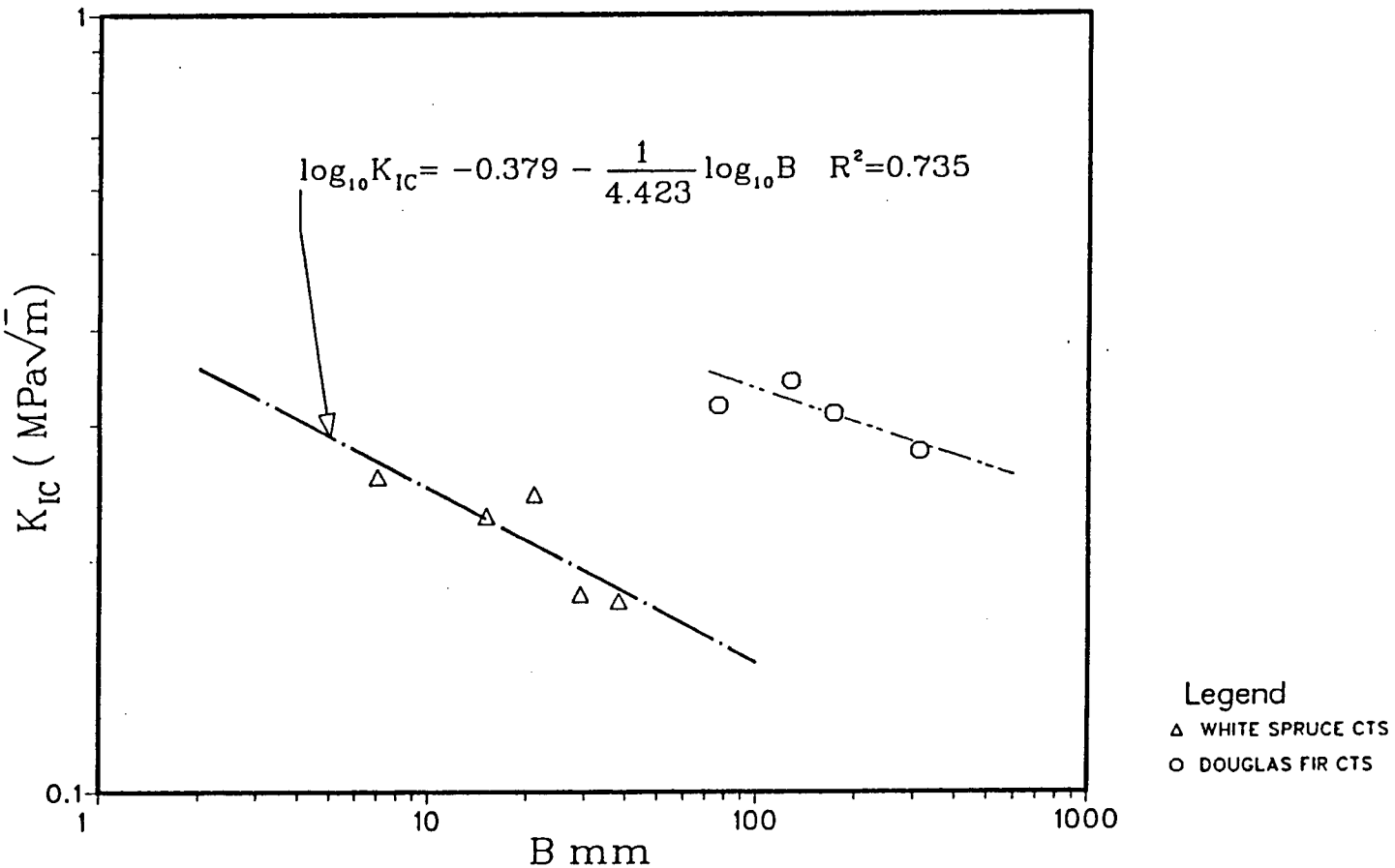

Figure 24 Effect of Crack-front Width on Mode I Fracture Toughness. (Based on the Weibull Weakest Link Model)

$$F(K_{IC}) = 1 - \exp[-(K_{IC}/0.384)^{4.423} B] \qquad (4.5)$$

which is comparable to the results of Douglas-fir.

The results of these tests confirmed that a relationship exists between the fracture toughness and the crack-front width. It has been shown that K_{IC} deceases as the crack-front width increases which can be explained by the weakest-link principle.

Another consistent model of the crack-front width effect is based on the stress state in the specimen. From equations (2.46b) and (2.47) we have :

$$K'_C = K_{C1} + 2H/D\ (K_{C2} - K_{C1})$$

$$H = \frac{1}{2\pi} \frac{K_{C2}^2}{\sigma_C^2}$$

where σ_C is the yield stress or that stress which results in gross deformation.

A graph of K_{IC} versus inverse thickness is shown in Figure 25 and a regression line is plotted based on the four data points. From the intercept at 1/D = 0 and equations (2.46b) and (2.47), we get :

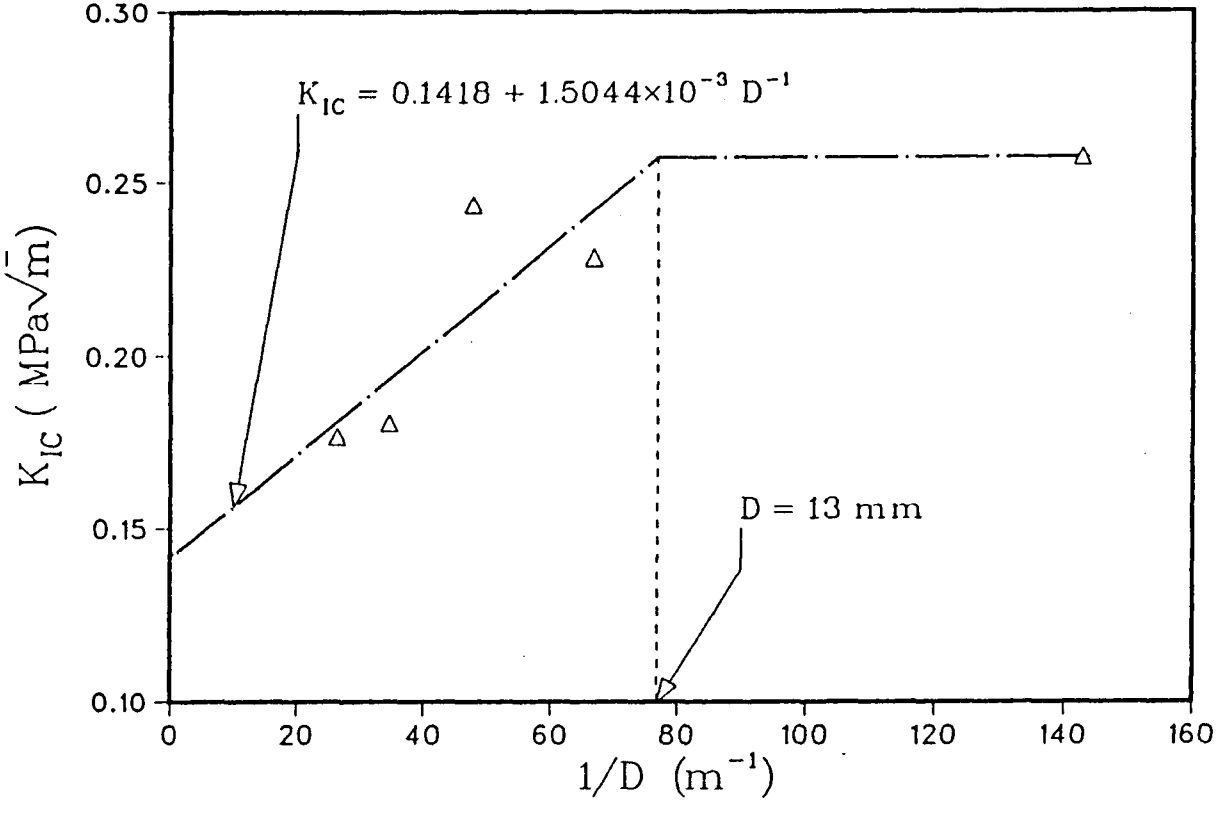

Figure 25 Effect of Crack-front Width on Mode I Fracture Toughness. (Based on the Stress-state Model)

K_{C1} = 0.1414 MPa$\sqrt{m}$

K_{C2} = 0.435 MPa$\sqrt{m}$

H = 6.95 mm

The transition thickness from plane stress to plane strain will be D = 2H which is equal to 13.90 mm. When D < 13.90 mm, a plane stress condition will be maintained, so the basic plane stress value, K_{C2} will be achieved.

For D > 13.90 mm, the plane strain condition will result in a decline in K_{IC} .

As seen from Figure 24 and Figure 25, both the Weibull theory model and the stress-state model fitted very well with the data points. However, if a specimen has a width less than the transition thickness, according to the stress-state theory, it is postulated that the width has no effect on the fracture toughness. For the Weibull model, it is proposed that the effect will exist no matter what the specimen thickness is. Since the transition thickness is usually less than 10 mm, the deviation between the Weibull model and the stress-state model is not significant at all and both models behaved well in the experiments conducted.

4.4 EXPERIMENT NO.3, CRACK-FRONT LENGTH VARIATION

4.4.1 EXPERIMENT DESIGN AND PROCEDURE

Because of the differences between the mode I fracture toughness values obtained from the CTS and DCB test results, Experiment No.3 was conducted. It aimed at investigating the influence of the crack-front length on the mode I fracture toughness. It was expected that the fracture toughness would follow a trend as the crack-front length i.e., the length in front of the crack increases. Experiments were carried out with the CTS with different crack-front length, nominally L = 50,75,100,125 mm, where L is defined in Figure 26. The crack is maintained at the same length as in experiment no.1. Five specimens were prepared for each case and a total of twenty specimens were cut from four boards. The experiments were conducted in room temperature with a average moisture content of 9%. The load was plotted against the COD recorded by the modified LVDT on a X-Y plotter. The design failure load were determined in the same way as ASTM Standard E399 and the time to failure were about 1 minute for all cases.

4.4.2 RESULTS

Table 4 summarize results of within-board experiments designed to determine the relation between K_{IC} and the crack-front length, L. Average values of K_{IC} , C.V., moisture content and specific gravity for each length are

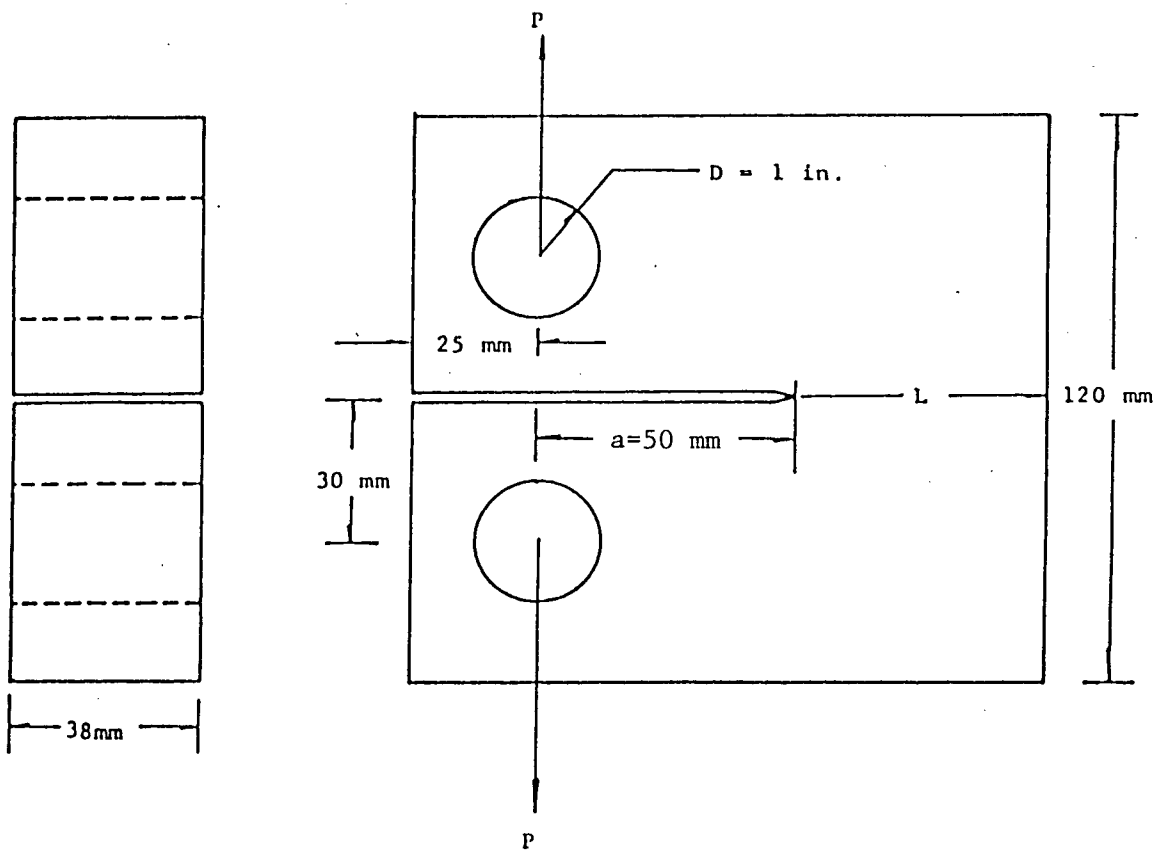

Figure 26 Specimen Configuration of the Crack-front Length Specimen.

Table 4

Effect of crack-front length on K_{IC} for compact tension specimens of white spruce

Board No.	Length L, mm	Sample size	Average M.C. %	Average S.G.	Average K_{IC}, MPa$\sqrt{m}$	C.V. %
A	75	2	8.43	0.413	0.2304	2.24
	100	1	8.49	0.420	0.2275	0.00
	125	2	8.68	0.414	0.2222	9.36
B	50	2	8.81	0.412	0.2817	4.63
	75	2	9.36	0.419	0.2918	5.28
	100	1	8.96	0.410	0.2762	0.00
	125	1	8.96	0.408	0.2569	0.00
C	50	2	9.69	0.335	0.2076	3.86
	75	1	9.68	0.334	0.1894	0.00
	100	2	9.75	0.322	0.2193	7.41
	125	1	9.54	0.342	0.1805	0.00
D	50	1	8.99	0.416	0.2640	0.00
	100	1	8.98	0.413	0.2518	0.00
	125	1	8.93	0.405	0.3145	0.00

also shown and the results are plotted in Figure 27. The results do not seem too helpful as it is not obvious any trend exists for all cases except for board A, for which the values of K_{IC} decrease as the length increases. The lack of consistent trends can be attributed to the limited number of specimens tested. However, comparing the average fracture toughness between the CTSs and the DCB specimens, surprisingly, the DCB specimens gave fracture toughness values twice as great as the CTSs. This may have different causes. Firstly, the CTSs were prepared from many different boards which implies a higher degree of variability, whereas the DCB specimens were prepared from only three boards. This can be observed by examining the coefficient of variations for both cases, as shown in Fig. 21 and 22.

The difference of the fracture toughness between CTSs and DCB specimens may also be explained by the stress-state condition in the specimens. As mentioned before, the fracture initiation constant, K_{IC} , is thickness dependent. The amount of material which yields at the crack tip must also be small. To ensure this, specimens must be of sufficient thickness so that a triaxial state of stress can exist at the flaw tip. It is postulated that K_{IC} decreases as the crack-front width increases. The lower limit occurs as the width approaches infinity and it is called the plane strain fracture toughness. The K_{IC} at this point is considered to be a geometric invariant material property. The size requirements recommended by Liu (1983) for this SSY

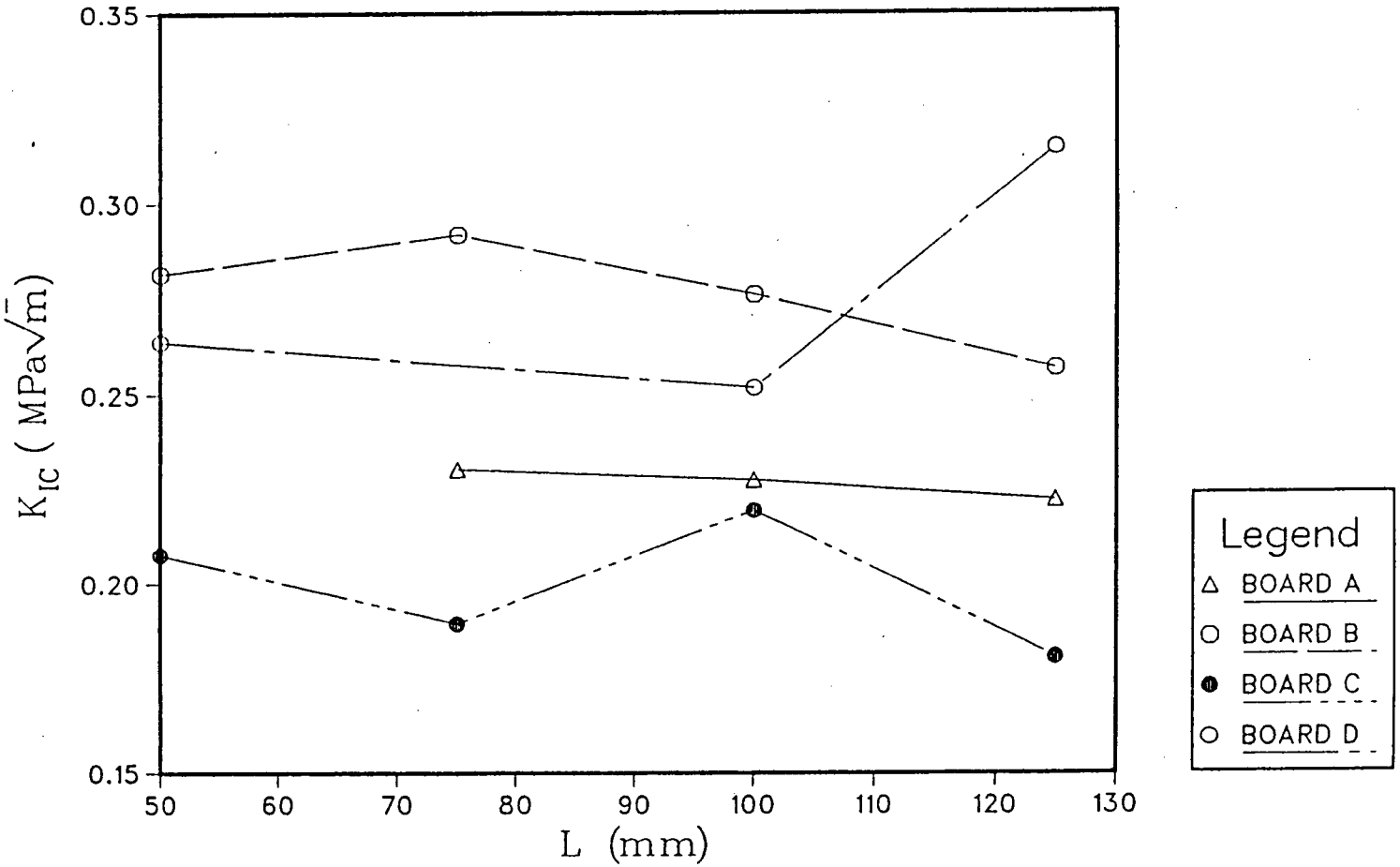

Figure 27 Effect of Crack-front Length on Mode I Fracture Toughness

and plane strain condition are :

$$\frac{t}{(\frac{a}{L})} > 2.5\ (\frac{K_{IC}}{\sigma_y})^2 \qquad (4.6a)$$

or

$$\frac{0.4t}{(\frac{a}{L})}\ (\frac{\sigma_y}{K_{IC}})^2 > 1 \qquad (4.6b)$$

where t is the specimen thickness, m; a,l are defined in Fig. 26.

This means that if the left-hand term is less that one, then a plane stress condition will exist; otherwise, the plane strain condition will result in a decline in K_{IC} .

Table 5 shows the data for the cases of CTSs and DCB specimens, the left-hand term for the CTSs is larger than the value for the DCB specimens. This indicates that the DCB specimens have a condition closer to the plane stress condition which implies a higher value of K_{IC} , which agrees with the results obtained. Further analysis of this difference is included in Appendix II.

4.5 EXPERIMENT NO.4 MOISTURE CONTENT EFFECT

4.5.1 EXPERIMENT DESIGN AND PROCEDURE

This experiment uses K_{IC} to examine the variation of fracture toughness in white spruce with the practically

Table 5

The size coefficient for CTSs and DCB specimens

Specimen type	Sample size	a mm	L mm	t mm	$t/\frac{a}{L}$ m	σ_Y MPa	$2.5(\frac{K_{IC}^2}{\sigma_Y})$	$\frac{0.4t}{\frac{a}{L}}(\frac{\sigma_Y^2}{K_{IC}})$
CTS	33	50	50	38	0.038	2.80	0.01288	2.9503
DCB	17	250	700	38	0.1064	2.80	0.04800	2.2164

important parameter -- moisture content.

Thirty-two compact tension specimens were prepared; most of them were in the TL system of crack propagation. The specimens were randomly divided into two groups and each group was conditioned in two different environments. Sixteen were placed in a dry air oven at 105°C to reduce the moisture content to zero; the remainder were conditioned in a humidity room to achieve a moisture content of 6%. When combined with the results from the 9% M.C. CTS of Experiment No.1, the three sets of specimens allows evaluation of K_{IC} at different moisture content. Specimen size and experimental procedures were exactly the same as Experiment No.1. The tests were conducted in the same humidity room.

4.5.2 RESULTS

Table 6 summarized the results from each set of experiments and a plot is given in Figure 28. As can be seen in the figure, the ovendried specimens failed at lower loads than the wet. The results indicate that the effect of moisture content on K_{IC} shows a decrease as the moisture content decreases from 9% to 0%. The average values for the kiln-dried condition,with moisture content approximately 9%, is 0.2051 MPa$\sqrt{m}$, and an average value of 0.1752 MPa$\sqrt{m}$ for the oven-dried specimens. This shows a decrease of 15% which is consistent with the results of the Newsletter of Technical Research Centre of Finland (1986) for spruce. According to the results obtained by P.D.Ewing (1979), the

Table 6

Effect of moisture content on K_{IC} for CTS in longitudinal propagation

Moisture content %	Sample size	Average K_{IC} MPa$\sqrt{m}$	C.V. %	Specific gravity
0.00	16	0.1752	21.46	0.383
6.34	16	0.1957	17.32	0.347
9.10	33	0.2051	24.67	0.380

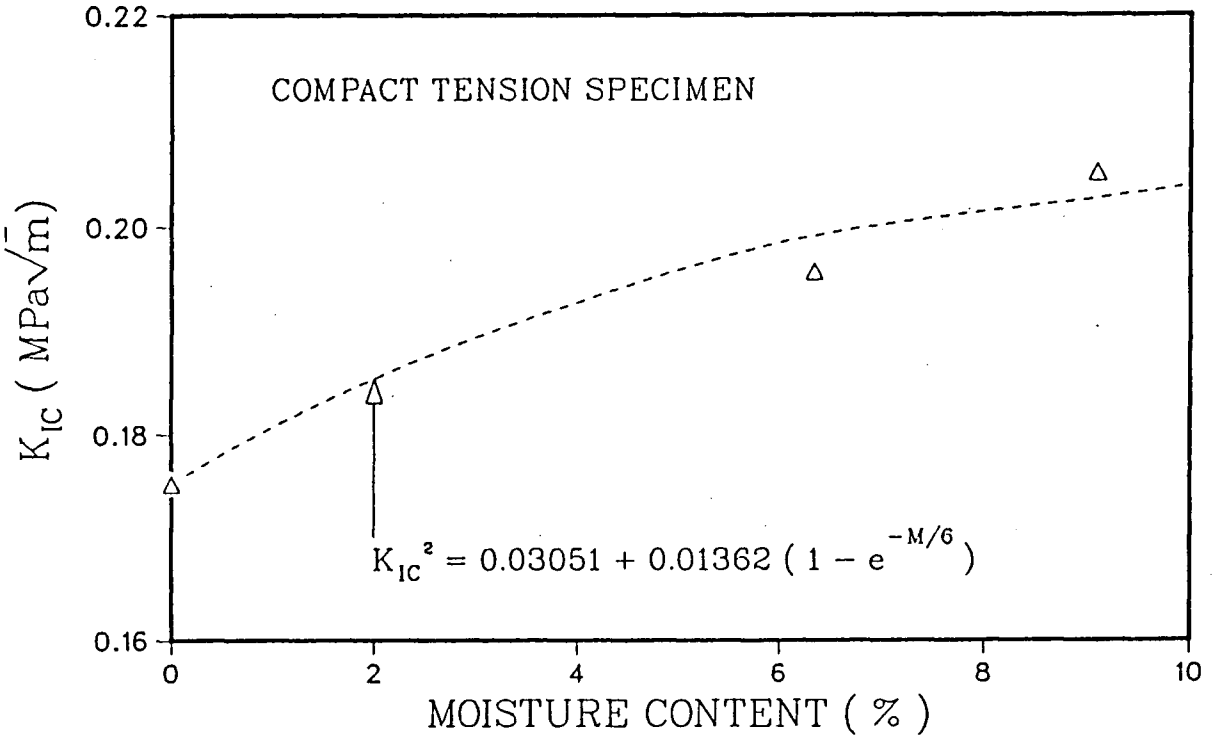

Figure 28 Effect of Moisture Content on Mode I Fracture Toughness

effect of moisture content on K_{IC} generally shows an increase as the moisture content decreases from 20% to a maximum at around 10% and then the K_{IC} values tend to decrease. This agrees with the results obtained from Experiment No. 4.

An exponential curve was fitted to the data points using the least-squares technique and the following relationship is obtained for M≤10 % :

$$K_{IC}^2 = 0.0305144 + 0.013619\ (1 - e^{-M/6}) \qquad (4.7)$$

$$R^2 = 0.9688$$

where

K_{IC} is the mode I fracture toughness, MPa$\sqrt{m}$;

M is the moisture content, %.

This equation shows good agreement with the experimental data points, as shown in Figure 28. However, this equation shows a limitation in that the fracture toughness will increase as long as the moisture content increases. According to Ewing's theory, this equation should only be valid in the range between 0% and 10%.

4.6 EXPERIMENT NO.5, MODE II FRACTURE TOUGHNESS

4.6.1 EXPERIMENT DESIGN AND PROCEDURE

Although mode I is usually dominant in crack propagation, for certain loading situations mode II can also

be of significance. In order to generate the interaction curve between mode I and mode II at failure; or to study the wood structure under the mode II failure condition, mode II fracture toughness values are required.

The end-split beam specimen suggested by Barrett. and Foschi (1977) was adopted here to study the mode II fracture toughness. The test method is shown in Figure 29 and the mesh for the finite element program is shown in Figure 30.

During the experiments, the relative displacement of the crack surfaces at points A and B shown in Figure 31 was recorded by a modified LVDT and plotted against the applied loads. Friction induced by the crack closure was avoided by placing a smooth plastic plate between the sawn notch as shown in Figure 29. Twenty-four specimens were prepared and the bandsawn notches were extended by a steel knife crack starter just before the testing. The specimens were tested in the Satec Testing Machine under room temperature and the crack orientation was recorded for each specimen. The experimental setup is shown in Figure 32.

4.6.2 RESULTS

A typical load versus crack displacement curve is also shown in Figure 31 which indicates some slow crack growth prior to the crack starting to propagate. The failure load were determined using the 5% offset line as suggested in ASTM Standard E399. The experiment results also indicated a dependence of mode II fracture toughness on the crack

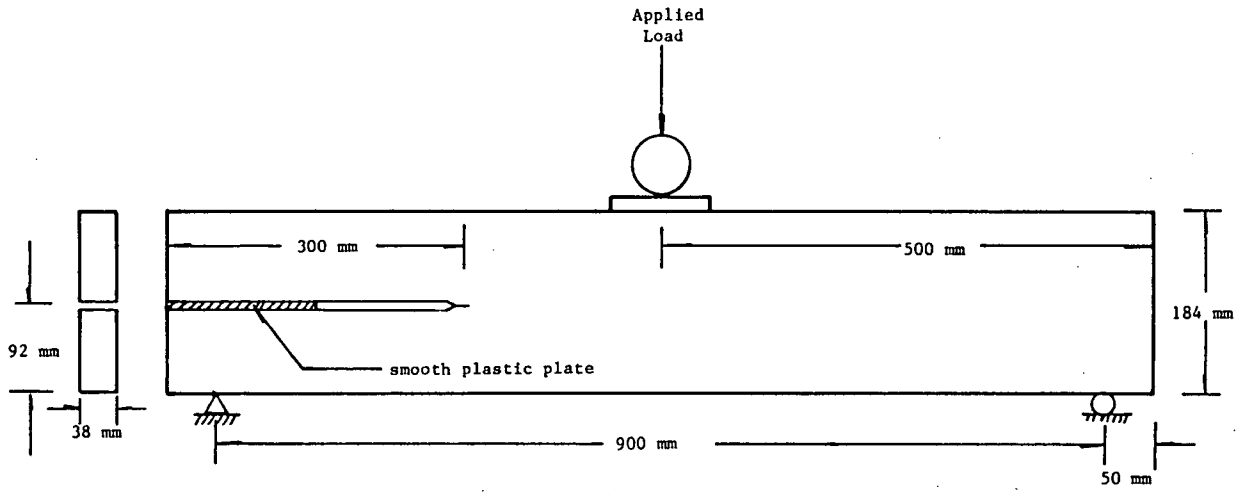

Figure 29 Experiment Setup of the Mode II Fracture Toughness Specimen.

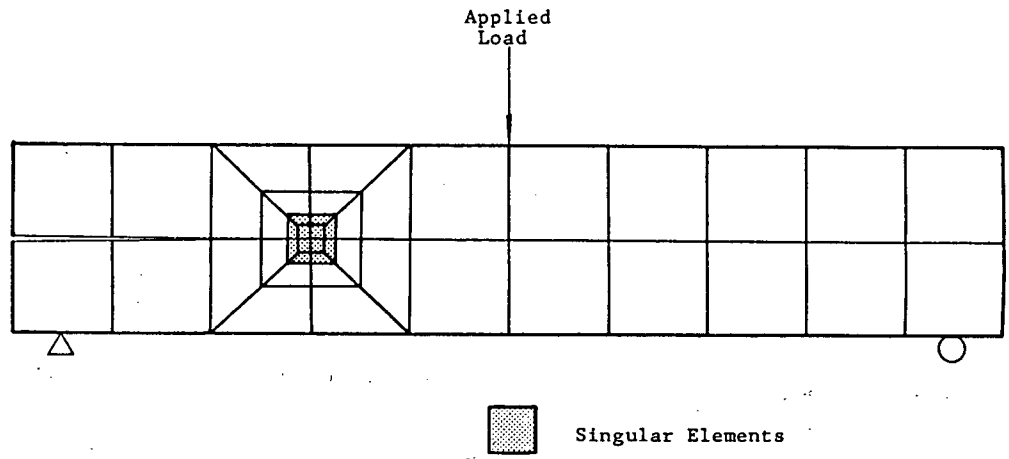

Figure 30 Finite Element Mesh for the Mode II Fracture Toughness Specimen.

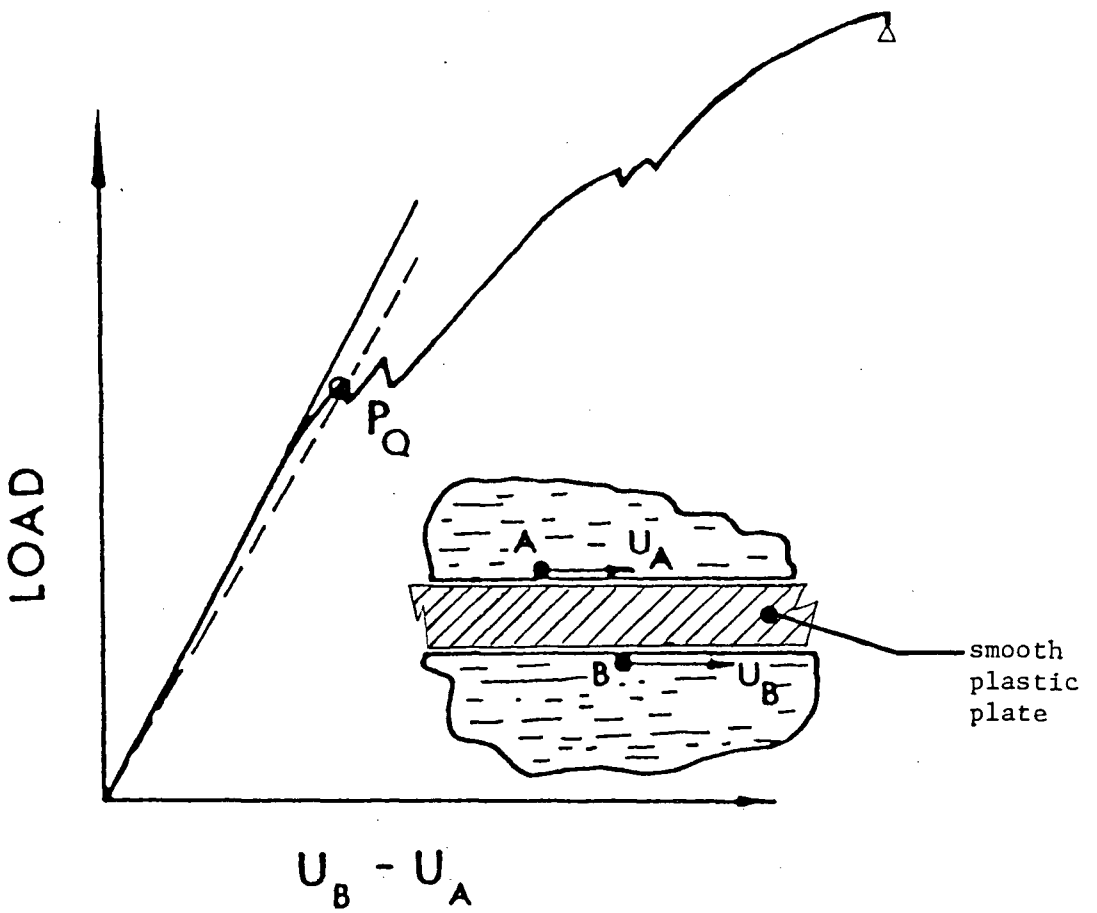

Figure 31 Applied Load versus Longitudinal Displacement.

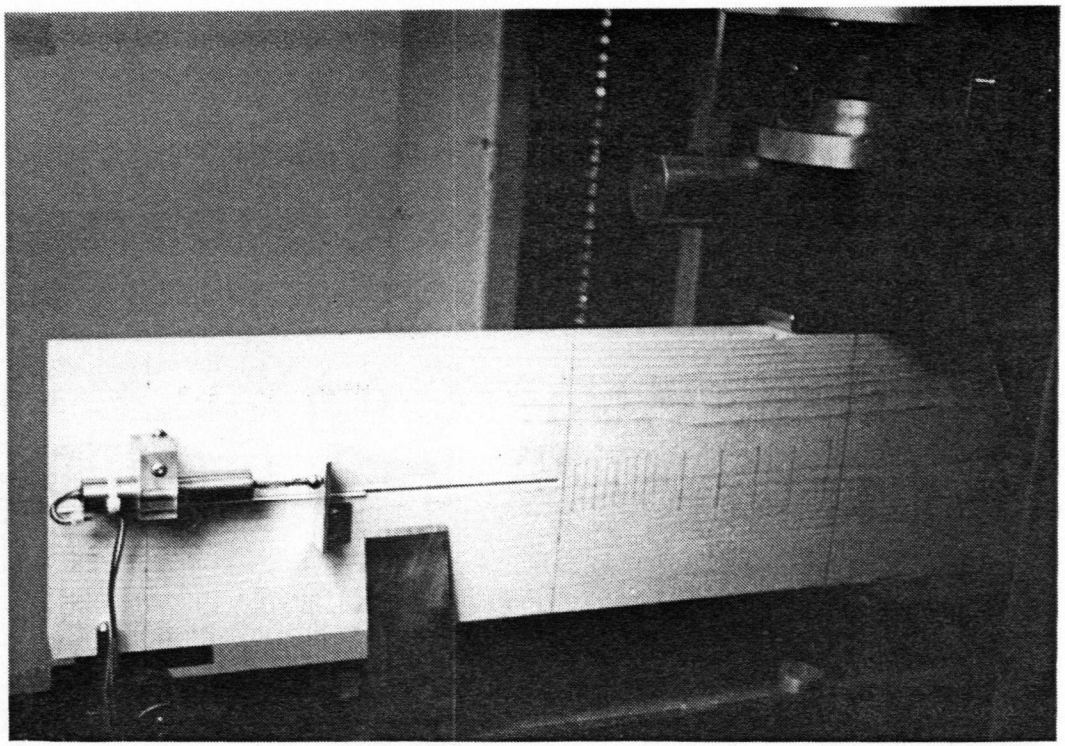

Figure 32 The apparatus and the experimental setup of the mode II fracture toughness test specimen.

orientation as shown in Table 7.

The K_{IIC} values were plotted against the annual rings angle, θ in Fig 33. The best-fitted polynomial curve calculated by the least-squares method is also shown in the figure, and the following relationship was derived :

$$K_{IIC} = 1.8798 + 2.5114 \times 10^{-2}\theta - 2.4828 \times 10^{-4}\theta^2 \qquad (4.8)$$

where

K_{IIC} is the mode II fracture toughness, MPa$\sqrt{m}$;

θ is the annual rings angle, degree.

The curve shows a maximum at a rings angle of 50 degrees which indicates a mode of cross-grain plane failure. This is reasonable as the cross-grain failure always require a higher failure load. The average mode II fracture toughness values obtained for white spruce were 2.16 MPa$\sqrt{m}$ and 2.05 MPa$\sqrt{m}$ for the TL and RL systems respectively. These values are comparable with the results obtained by Barrett (1981) for white spruce -- K_{IIC} for the TL mode is 1.89 MPa$\sqrt{m}$ which is in the same order of magnitude.

Figure 34 shows the cumulative distribution funmction for K_{IIC} based only on all the specimens tested in the TL system. The coefficient of varience is 16% with the fifth percentile being 1.925. MPa$\sqrt{m}$.

Table 7

Effect of the annual rings angle on K_{IIC}

Specimen type	Angle to RL degree	Sample size	M.C. %	S.G.	K_{IIC} MPa$\sqrt{m}$	K_{IIC} psi$\sqrt{in}$
End-split Beam	0 - 10	2	13.38	0.384	2.0180	1836.33
	11 - 20	2	13.75	0.369	2.1000	1911.00
	21 - 30	0	-	-	-	-
	31 - 40	3	12.83	0.410	2.2597	2056.30
	41 - 50	4	13.13	0.418	2.6935	2451.09
	51 - 60	2	13.78	0.371	2.3942	2178.72
	61 - 70	1	14.50	0.423	3.0098	2738.90
	71 - 80	1	12.75	0.324	1.9359	1761.70
	81 - 90	8	12.91	0.345	2.1561	1962.01

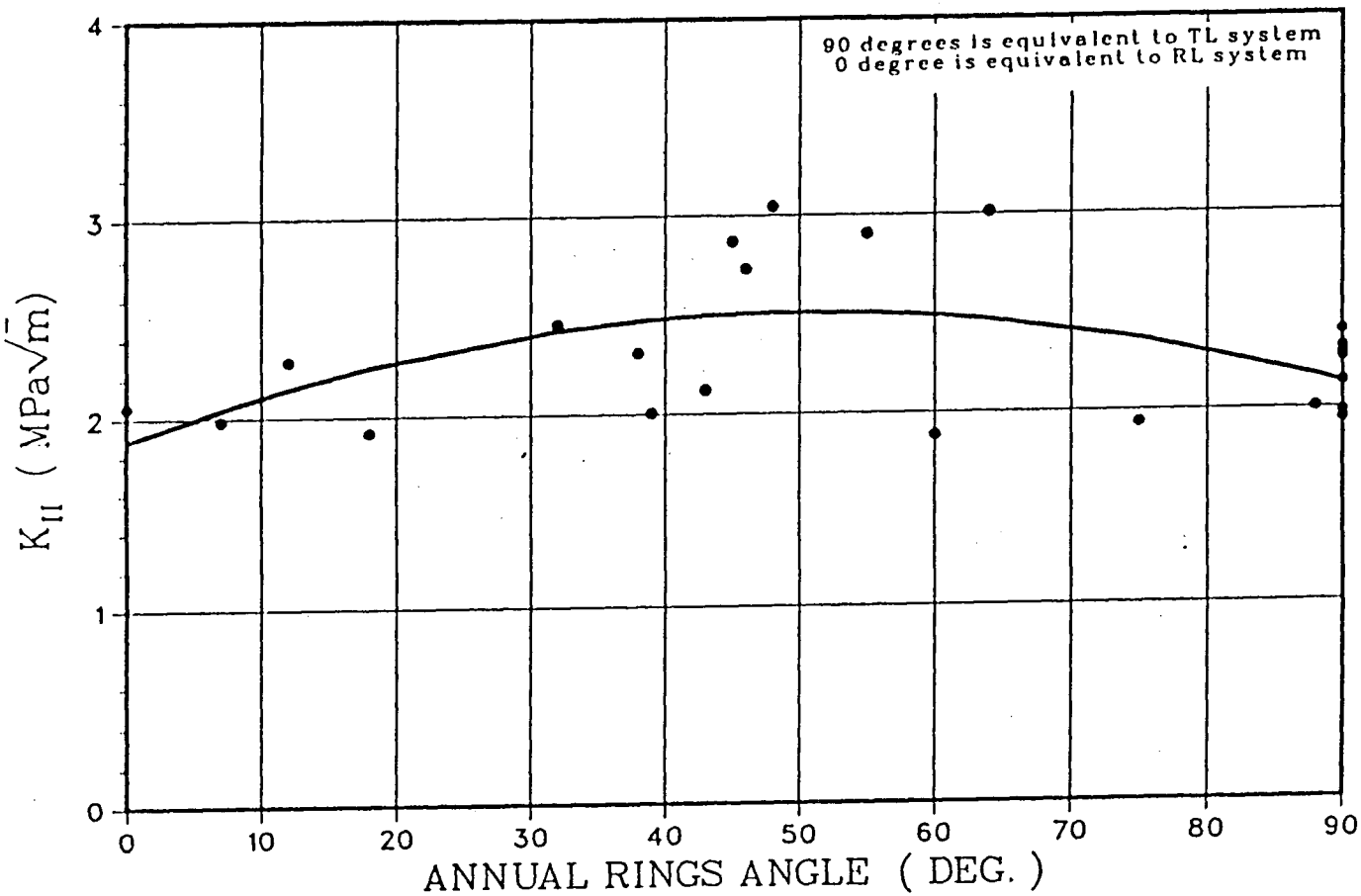

Figure 33 Mode II Fracture Toughness Variation with Annual Rings Angle

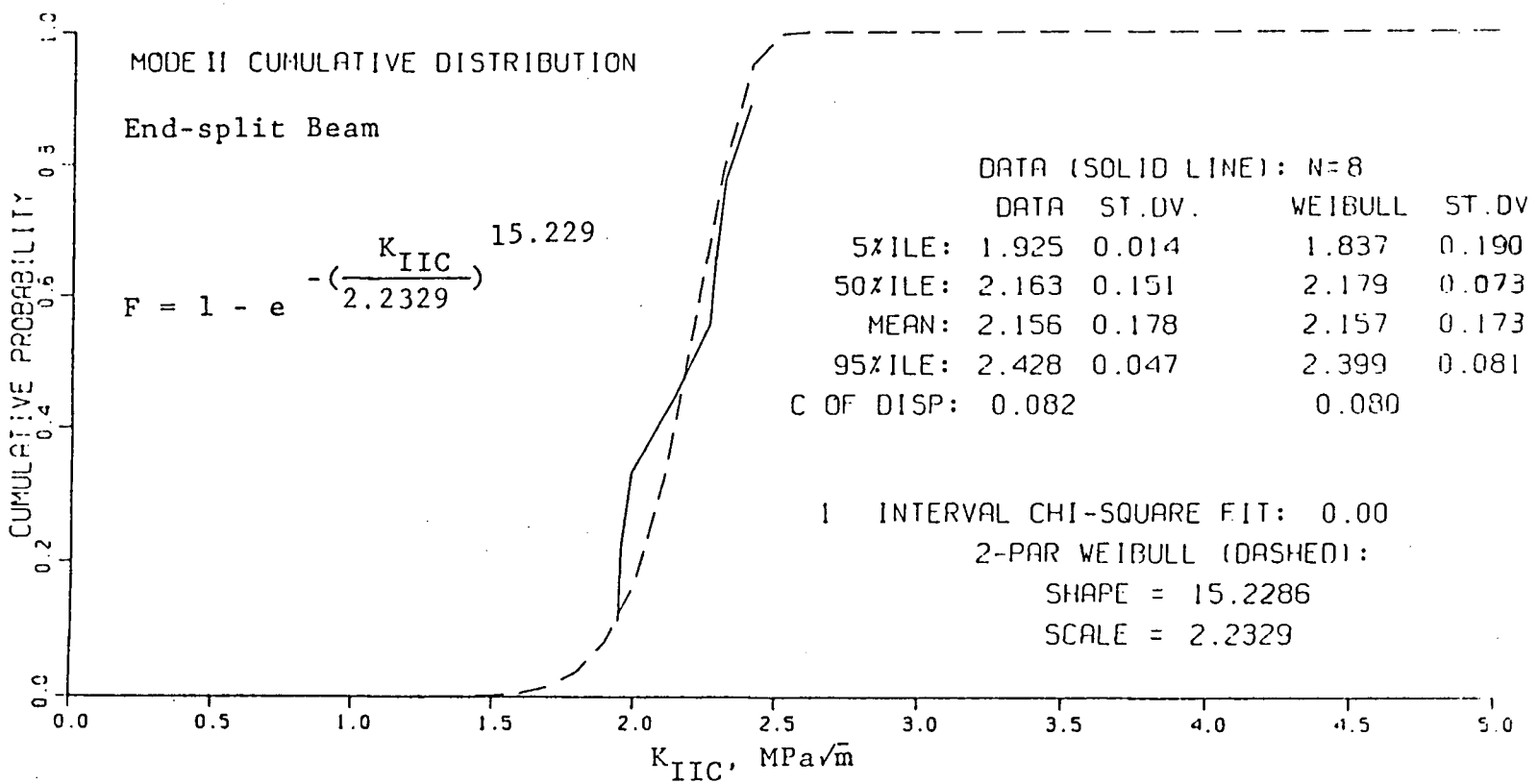

Figure 34 Cumulative Distribution Curve of the End-split Beam Specimens.

4.7 EXPERIMENT NO.6, MIXED MODE MID-CRACKED BEAMS

4.7.1 EXPERIMENT DESIGN AND PROCEDURE

Since wood structural members are often subjected to complex loading conditions that result in mixed mode fracture, a failure criterion should be expressed in terms of combinations or interations of the mode I and mode II failure modes.

Experiment No.6 was designed to investigate the fracture strength of mid-cracked beams under the mixed mode loading condition. Difficulties were encountered in designing the specimen geometry in order to produce the desired ratio of K_I to K_{II} . This had to be done by trial and error, and finally the 45 degrees and the 90 degrees mid-cracked beams were adopted for testing.

This investigation had two principal phases. In the first phase, the 45 degrees mid-cracked beams were loaded at the centerpoint as well as at a distance of 200 mm from the support as shown in Figure 35. Twenty-four specimens were cut and prepared for each case with mostly in the TL system of crack propagation.

The second phase consists of the 90 degrees mid-cracked beams loaded at the centerpoint as shown in Figure 36. Sixteen specimens were prepared for the TL propagation and the tests were performed in the Satec Testing Machine at room temperature.

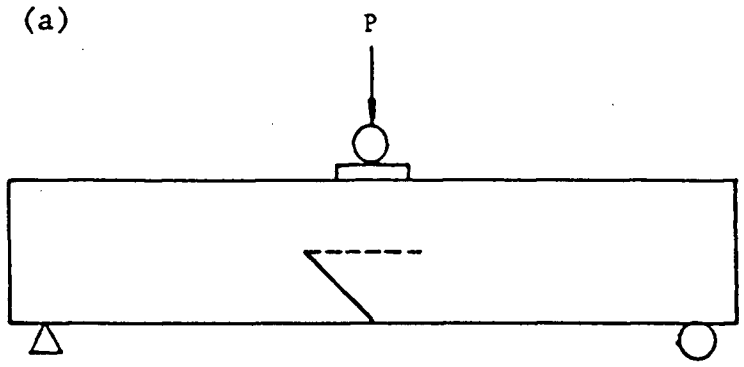

Type A

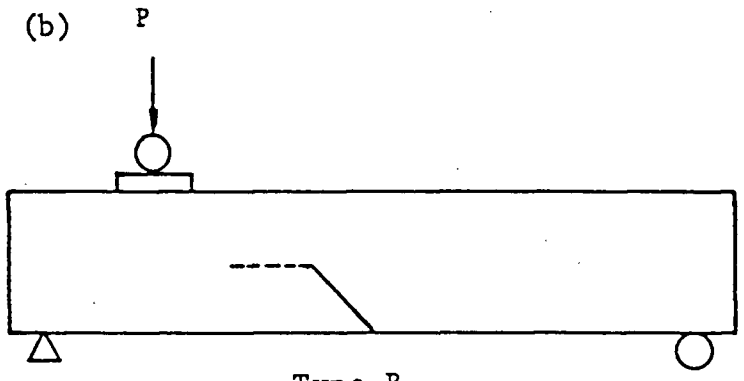

Type B

Figure 35 Specimen Configuration of the 45 deg. Beam
(a) Loading at the centerpoint.
(b) Loading at 200mm from the left support.

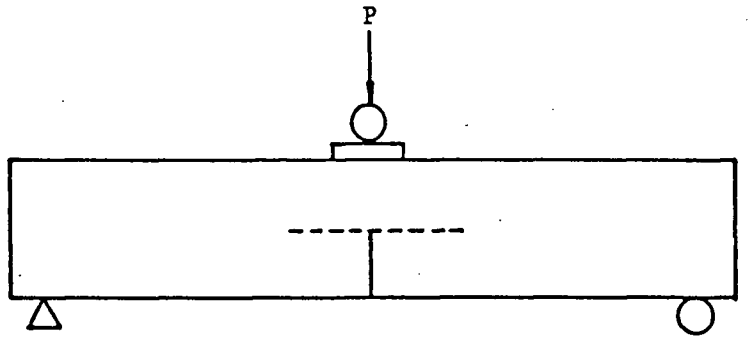

Type C

Figure 36 Specimen Configuration of the 90 deg. Beam

Prior to testing, the band-sawn notches were also sharpened with the crack starter in the direction of the sawn crack. In fact, the cracks propagated along the grain at maximum load.

The K_I and K_{II} values corresponding to a load of 100 N were calculated with the program NOTCH using the finite elements meshes shown in Figure 37. The predicted direction of propagation was determined by comparing the K_I and K_{II} values for both directions from the computer output. A higher value of K_I and K_{II} indicates a lower failure load during the testing. The predicted failure direction is also shown in Figure 35 and Figure 36.

Because of the difficulties of measuring the COD values in the experiments or the opening at the lowest midpoint of the initial crack, the mid-span deflections were measured instead.

4.7.2 RESULTS

Table 8 summarizes the results for each phase of experiment with the average K_{IC} , K_{IIC} values shown as well. As can be seen from Figures 35, 36 and Table 8, there are two potential directions of propagation for the 90 degrees mid-cracked beams. Since cracks started at the weaker direction of the two, it implies a double chance of failure. The experimental curves were corrected based on the following formulae :

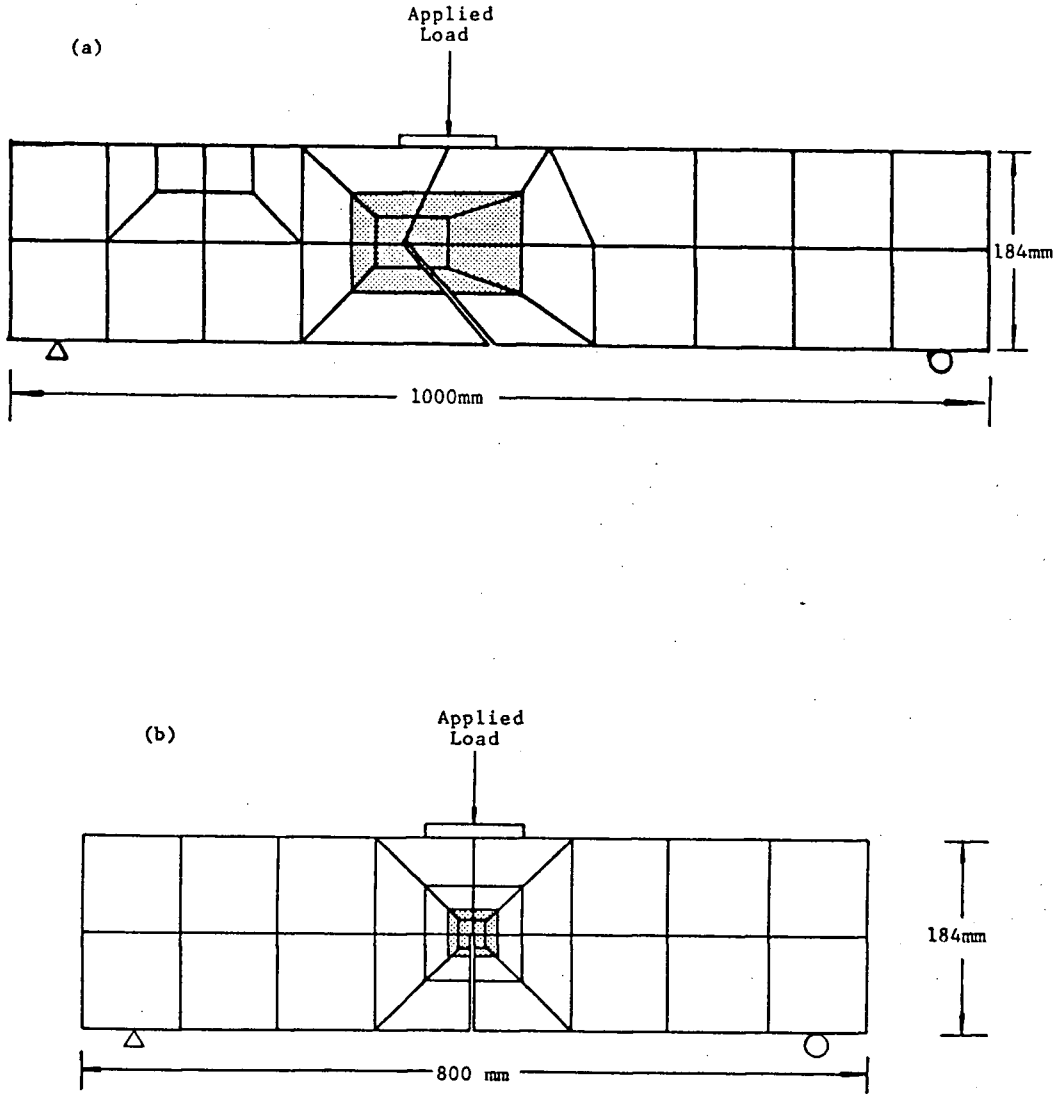

Figure 37 Finite Element Mesh for the Mid-cracked Beam Specimen.
(a) 45 degrees Mid-cracked Beam.
(b) 90 degrees Mid-cracked Beam.

Table 8

Results of the mid-cracked beam specimens

Specimen type	Sample size	Average K_{IC} MPa$\sqrt{m}$	Average K_{IIC} MPa$\sqrt{m}$	C.V. %	Predicted prop. direction	$\frac{K_I}{K_{IC}}$ Mean	C.V. %	$\frac{K_{II}}{K_{IIC}}$ Mean	C.V. %	R* %
Type A	20	0.3013	0.7470	19.0	0	0.7765	9.0	0.3433	12.5	100
Type B	18	0.3539	0.5183	18.7	180	0.9073	6.4	0.2341	14.9	100
Type C	16	0.3084	0.6571	17.4	0 , 180	0.8496	3.8	0.3160	10.7	100

* - R is the percentage of the specimens failed in the predicted direction.

$$F_E = 1 - [1 - F_c]^2 \tag{4.9}$$

$$F_c = 1 - \sqrt{1 - F_E} \tag{4.10}$$

where

F_E is the experimental cumulative probability.

F_C is the corrected cumulative probability.

These cumulative distribution curves are shown in Figure 38 and Figure 39 together with the best-fitted Weibull curves and equations. It can be seen that the curves are rotated to the right i.e., higher values of K_{IC} and K_{IIC} correspond to the same percentile.

For the mode I stress intensity factors of the 90 degrees beams, the K_{IC} has a mean value of 0.3084 MPa$\sqrt{m}$ for the experimental cumulative distribution and a value of 0.3556 MPa$\sqrt{m}$ for the corrected cumulative distribution.

In order to determine the normalized interaction curve between mode I and mode II fracture toughness, the K_I and K_{II} values for mixed mode failure are normalized by the critical mode I and mode II stress intensity factors respectively. If we just divide the K_I and K_{II} values by the average K_{IC} and K_{IIC} respectively, we are comparing the values at different percentiles. One method to tackle this problem is to normalize the K_I and K_{II} values at failure by the K_{IC} and K_{IIC} values which correspond to the same percentile.

This method is shown diagramatically in Figure 40. The solid curve and the dashed curve correspond to the pure mode

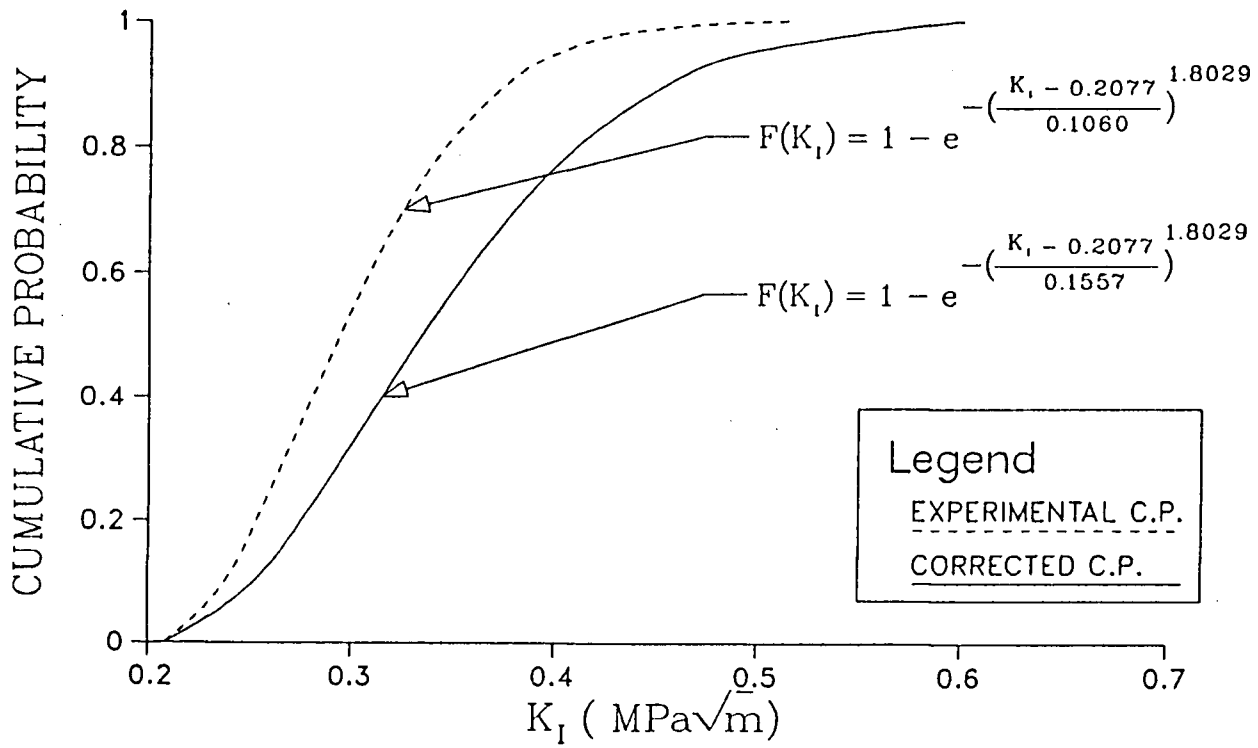

Figure 38 Experimental and Corrected Cumulative Probability Curves of the Mode I Fracture Toughness for the 90 degrees beam.

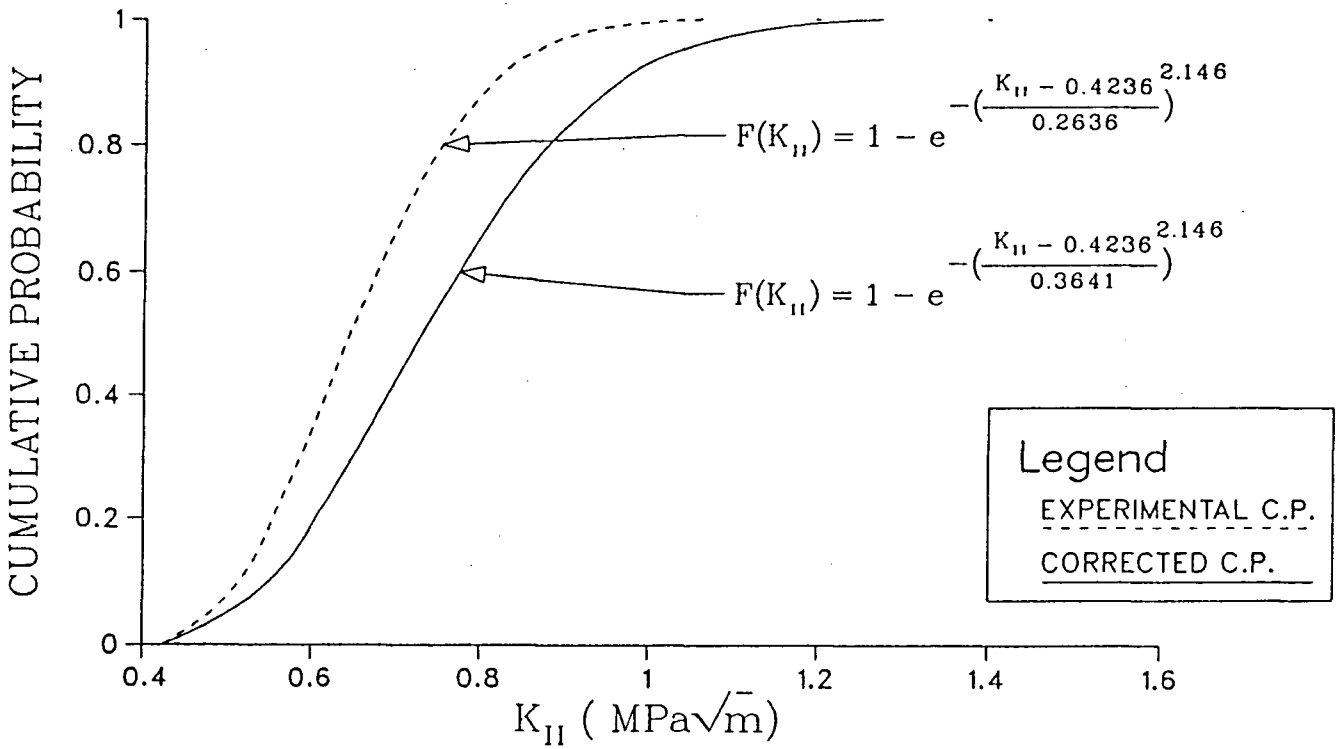

Figure 39 Experimental and Corrected Cumulative Probability Curves of the Mode II Fracture Toughness for the 90 degrees beam.

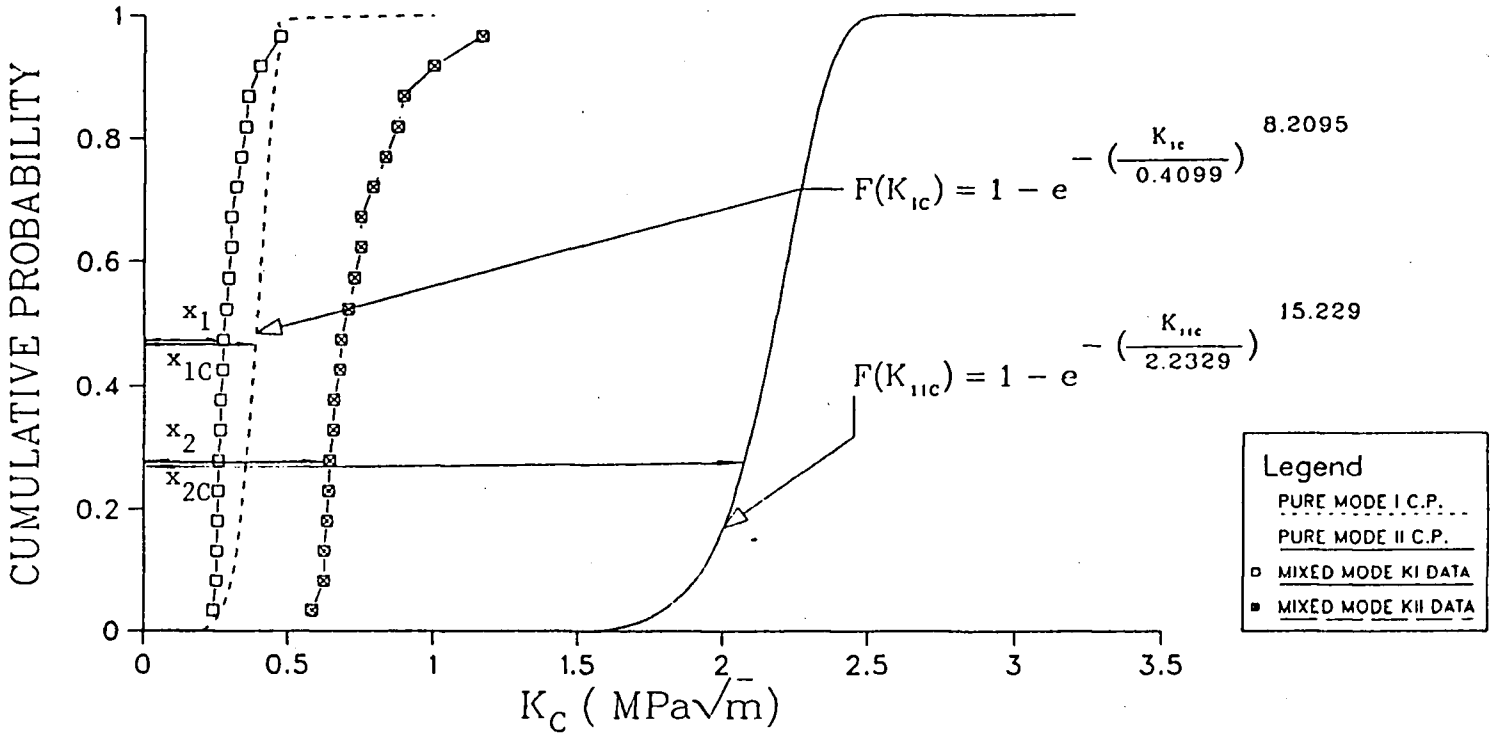

Figure 40 Method of Normalizing the Cumulative Probability Curves for the 45 degrees mid-cracked beam.

I and mode II fracture toughness Weibull curves respectively. Each data point is divided by the K_C value which refers to the same level of cumulative probability. Refering to Figure 40, we have :

$$\frac{K_I}{K_{IC}} = \frac{x_1}{x_{1c}} \qquad \frac{K_{II}}{K_{IIC}} = \frac{x_2}{x_{2c}} \tag{4.11}$$

where

K_I is the mode I stress intensity factor at failure.

K_{II} is the mode II stress intensity factor at failure.

K_{IC} is the pure mode I fracture toughness.

K_{IIC} is the pure mode II fracture toughness.

x_1, x_{1C}, x_2, x_{2C} are as shown in the figure.

Both the 45 degree and the 90 degree mid-cracked beam data points are treated by this method. For the 90 degrees beams data, the corrected cumulative distribution functions were used to calculate the required ratios.

The average values for the K_I / K_{IC} and K_{II} / K_{IIC} for this experiment are listed in Table 8 and are plotted in Figure 41.

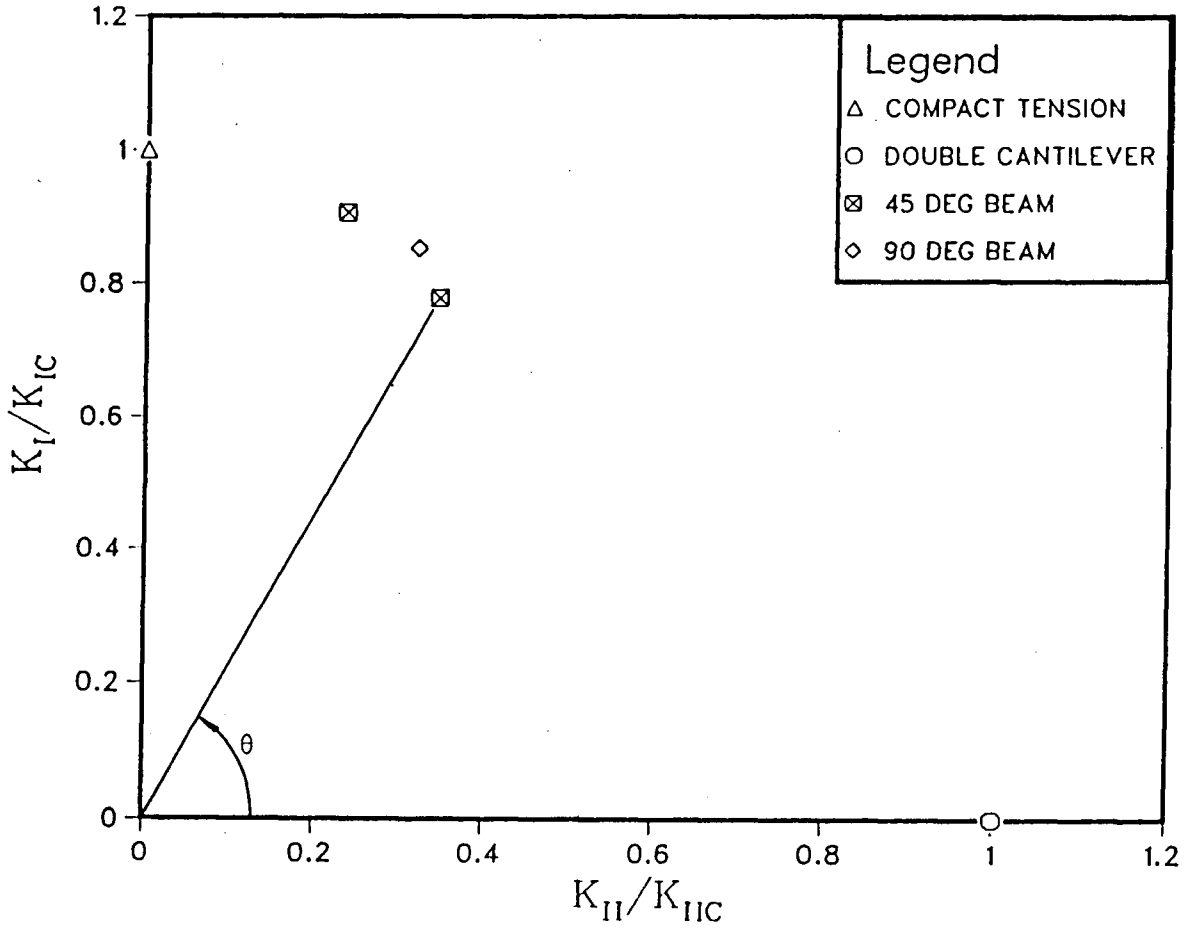

Figure 41 K_I-K_{II} Interaction Diagram based on the Mid-cracked Beams Result.

4.8 EXPERIMENT NO.7, DCB UNDER MIXED-MODE LOADING

4.8.1 EXPERIMENT DESIGN AND PROCEDURE

Experiment no.7 served the purpose of generating more points on the interaction curve and to check the consistency of the interaction curve for describing the mixed mode fracture failure for different geometries.

The main difficulty in generating a interaction curve occurs because of the limited range of K_I / K_{II} (or $(K_I / K_{IC})/(K_{II} / K_{IIC})$) in the specimen design. It was found that for most beam geometries, the mode I stress intensity factor often dominates the fracture failure. This is equivalent to the failure points on the upper region of the interaction curve or a high value of θ as shown in Figure 41.

The practical difficulty was overcome by applying two separate loads on the DCB specimens which could be controlled to produce different mode I and mode II stress fields around the crack tip. This is the same as superimposing the mode I and mode II DCB loading as shown in Figure 16 and 29. Although the two stress modes are not absolutely independent with respect to the two loads, it is possible to control the ratio of K_I to K_{II} at fracture. The test method is shown in Figure 42. The midspan load was produced by the Satec Testing Machine while the end-support load was achieved by a hydraulic jack with a calibrated load cell. The experimental setup is shown in Figure 43.

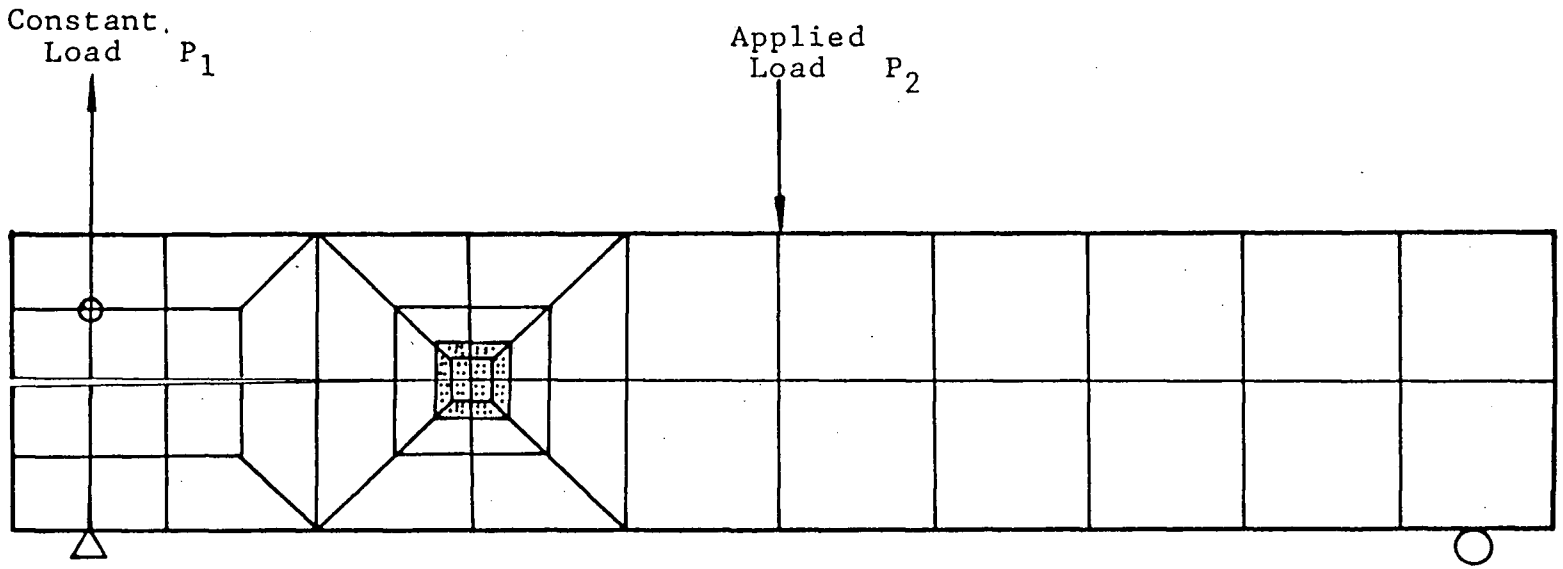

Figure 42 Specimen Configuration of the Two-loads Beam Specimen.

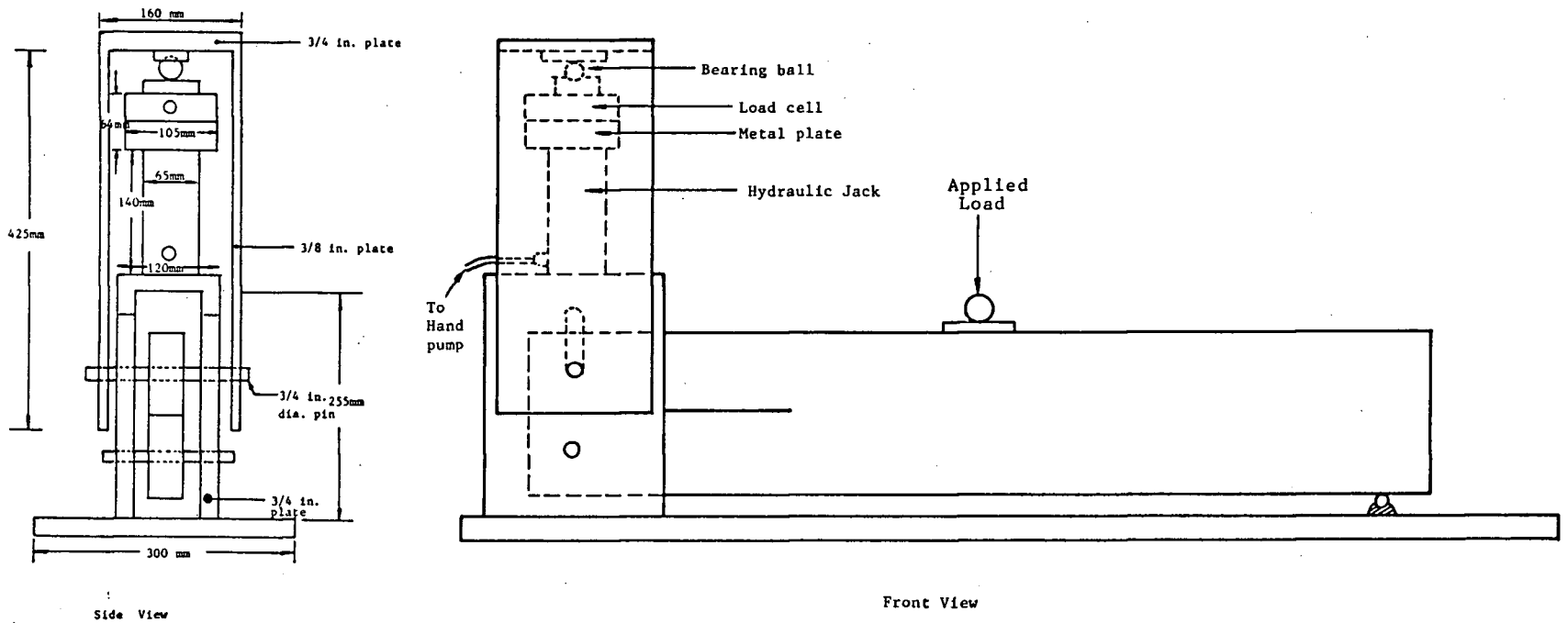

Figure 43 Experiment Setup of the Two-loads Beam Specimen.

The relationship between the stress intensity factors and the applied loads are :

$$K_I = 4.0488 \times 10^{-4} P_1 - 9.894 \times 10^{-5} P_2 \qquad (4.12a)$$

$$K_{II} = -1.5060 \times 10^{-4} P_2 \qquad (4.12b)$$

Using the results from before for the TL system :

$$K_{IC} = 0.388 \text{ MPa}\sqrt{\text{m}} \qquad K_{IIC} = 2.13 \text{ MPa}\sqrt{\text{m}}$$

For pure mode I fracture : (P_2=0)

$$P_1 = \frac{0.388}{4.0488 \times 10^{-4}} = 958.3 \text{ N}$$

For pure mode II fracture : (P_1=0)

$$P_2 = \frac{2.13}{1.5060 \times 10^{-4}} = 14143.5 \text{ N}$$

Introducing the condition $K_I \geq 0$ i.e., that the crack does not close, from Equation (4.12a) we have :

$$4.0488 \times 10^{-4} P_1 - 9.894 \times 10^{-5} P_2 = 0$$

or

$$P_2 < 4.1\ P_1 \tag{4.13}$$

Assuming the interaction curve to be :

Case I :

$$\left(\frac{K_I}{K_{IC}}\right) + \left(\frac{K_{II}}{K_{IIC}}\right)^2 = 1$$

$$\text{Let} \quad r = \frac{K_I/K_{IC}}{K_{II}/K_{IIC}} = \tan\theta$$

we have,

$$P_1 = (\sqrt{r^2+4} - r)[1234.93r\ K_{IC} + 811.29\ K_{IIC}] \tag{4.14a}$$

$$P_2 = 3320.062\ (\sqrt{r^2+4} - r)[K_{IIC}] \tag{4.14b}$$

Case II :

$$\left(\frac{K_I}{K_{IC}}\right)^2 + \left(\frac{K_{II}}{K_{IIC}}\right)^2 = 1$$

we have,

$$P_1 = 1/\sqrt{1+r^2}\ \ [2469.9\ K_{IC} \cdot r + 1622.6\ K_{IIC}] \tag{4.15a}$$

$$P_2 = 6640.12\ \frac{K_{IIC}}{\sqrt{1+r^2}} \tag{4.15b}$$

Since case I is more conservative than case II, in designing the fracture criterion, case I is adopted.

The interaction failure envelope for the P_1-P_2 mixed mode loading is shown in Figure 44. Outside the curve is the failure region, where as inside, the specimen is intact.

To obtain the desired ratio of fracture toughness, the following procedure was followed :

1. A ratio r was selected.
2. From equations (4.14a) and (4.14b), failure loads P_1 and P_2 were obtained.
3. The corresponding K_I and K_{II} values from equations (4.12a) and (4.12b) were calculated.
4. From Figure 44, a loading path was designed within the safe region to achieve the P_1 and P_2 calculated.

Experiment no.7 was carried out in determining the K_I and K_{II} value at failure for two different ratios as shown in Figure 44 together with the loading path.

Ten specimens were prepared and tested for each case under room temperature with the dominant system of crack propagation being TL. The applied mid-span load and the COD were recorded by a X-Y plotter.

4.8.2 RESULTS

The experiment results are summarized in Table 9 and Figure 44, with the failure load shown as well. This gives the ratio of K_I to K_{II} values of 0.64 and 0.229, with corresponding θ values of 74° and 52°. These values were

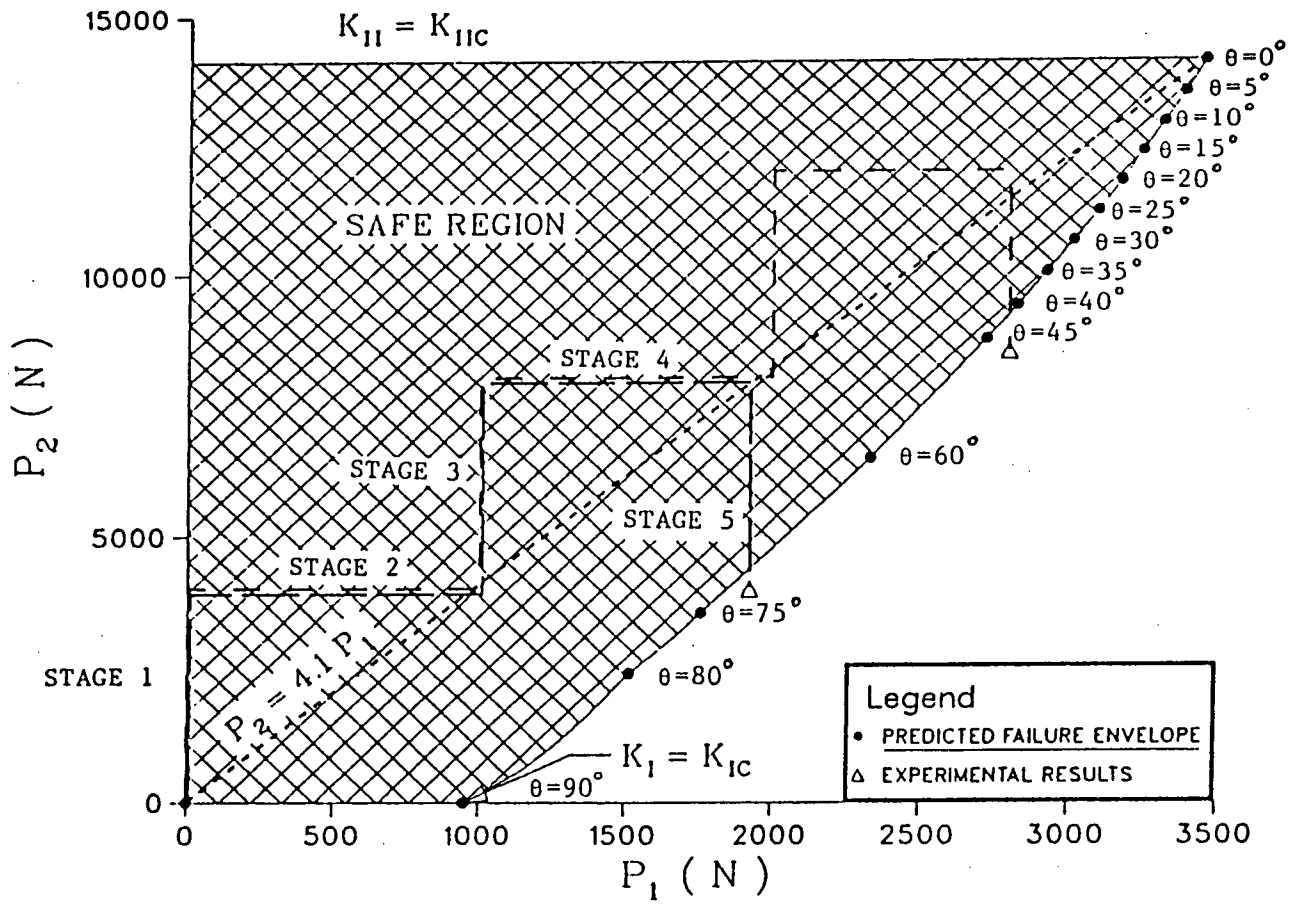

Figure 44 Failure Envelope of the Two-loads Beam Specimen.

Table 9

Results of the two-loads beam tests

Specimen type	Sample size	P_1 N	P_2 N	Average K_I MPa$\sqrt{m}$	C.V. %	Average K_{II} MPa$\sqrt{m}$	C.V. %	$\frac{K_I}{K_{IC}}$	C.V. %	$\frac{K_{II}}{K_{IIC}}$	C.V. %	Average r
5-steps	10	1925.0	3985.4	0.3851	9.6	0.6002	9.6	0.998	5.3	0.282	9.3	3.525
9-steps	9	2800.0	8488.3	0.2938	16.7	1.2783	16.7	0.754	5.4	0.600	5.9	1.260

used to generate the interaction curve later.

Theoretically, it is possible to attain any stress intensity factors ratio even for θ close to zero, however, in practice it may require the specimen loaded close to the mode II fracture toughness, which may cause the specimen failed in mode II instead of the mixed mode condition wanted.

The onset of the crack propagation were determined by a change of the slope of the load verses COD curve in the final phase as shown in Figure 45. Some slow crack growth was observed during the tests. A 5% offset method is used here to determine the failure load.

4.9 EXPERIMENT NO.8, NOTCHED BEAM SPECIMENS

4.9.1 EXPERIMENT DESIGN AND PROCEDURE

The final phase of the experiment concerned the notched beam specimens under the mixed mode loading condition. As mentioned before, the stress intensity factor for notches has a unit of $(\text{Load})\times(\text{Length})^{2-\lambda}$, which depends on the eigenvalue λ. Therefore, the interaction curve for notched specimens include three variables, i.e., K_I / K_{IC}, K_{II} / K_{IIC} and λ.

Experiment no.9 was designed to produce data points for notches with λ = 1.6 and 1.7. Three types of specimens were used in these experiments as shown in Figure 46.

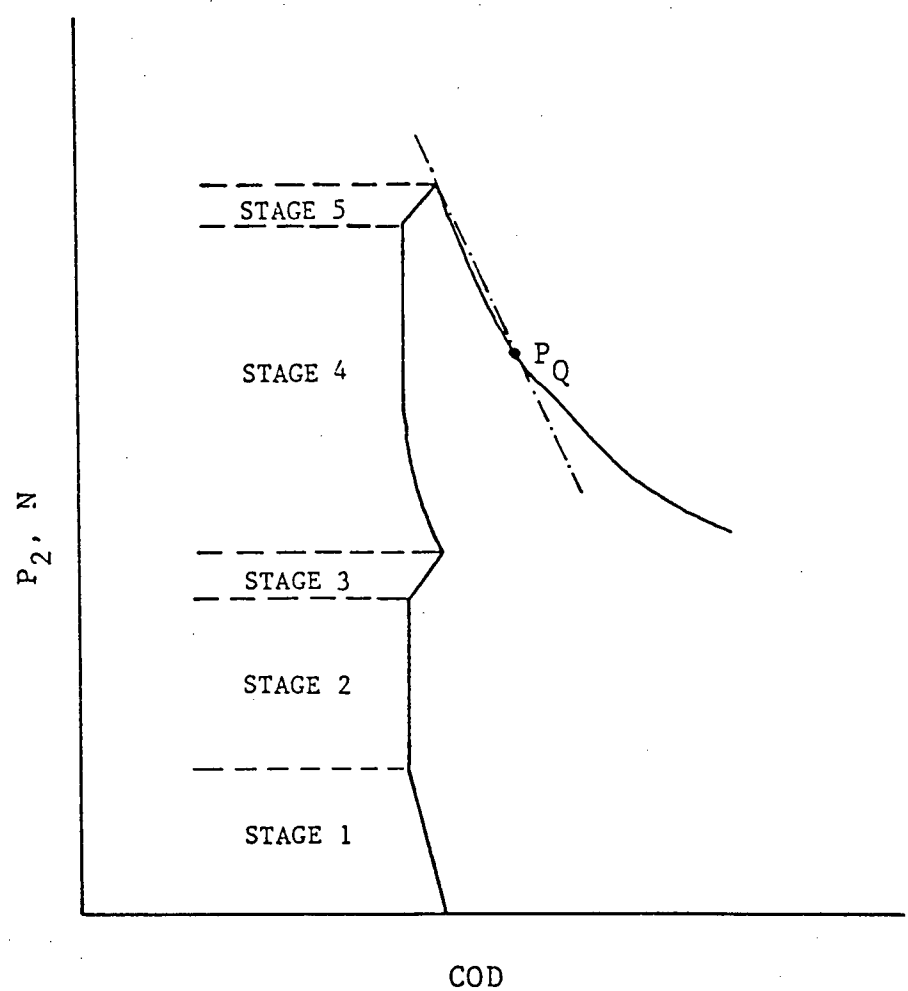

Figure 45 Typical Load-Displacement curve of Two-loads Beam Specimen.

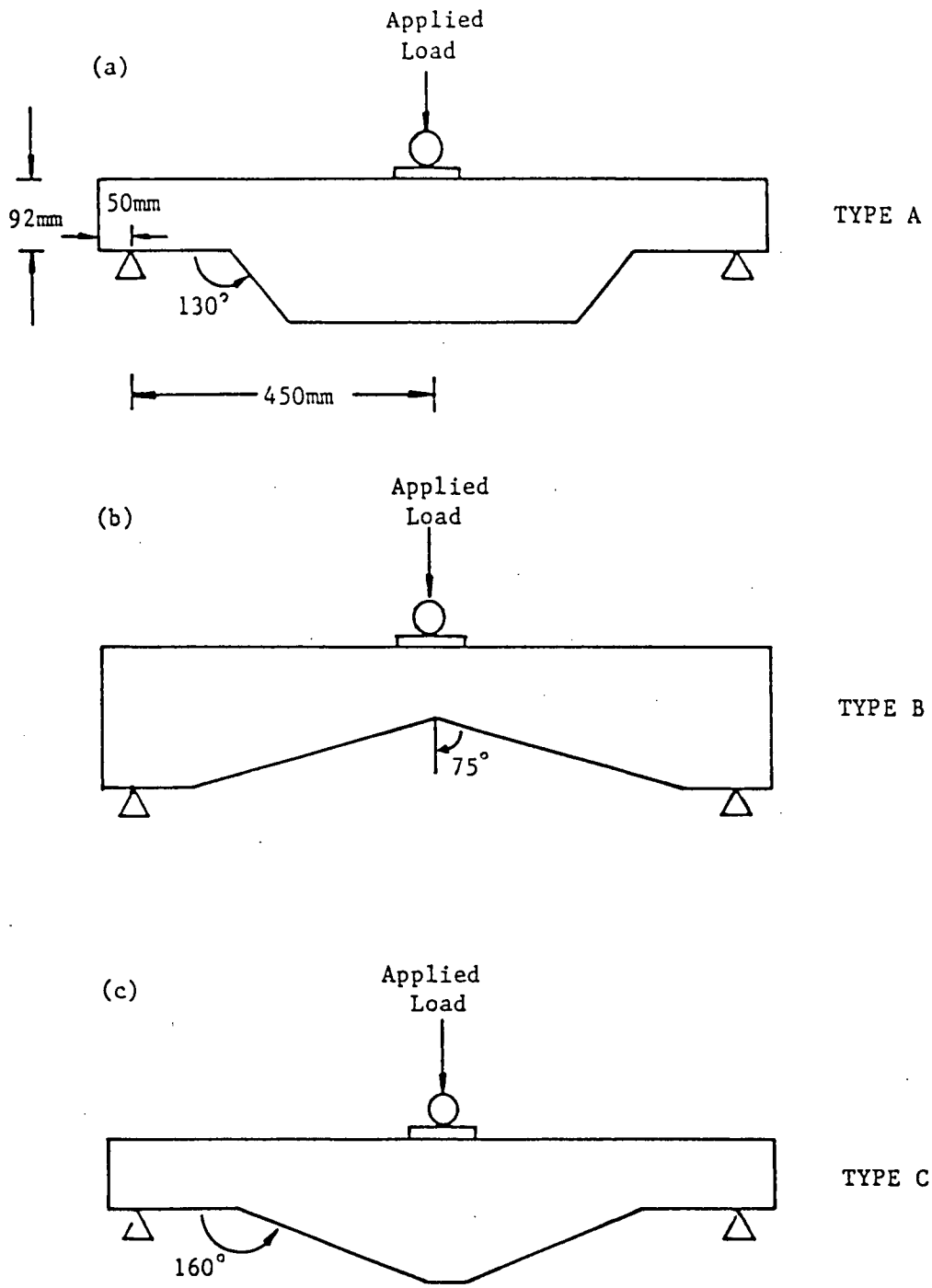

Figure 46 Specimen Configurations for Notched Beam

(a) Type A specimen; λ=1.60
(b) Type B specimen; λ=1.60
(c) Type C specimen; λ=1.70

Eight specimens were prepared for each case and the tests were carried out with the Satec Testing Machine at room temperature. The initial notches were not extended by the crack starter and the loads were plotted against the midspan deflection for all cases.

The pure mode I and mode II fracture toughness tests for these λs were not done due to the difficulty of obtaining feasible specimen dimensions and loading method. For example, to obtain the K_{IC} and K_{IIC} for λ=1.6, we need to test a 77° notch in the compact tension specimen, and a 13° notch in shear.

4.9.2 RESULTS

The results were summarized in Table 10. Since the specimens are symmetrical with respect to the midspan neutral axis, there is a equal probability of crack initiation at both notches. Similar treatment of the experiment data were preformed according to the equations (4.9) and (4.10). The average corrected K_I and K_{II} values are given in Table 10 as well.

The failure of specimens type A and type C was very brittle and the rate of crack propagation was extremely fast while the failure of type B specimens were more ductile due to the slow crack growth.

The average values of the stress intensity factors at failure for notches were showed to be less than the values for cracks. It is expected that the interaction curves will

Table 10

Results of the notched beam specimens

Specimen type	Sample size	M.C. %	S.G.	Average K_I $MPam^{2-\lambda}$	Average K_{II} $MPam^{2-\lambda}$	C.V. %	λ
Type A	7	8.81	0.361	0.2877	0.4997	17.94	1.60
Type B	8	8.59	0.347	0.2370	1.2044	12.11	1.60
Type C	8	8.00	0.315	0.2122	0.7326	24.54	1.70

move towards the origin as the value of λ increases.

4.10 SUMMARY

This chapter has served to provide the full descriptions of the experiment design, procedures and results. Each experiment contributed to a better understanding of how wood specimens performed under different geometries and loading conditions. The experiments also provide the data points which are necessary in generating the interaction curve for the mode I and mode II stress intensity factor.

5. DISCUSSION

5.1 INTRODUCTION

This chapter first explains the method of generating an interaction curve for a cracked beam, and then presents the results obtained. The method is then extended to a notched specimen, to establish the family of interaction curves. Following is a detailed discussion of the treatment of data in order to obtain the curves, including assumptions that had been made during the process and the limitations of the experiments. Finally, rules for the design of cracked beams and notched beams are suggested.

5.2 STRESS INTENSITY FACTOR INTERACTION CURVE FOR CRACKS

Using the results of all the cracked specimens tested - DCB specimens, two-loads specimens, mid-crack beam specimens, it is possible to establish the interaction curve for the cracked beams. Figure 47 shows all the experimental data points obtained which had been normalized with the critical mode I and mode II stress intensity factors. An interation curve has been derived by the least-squares technique based on equation (2.65) and is shown in Figure 47 with all the data points, and in Figure 48 with their average values. This gives the formula :

$$\frac{K_I}{K_{IC}} + \left(\frac{K_{II}}{K_{IIC}}\right)^{2.5587} = 1 \qquad (5.1)$$

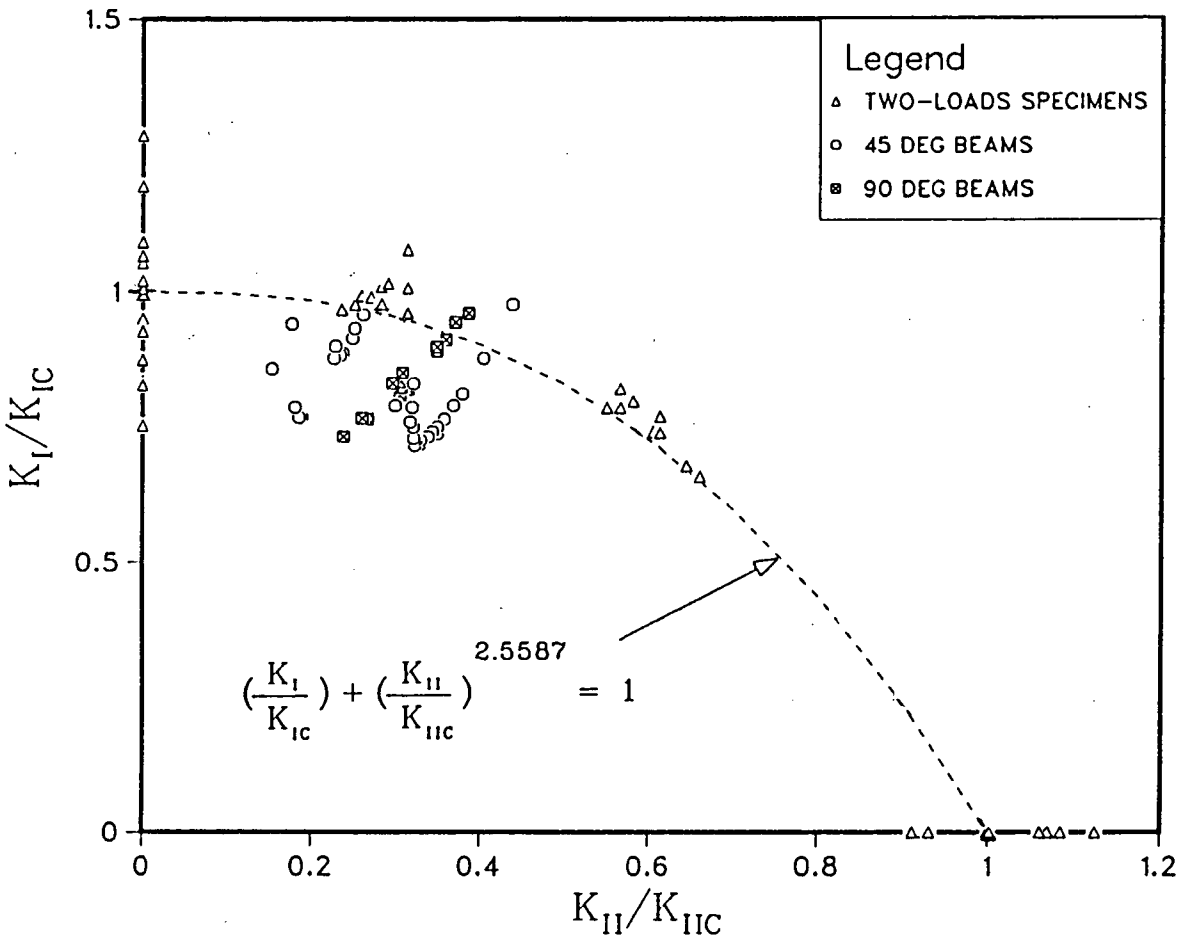

Figure 47 Interaction between K_I/K_{IC} and K_{II}/K_{IIC} for cracked beam specimens.

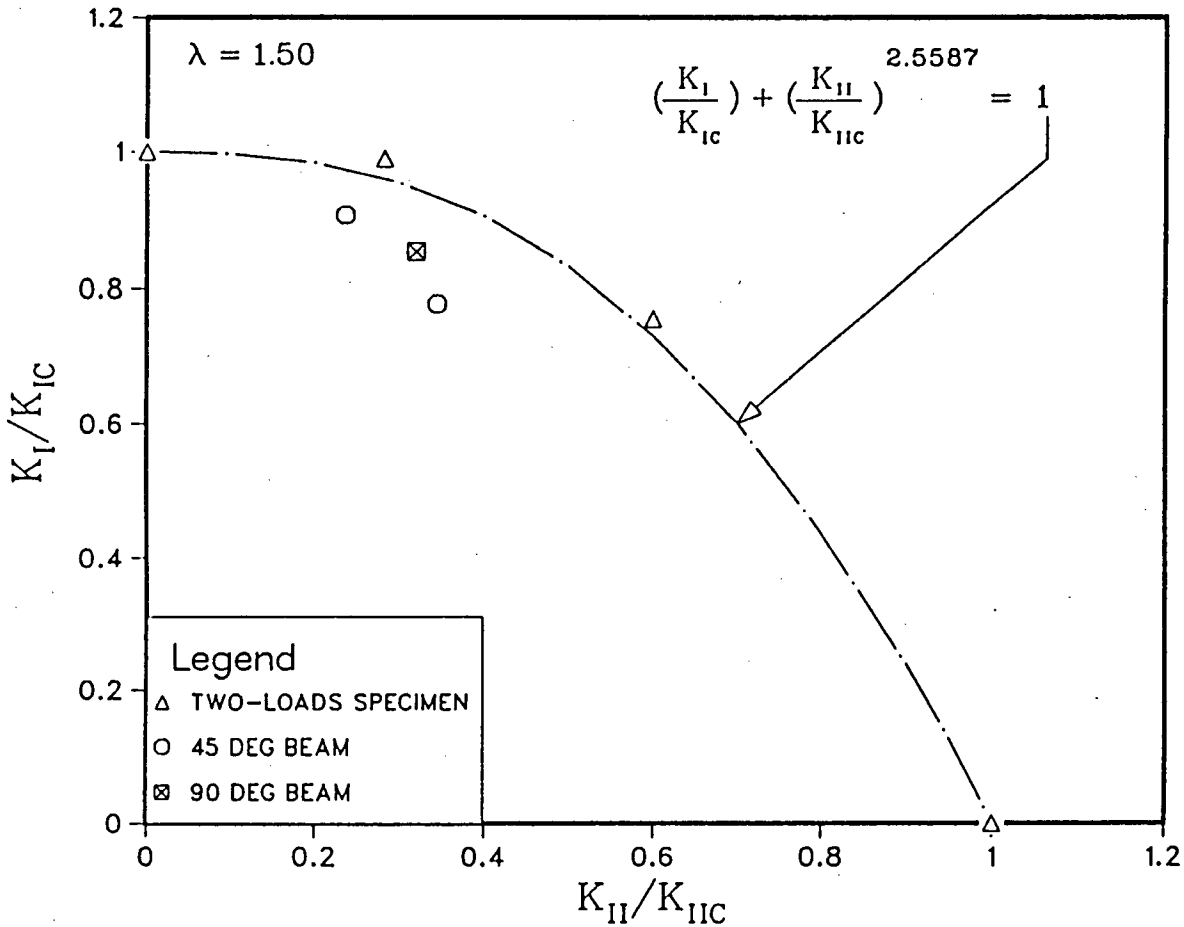

Figure 48 Interaction curve derived between K_I/K_{IC} and K_{II}/K_{IIC} for cracked beam specimens.

This is close to the model proposed by Wu (1967),i.e.:

$$\frac{K_I}{K_{IC}} + \left(\frac{K_{II}}{K_{IIC}}\right)^2 = 1 \qquad (5.2)$$

This formula is replotted in Figure 49 together with other suggested models. The linear relation of Leicester (1974) seems to be too conservative. The model proposed by Williams and Birch (1976) that the shear stress causing sliding mode has no effect on the mixed mode failure, does not follow the data trend. The present experiments on white spruce corroborate the findings of Wu (1976) on balsa. The question might be raised whether this interaction relation is applicable to other species of wood, but it cannot be answered until further results are obtained.

5.3 STRESS INTENSITY FACTOR INTERACTION CURVE FOR NOTCHES

As mentioned before, the stress intensity factors for notches have dimensions of stress*length$^{2-\lambda}$, where λ is a non-linear function of the material and notch orientation in orthotropic materials. Consequently, for any given value of λ, there may be an infinite number of compatible notch geometries and material combinations.

In a general case of a notch, a minimum of three parameters are essential to uniquely specify the stress fields at the notch root : K_I , K_{II} and λ. K_I and K_{II} indicate the strength of each of the stress fields while λ

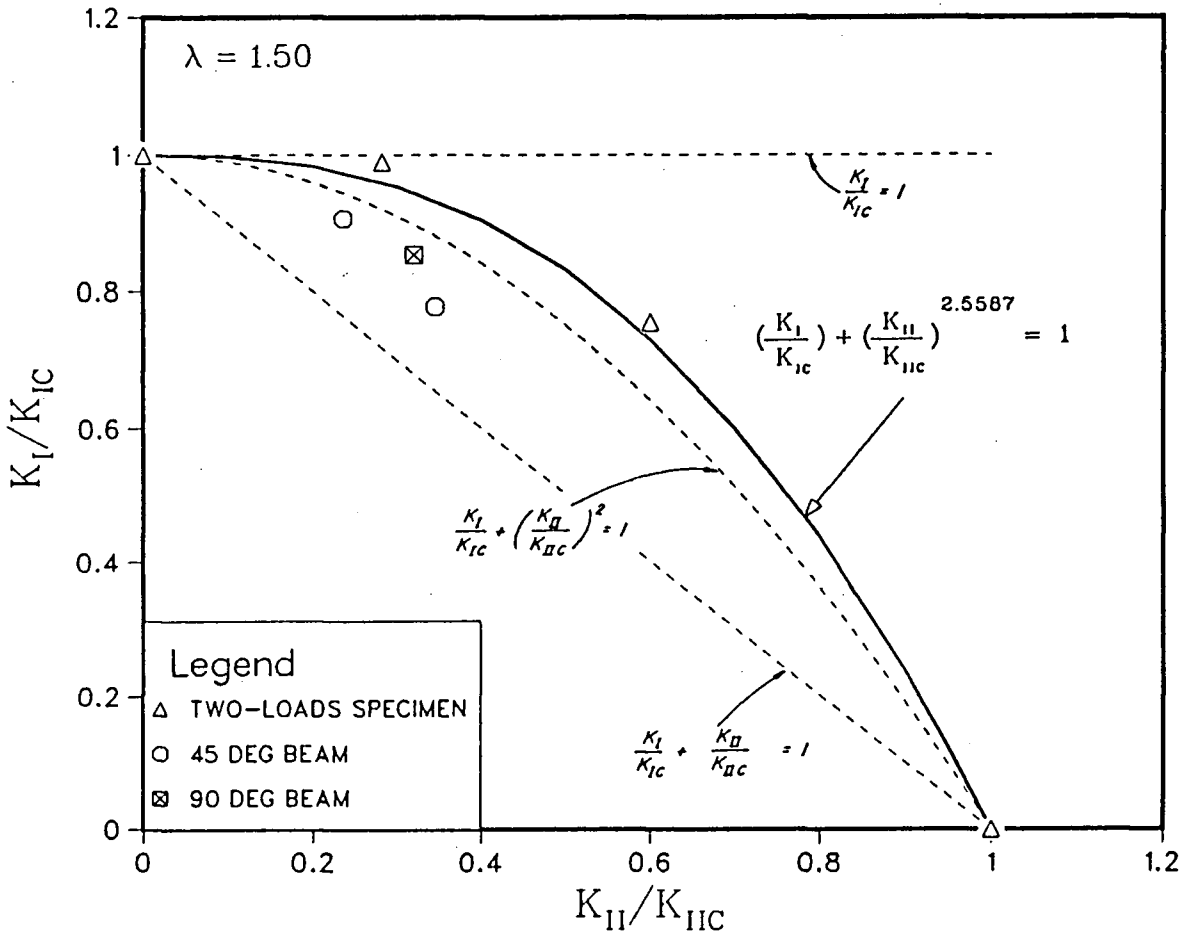

Figure 49 Interaction models between K_I/K_{IC} and K_{II}/K_{IIC} for cracked beam specimens.

shows the rate at which the stresses change when the distance to the notch root varies.

To establish the family of interaction curves, it is necessary to obtain interaction curves for λ values from 1.5 to 2.0. This is rather tedious as compared to sharp cracks, for which the primary and secondary modes have equal eigenvalues. In order to obtain data points on the interaction curve, different notch geometries are required.

The experiments contributed two data points for λ=1.6 and one data point for λ=1.7. These are the more general cases since a larger value of λ corresponds to a large notch angle. As λ approaches the value of 2.0, the notch open to 180 degrees to produce a flat surface.

Due to the limited number of the data points, the assumption that the shape of the interaction curves for notches would be the same as for the case of cracks had to be made.

A plot of the family of the interaction curves obtained is shown in Figure 50. The curves are best-fitted based on the following interaction relationship:

$$A K_I + B K_{II}^{2.5587} = 1 \qquad (5.3)$$

$$A/B = 17.84 \qquad (5.4)$$

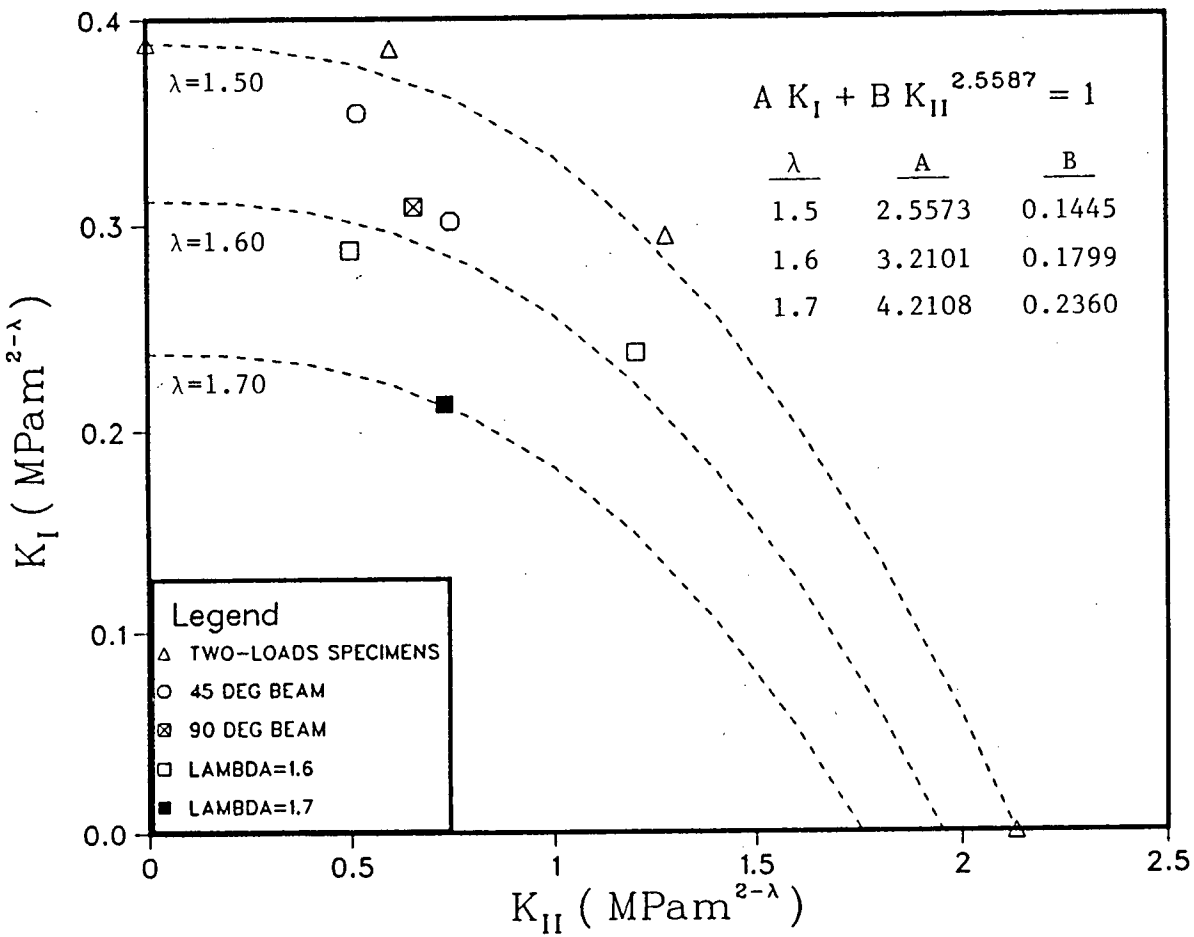

Figure 50 Interaction relations between K_I and K_{II} for notches.

where

K_I , K_{II} are the mode I and mode II fracture toughness respectively, $MPam^{2-\lambda}$;

A, B are some constants as shown in Figure 50.

This give values of K_{IC} of 0.3880 $MPa\sqrt{m}$, 0.3115 $MPam^{0.4}$, 0.2375 $MPam^{0.3}$ for λ=1.5, 1.6, 1.7 respectively; K_{IIC} of 2.183 $MPa\sqrt{m}$, 1.955 $MPam^{0.4}$, 1.758 $MPam^{0.3}$ for λ=1.5, 1.6, 1.7 respectively. A more general interaction equation was derived for white spruce using the least-squares method on the experimental results :

$$K_I + 0.05605\, K_{II}^{2.5587} = 1.8355 - 1.1525\,\lambda + 0.125\,\lambda^2 \qquad (5.5)$$

where

K_I , K_{II} are the mode I and mode II fracture toughness respectively, $MPam^{2-\lambda}$;

The individual interaction curve for notched beams for λ=1.6 and 1.7 are also showned in Figure 51 and Figure 52 respectively.

After establishing the interaction curves, we are now able to compute the strength of any notched or cracked specimen of different geometries, materials and grain orientations under any kind of loading. But using of these curves for beam design seems to be too troublesome as one needs the stress intensity factors. However, we can alter these curves in order to obtain a design method for the

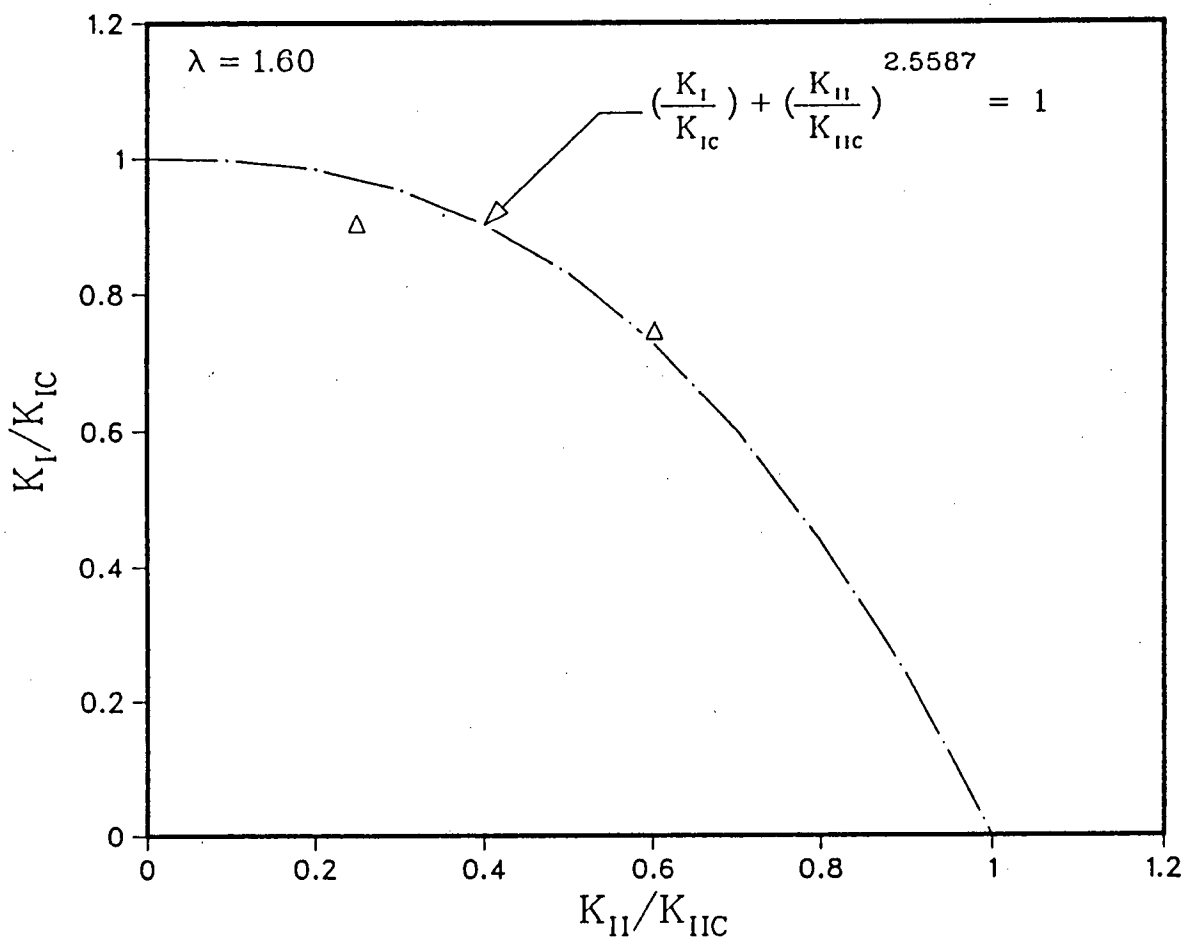

Figure 51 Interaction curve for notches with λ=1.60

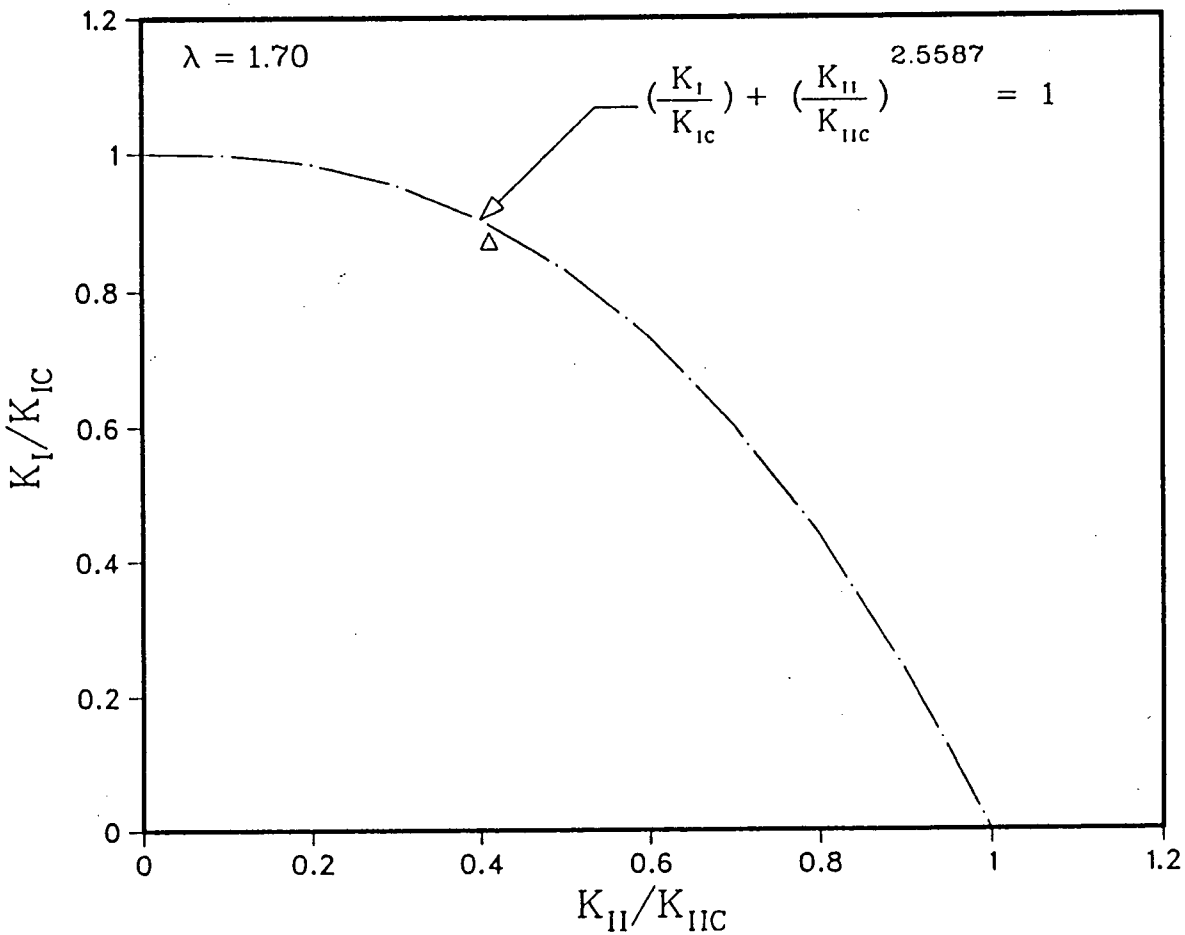

Figure 52 Interaction curve for notches with λ=1.70

cracks and notches.

5.4 APPLICATION

The application of linear elastic fracture mechanics methods for beam design allows estimates of the strength of notched beams. Murphy (1978) had shown that the recent code has underestimated the effect of the presence of a notch based on the net-section theory. A more rational method of treating the notches and cracks is presented herein which provides rules for the strength design of notched beams. These rules were based on theoretical studies combined with the test data.

The design method includes two essential features - the 90 degrees cracked beam and the 90 degrees notched beam. The essential feature of the 90 degree cracked beam problem under investigation is shown in Figure 53. The geometrical dimensions a, b, d are indicated therein as well as the sign convention of bending moment M and shear force V acting on the beam at the cross-section containing the crack root.

Figure 53 also shows the individual contribution of the applied moment and shear to the mode I and mode II stress intensity factors for varying notch-depth ratios. The curves were obtained by using the program NOTCH and followed the "transformed stress intensity factors method" proposed by Murphy (1978).

In application, one can obtain the stress intensity factors for specific configuration by evaluating the moment

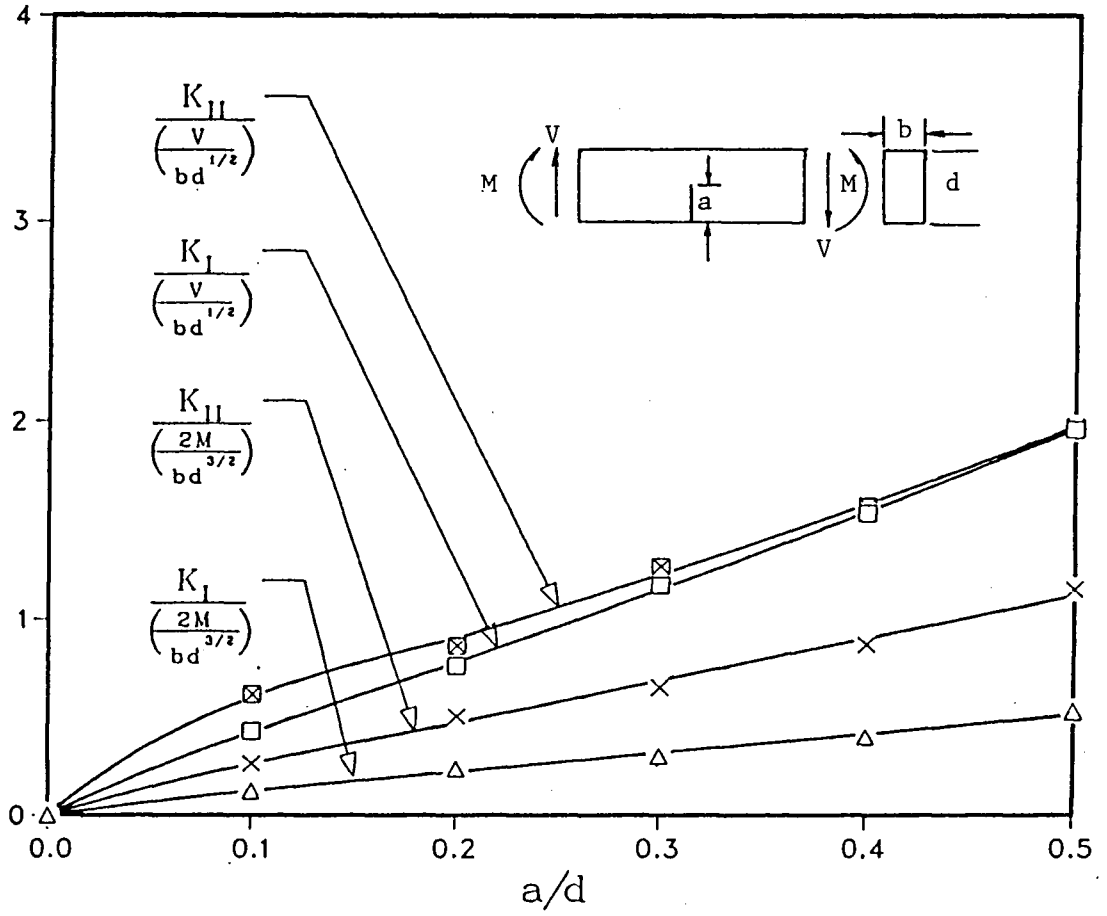

Figure 53 Dimensionless Stress Intensity Factors for pure moment and pure shear loadings as a function of notch-to-depth ratio for 90 degrees cracked beam.

and shear at the notch root and entering the figures.

Since the stress intensity factors are also affected by the nominal stress field surrounding the eigenfield, the accuracy of the proposed curves for computing stress intensity factors depends on how similar the nominal stress field of the beam being analyzed is to the stress field of the beam shown in Figure 53.

To verify the validity of these curves, a comparison had been made between the results obtained by these curves and the the program NOTCH. Five cases, with two simple structural configurations under different loadings were investigated. The notch-to-depth ratio is 0.5 and the five cases are shown in Figure 54.

The results are presented in Table 11. As can be seen, the difference between the two methods is larger in cases 3 and 5, which might be explained by the high discrepancy between the nominal stress field of the off-center cracked beam and the nominal stress field of the beam from which the curves were derived. The difference of the beams under uniform loading can be explained in the same manner.

Interaction relation between the ultimate moment and shear force can be established by using the interaction curves for the stress intensity factors obtained and substituting the K_I and K_{II} values by the applied moment and shear. The interaction relation between the moment and shear for 90 degrees crack for various notch-depth ratio is shown in Figure 55. The curves show a linear relationship between

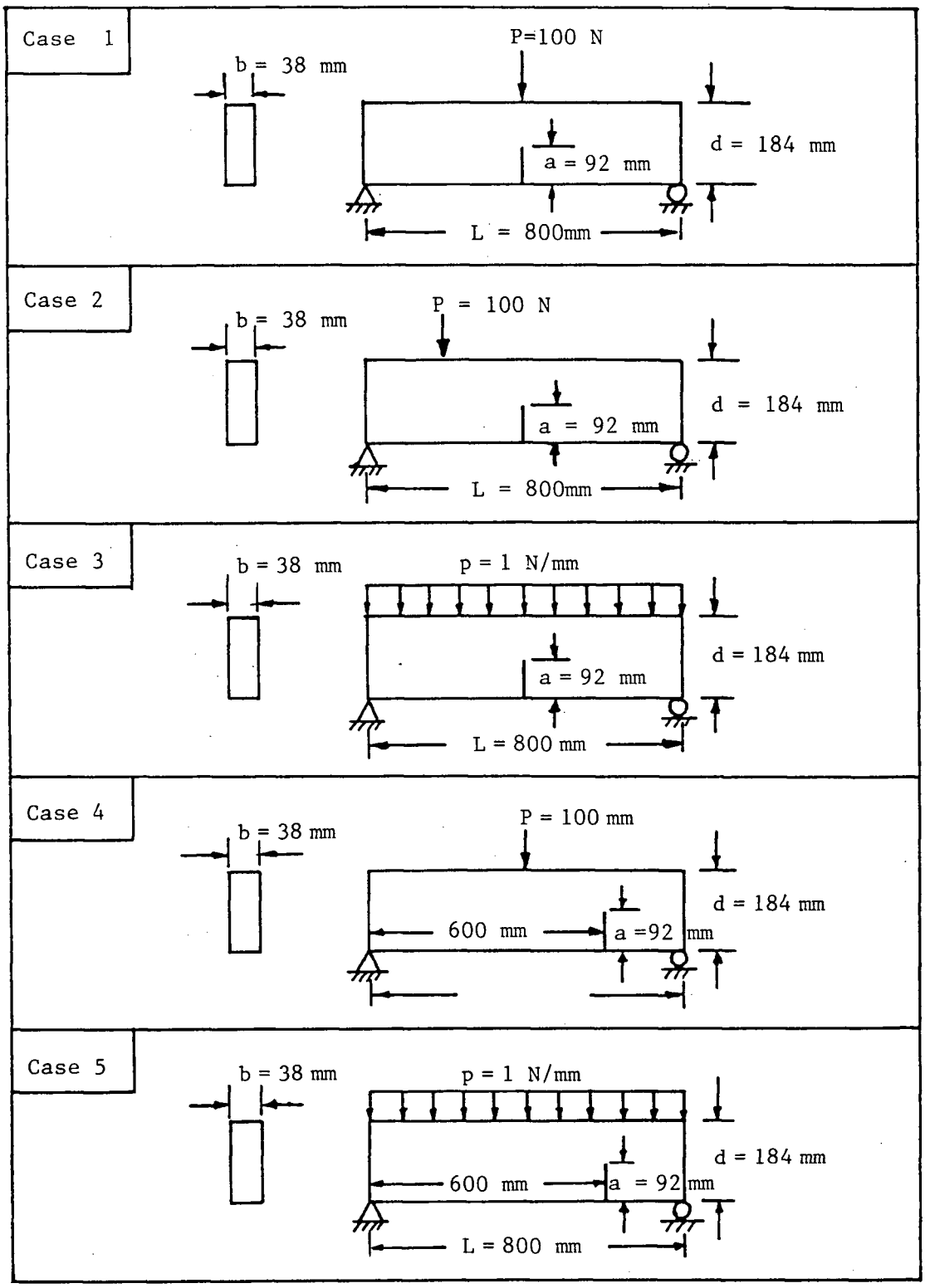

Figure 54 Several Sharp Crack Problems.

Table 11

Stress intensity factors for various sharp crack problems

Case	From curves		From NOTCH		Accuracy* of K_I %	Accuracy of K_{II} %
	K_I MPa$\sqrt{m}$	K_{II} MPa$\sqrt{m}$	K_I MPa$\sqrt{m}$	K_{II} MPa$\sqrt{m}$		
1	7.210×10^{-3}	0.0154	7.005×10^{-3}	0.0149	2.9	2.7
2	6.606×10^{-3}	0.0107	6.372×10^{-3}	0.0101	3.7	5.7
3	0.0288	0.0614	0.0317	0.0672	8.9	8.6
4	9.606×10^{-3}	0.0137	9.280×10^{-3}	0.0133	3.5	3.3
5	0.0216	0.0461	0.0241	0.0502	10.1	8.3

* Accuracy is based on the results obtained from the program NOTCH.

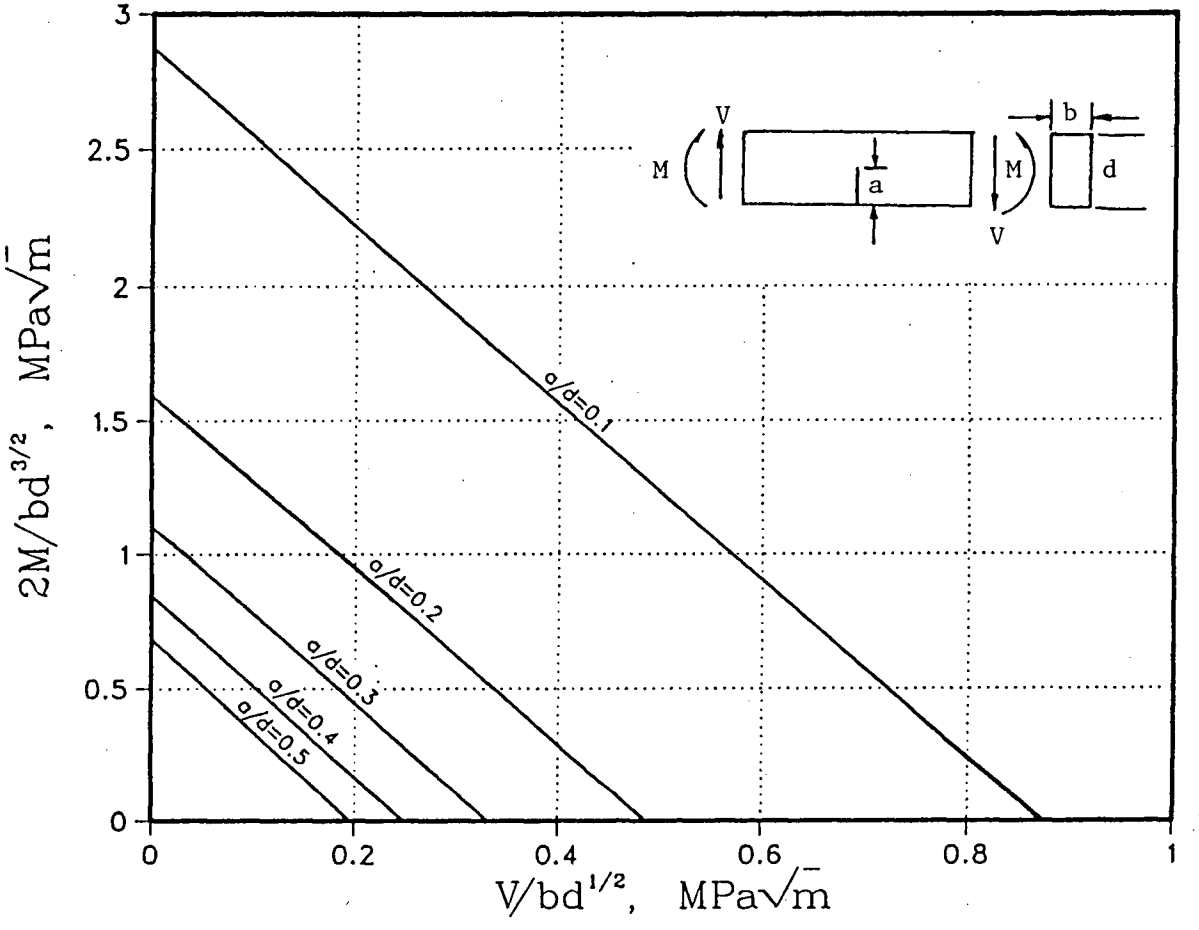

Figure 55 Design curves for 90 degrees cracked beam as a function of notch-to-depth ratio.

moment and shear with different intercepts and slopes for different notch-depth ratio.

These relationship can be expressed in formulae in terms of the nominal maximum bending stress $f_b=6M/bd^2$ and nominal maximum shear stress $f_s=3V/2bd$ calculated for the total beam depth.

This gives,

For 90 degrees cracked beam :

$$\frac{\alpha f_b + f_s}{\beta d^{-0.5}} \leq 1 \qquad (5.6)$$

where

α, β are constants listed below;

d is the total beam depth, m;

f_b is the maximum bending stress, MPa;

f_s is the maximum shear stress, MPa.

a/d	α(dimensionless)	$\beta(\sqrt{m}/MPa)$
0.5	0.0644	0.1271
0.4	0.0797	0.1815
0.3	0.0787	0.2374
0.2	0.0913	0.3532
0.1	0.1004	0.8544

Equation (5.6) is analogous to the design equations for notches from the S.A.A. Australian Timber Engineering Code

CA65-1972 (S.A.A. 1972) :

$$\frac{0.3f_b + f_s}{C_3 F_{sj}} < 1 \qquad (5.7)$$

where

$$f_b = \frac{6M}{Bd^2_{min}} \qquad f_s = \frac{1.5V}{Bd_{min}}$$

F_{sj} = shear block strength for the species of interest;

C_3 = constant for specific notch angle. For the 90 degrees notched beam, the stress intensity factors do not show a consistent relationship with the applied moment and shear. This means the stress distribution around the eigenfield of a notch is very sensitive and varies with different loadings and geometries. Consequently, the stress intensity factors for notches have to be computed by using singular finite element program, and general design curves for different loadings can not be obtained.

One particular case of a one-metre rectangular end-notched white spruce 2x8's beam under centerpoint loading (P) was analyzed with various notch-to-depth ratio. The ratio K_I /P were plotted against the notch length for various notch-to-depth ratio. (see Figure 56) Since the K_I to K_{II} ratio is constant for a given notch geometry and

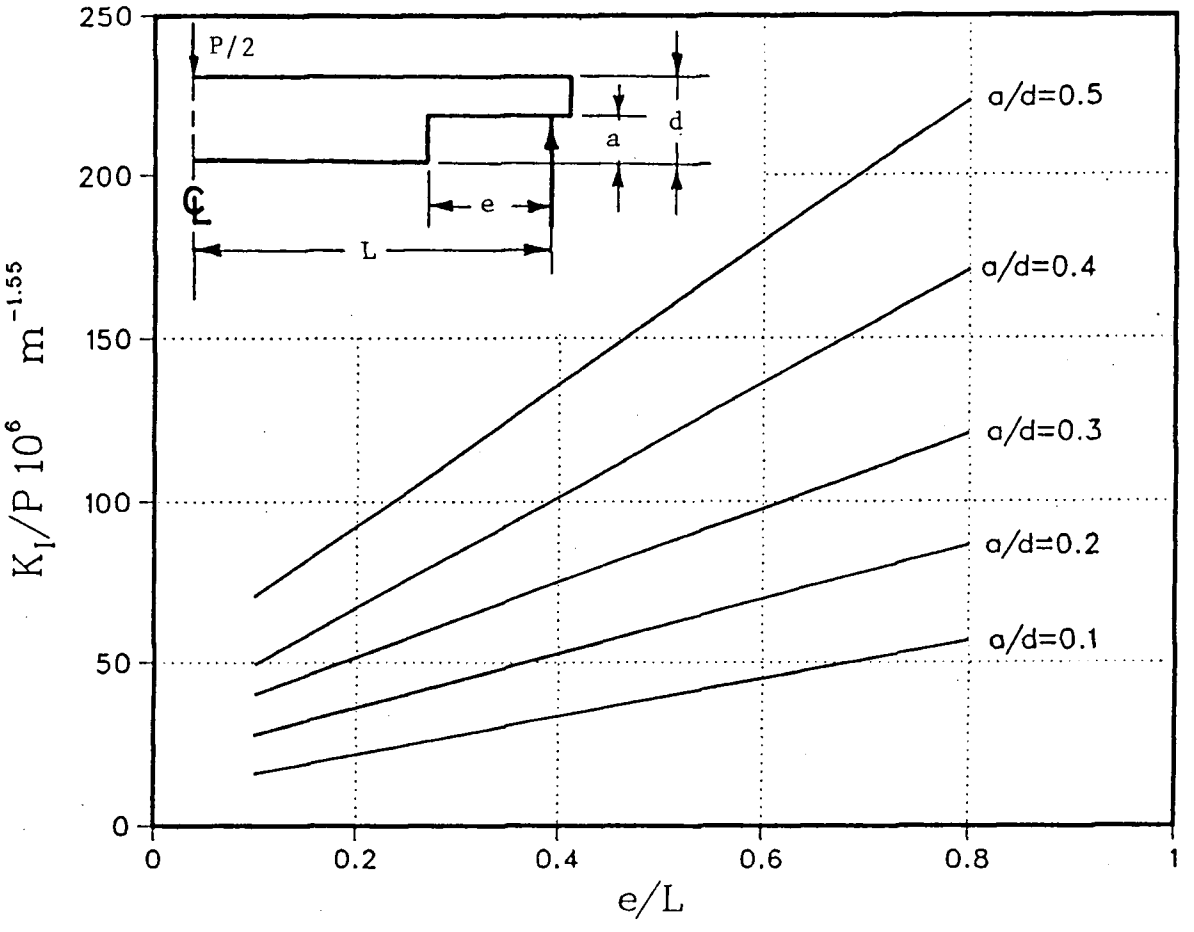

Figure 56 K_I/P versus Notch Length for various notch depth of a 2"x8" beam.

material, K_{II} can be obtained from the relation $K_{II} = 1.096 K_I$ after obtaining the K_I value from the figure. Using equation (5.5) and substituting K_{II} by $1.096 K_I$, the critical mode I and mode II stress intensity factors can be computed. The values obtained are 0.3823 $MPam^{0.4521}$ for the critical mode I stress intensity factor and 0.3487 $MPam^{0.4521}$ for the critical mode II stress intensity factor. Using these values and Fig. 56, a plot of the critical applied load against the notch length for various notch depths can be obtained as shown in Figure 57. It should be noted that for notches close to the end support, the stress intensity factors might be affected by the bearing stress, which causes the distortion of the stress field around the notch. Therefore the stress intensity factors cannot be represented in the same plot.

Although the relation between the critical stress intensity factors and the applied load seems to be very complicated for notches, design curves for other beam configurations and loadings can be established in a similar way based on the notch length and the notch-to-depth ratio.

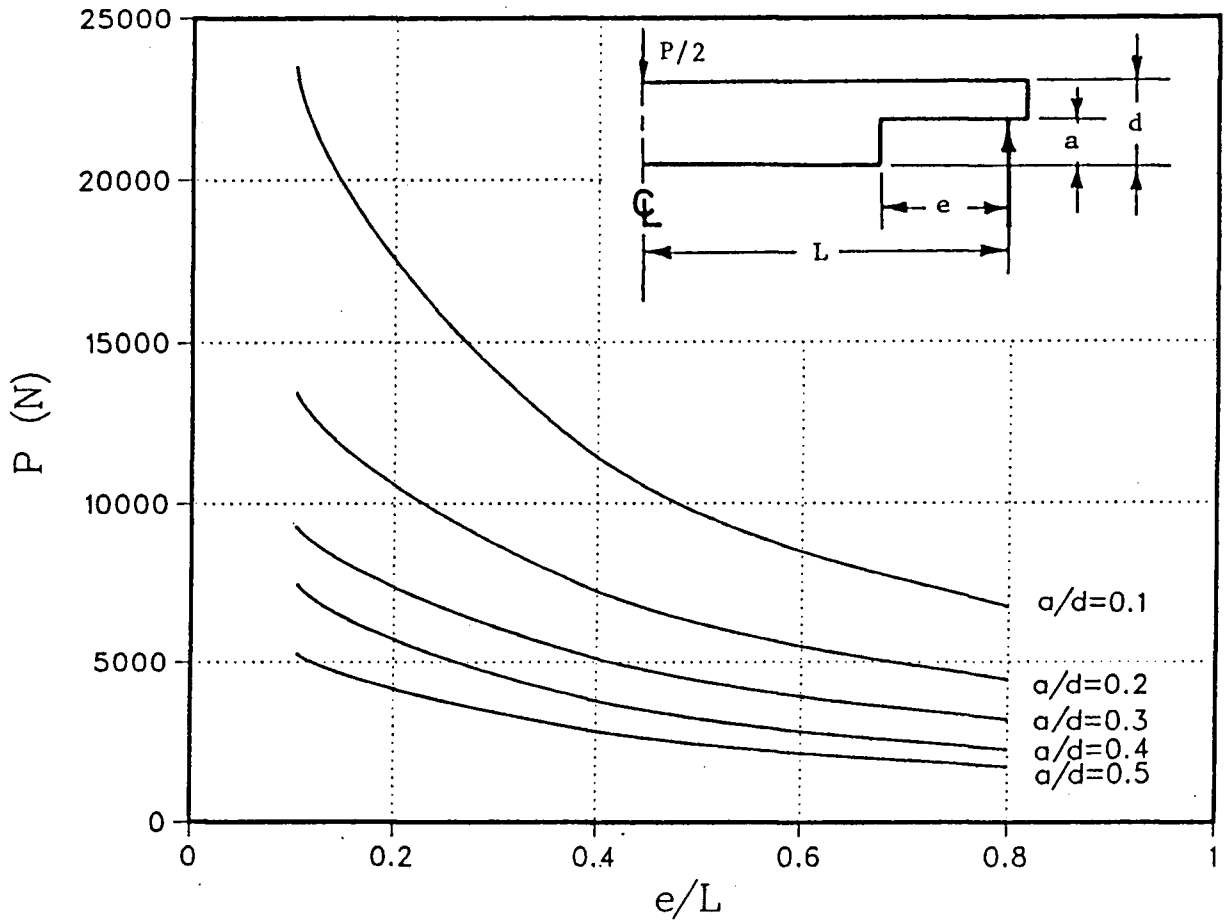

Figure 57 Critical Load versus Notch Length for various notch depth of a 2"x8" beam.

6. CONCLUSIONS AND RECOMMENDATIONS

6.1 CONCLUSIONS

The linear elastic fracture mechanics method has been found to be appropiate and to apply well to the characterization of the fracture behavior of wood. The fracture toughness for white spruce has been shown to vary with the annual ring orientation in the specimens. It has also been shown that there is a dependence of the mode I fracture toughness, K_{IC}, on the width of the crack front and the moisture content in the specimens.

The mode II critical stress intensity factor, K_{IIC}, has been shown to govern the fracture of end-cracked wood beams and it has also shown a dependence on the annual ring orientation.

The mixed mode interaction curves, which incorporate the mode I and mode II fracture toughness, have been presented and applied successfully to the fracture behavior of white spruce. The criterion that the mode I fracture toughness is independent of forward shear effect has not been observed here while an interaction relationship between K_I and K_{II} in the mixed mode fracture of white spruce is more obvious. This relation applied equally well to the notched specimens, and a family of interaction curves for predicting the onset of rapid crack propagation has been established for white spruce.

Design methods has been provided herein for 90 degrees cracked beam based on the applied moment and shear. Interaction formulae between nominal maximum bending stress and nominal maximum bending stress has been presented which is analogous to the rules outlined by the Australian Timber Design Code. Design curves for 90 degree notched beam has also been presented here for a particular case of a simple-supported mid-span loaded beam.

6.2 RECOMMENDATIONS FOR FUTURE RESEARCH

The crack-front width theory has been found to apply well to the experiments conducted and an extension of applying to notches should be studied.

The moisture content effect should be investigated with wider range of moisture content variation as well as possibility of applying on notches.

The pursuit of a valid size effect on the mode I fracture toughness has not been completed successfully and a consistent method to characterize the effect of the specimen size on the mode I fracture toughness should be developed.

This work has also given a simplified picture of mixed mode failure for notches which has not been studied before. A proposed design method has also been presented here which can be adopted by the timber design code. Further research should include performing experiments to study this interaction relation for other geometrical configurations and other species of wood.

BIBLIOGRAPHY

ASTM-E399-B3, "Standard Test Method for Plane-Strain Fracture Toughness of Metallic Materials," *ASTM Vol. 03.01*, Sec.3, 547-582, (1985).

Barrett, J.D., "Effect of size on mode I stress intensity factors for Douglas-fir," *IUFRO wood engineering meeting*, Delft, Holland, (1976).

Barrett, J.D., "Mode II stress-intensity factors for cracked wood beams," *Engineering Fracture Mechanics*, 9, 371-378, (1977).

Benzley, S.E., "Representation of singularities with Isoparametric Finite Elements," *Int. J. Numerical Methods in Engineering*, 8, 537-545, (1974).

Bodig, J., Goodman, J.R., "Prediction of Elastic Parameters for Wood," *Wood Science*, Vol. 5, No.4, 249-264, (1973).

Broek, David, *Elementary Engineering Fracture Mechanics*, 3rd ed., The Hague: Martinius Nijhoff Publishers, (1982).

CAN3-086-M84, *Engineering Design in Wood (Working Stress Design)*, Canadian Standards Association, (1984).

Debaise, G.R., Porter, A.W., Pentoney, R.E., *Morphology and Mechanics of Wood Fracture*, Materials research and standards, 6(10), 493-499, (1966).

Dolan, J.D., Madsen, B., "Experimental determination of the shear strength of lumber," *Thesis Sec. (Civil) University of British Columbia*, (1985).

Ewing, P.D., Williams, J.G., "Thickness and moisture content effect in the fracture toughness of Scots Pine," *J. Materials Science*, 14, 2959-2966, (1979).

Foschi, R.O., Barrett, J.D., "Stress intensity factors in anisotropic plates using singular isoparameter elements," *Int. J. Numerical Methods in Engineering*, 10, 1281-1287, (1976).

Gandhi, L.R., "Analysis of an Inclined Crack Centrally Placed in an Orthotropic Rectangular Plate," *Journal of Strain Analysis*, 3(3), 157-162, (1972).

Griffith, A.A., "The phenomena of rupture and flow in solids," *Philosophical Trans. R. Soc. (London) Series A*, 221, 163-198, (1921).

Gross, B., Mendelson, A., "Plane Elastiostatic Analysis of

V-Notched Plates," *Int. J. Fracture Mechanics*, 8, 267-276, (1972).

Hellan, K., *Introduction to Fracture Mechanics*, Montreal: McGraw-Hill, (1984).

Hilton, P.D., Gifford Jr., L.N., "Stress Intensity Factors by Enriched Finite Elements," *Engineering Fracture Mechanics*, 10, 485-496, (1978).

Hunt, D.G., Croager, W.P., "Mode II fracture toughness of wood measured by a mixed mode test method," *J. Materials Science Letters*, 1, 77-79, (1982).

Inglis, C.E., "Stress in a cracked plate due to the presence of cracks and sharp corners," *Transaction of Naval Architects (London)*, 60, 213, (1913).

Irwin, G.R., "fracture dynamics," *Fracturing of Metals*, 147-166, Am. Society for Metals, Cleveland, (1948).

Irwin, G.R., "Analysis of stresses and strains near the end of a crack traversing a plate," *J. Appl. Mech.*, 24(3), (1957).

Johnson, J.A., "Crack Initiation in wood plates," *Wood Science*, 6(2), 151-158, (1973).

Knott, J.F., *Fundamentals of Fracture Mechanics*, 1st ed., London: Butterworth, (1973).

Leicester, R.H., "The size effect of notches," *Proc. 2nd Australian Conf. Mech. of Structures and Materials*, 4.1-4.20, (1969).

Leicester, R.H., "Some Aspects of stress fields at sharp notches in Orthotropic Materials," *CSIRO Aust. Div. Forest Prod. Technol. Paper No. 57*, Melbourne, (1971).

Leicester, R.H., "Effect of size on the strength of structures," *CSIRO Aust. Div. of Building Research Technol. Paper No.71*, Melbourne, (1973).

Leicester, R.H., "Application of Linear Fracture Mechanics in the Design of Timber Structures," *Proceedings, Conference Australian Fractured Group 23*, Melbourne, Australia, 156-164, (1974).

Leicester, R.H., Walsh, P.F., "Numerical Analysis for Notches or Arbitrary Notch Angle," *Proceedings of the International Conf. on Fracture Mechanics Technol. Applied to Material Evaluation and Structure Design*, Melbourne, Australia, (1982).

Liu, H.W., "Discussion to 'A Critical Appraisal of Fracture

Mechanics,'" *STP 381*, ASTM-NASA, 23-26, (1965).

Liu, H.W., "Fracture criteria of cracked metallic plate," *Int. J. Fracture Mech.*, 2, 393-399, (1966).

Liu, H.W., "On the fundamental basis of fracture mechanics," *Engineering fracture mechanics*, 17(5), 425-438, (1983).

Lin, K.Y., Tong, P., "Singular Finite Elements for the Fracture Analysis of V-Notched Plate," *Int. J. Numerical Methods in Engineering*, 15, 1343-1354, (1980).

Lum, C., "Stress Intensity Factors for V-Notches in Orthotropic plates using singular finite elements," *Thesis Sec. (Civil) University of British Columbia*, (1986).

Mall, S., Murphy, J.F., Schottafer, J.E., "Criterion for the mixed mode fracture in wood," *ASCE J. Eng. Mech.*, 109(3), 680-690, (1983).

Orowan, E., "Energy criteria of fracture," *Welding Res. Suppl.*, 20, 1575, (1955).

Paris, P.C., "The Mechanics of Fracture Propagation and Solutions to Fracture Arrestor Problems," *Document No. D2-2195*, Boeing Co., (1957).

S.A.A., *AS 1720-1979, Timber Engineering Code*, Sydney: Standards Association of Australia, (1975).

Saven, S.G., *Stress Concentration Around Holes*, Trans. from Russian by E. Gros., New York: Pergamon Press, (1961).

Schniewind, A.P., R.A. Pozniak, "On the Fracture Toughness of Douglas Fir Wood," *Engineering Fracture Mechanics*, 2, 223-233, (1971).

Sih, G.C., Paris, P.C., Irwin, G.R., "On crack in rectilinearly anisotropic bodies," *Int. J. Fracture Mechanics*, 1, 189-203, (1965).

Tada, H., *The Stress Analysis of Cracks Handbook*, Del Research Corp., Penn., (1973).

Technical Research Centre of Finland, Laboratory of Structural Engineering, "Application of Fracture Mechanics: Fracture Toughness of Finnish wood," *Research Newsletter*, (1986).

Walsh, P.F., "The computation of stress intensity factors by a Special Finite Element Technique," *Int. J. Solids and Structures*, 7(10), 1333-1342, (1971).

Walsh, P.F., "Linear fracture mechanics in orthotropic

materials," *Engineering Fracture Mechanics*, 4, 533-541, (1972).

Walsh, P.F., "Linear fracture mechanics solutions for zero and right angle notches," *CSIRO Aust. Div. of Building Research Technical Paper (Second series) No. 2*, 1-16, Melbourne, (1974).

Westergaard, H.M., "Bearing Pressures and Crack," Transactions, Am Soc. Mechanical Engrs., *J. Applied Mechanics*, (1939).

Williams, J.G., Birch, M.W., "Mixed Mode Fracture in Anisotropic Media," *Cracks and Fracture STP 601*, ASTM, 125-137, (1976).

Williams, M.L., "On the stress distribution at the base of a stationary crack," *J. Appl. Mech.*, 24(1), (1957).

Woo, C.W., Chow, C.L., "Mixed Mode Fracture in Orthotropic Media," *Proceedings, Fracture Mechanics in Engineering Application*, India, 387-396, (1979).

Wu, E.M., "Application of fracture mechanicxs to anisotropic plates," *J. Applied Mechanics*, E34(4), 967-974, (1967).

APPENDIX I

Test Data of Experiment No. 1

Compact Tension Specimen

Spec. no.	M.C. %	S.G.	Angle to RL degree	P_{max} N	P_Q N	P_{max}/P_Q	K_{IC} MPa$\sqrt{m}$
1	9.92	0.372	90	248.0	227.5	1.09	0.1570
2	9.92	0.324	90	216.1	208.1	1.04	0.1436
3	10.05	0.411	90	307.2	290.1	1.06	0.2002
4	10.18	0.408	90	324.2	312.9	1.04	0.2159
5	10.05	0.377	90	199.1	147.9	1.35[a]	0.1021
6	8.87	0.450	90	492.5	489.2	1.01	0.3376
7	10.10	0.330	90	238.8	227.5	1.05	0.1570
8	10.00	0.414	90	291.2	272.9	1.07	0.1883
9	9.80	0.374	90	341.3	332.1	1.03	0.2296
10	9.60	0.378	90	335.6	329.9	1.02	0.2277
11	9.60	0.369	90	244.5	248.0	1.00	0.1711
12	9.80	0.405	90	238.8	236.6	1.01	0.1633
13	9.70	0.412	90	261.6	252.5	1.04	0.1743
14	9.70	0.375	90	329.9	295.8	1.11	0.2041
15	9.80	0.410	90	307.2	284.4	1.08	0.1963
16	9.60	0.328	90	270.7	260.5	1.04	0.1798
17	6.60	0.408	90	432.2	415.2	1.04	0.2865
18	9.95	0.417	90	238.8	213.9	1.12	0.1476
19	9.70	0.373	90	318.5	304.8	1.05	0.2103
20	9.40	0.386	90	261.6	254.9	1.03	0.1759
21	9.20	0.384	90	204.7	184.3	1.11	0.1272
22	9.50	0.386	90	204.7	199.1	1.03	0.1374
23	9.10	0.389	90	298.0	275.3	1.08	0.1900
24	8.45	0.370	90	227.5	224.1	1.02	0.1547
25	8.70	0.378	90	398.1	389.1	1.02	0.2685
26	9.10	0.386	90	394.6	378.7	1.04	0.2613
27	8.95	0.386	90	409.5	407.3	1.01	0.2811
28	9.30	0.394	90	301.5	278.7	1.06	0.1923
29	9.20	0.394	90	394.7	381.1	1.04	0.2630
30	8.70	0.374	90	420.8	415.2	1.01	0.2865
31	8.40	0.441	90	272.9	255.9	1.07	0.1766
32	8.95	0.390	90	369.7	364.0	1.02	0.2512
33	9.40	0.411	90	261.6	252.5	1.04	0.1743
34	8.80	0.389	90	364.0	345.8	1.05	0.2386
35	9.30	0.381	80	184.3	177.5	1.03	0.1225
36	9.00	0.400	76	382.2	364.0	1.05	0.2512
37	8.70	0.399	75	449.3	434.5	1.03	0.2998
38	7.70	0.402	65	466.3	443.6	1.05	0.3061
39	9.20	0.388	60	537.0	536.8	1.00	0.3704
40	9.40	0.359	60	278.8	263.9	1.06	0.1635

a - rejected because $P_{max} > 1.2P_Q$.

Test Data of Experiment No. 1 - Cont'd

Compact Tension Specimen

Spec. no.	M.C.[b] %	S.G.	Angle to RL[c] degree	P_{max} N	P_Q N	P_{max}/P_Q	K_{IC} MPa$\sqrt{m}$
41	8.08	0.390	57	473.2	460.7	1.03	0.3179
42	7.40	0.383	55	445.9	437.9	1.02	0.3022
43	9.65	0.350	54	420.8	406.1	1.04	0.2802
44	9.90	0.350	53	445.9	436.8	1.02	0.3014
45	9.67	0.457	52	403.8	392.4	1.03	0.2708
46	8.40	0.364	51	374.2	364.0	1.03	0.2512
47	8.70	0.356	50	364.0	344.7	1.06	0.2379
48	7.80	0.386	50	464.1	460.7	1.01	0.3179
49	7.90	0.455	50	523.3	494.8	1.09	0.3415
50	8.57	0.453	49	523.3	489.1	1.07	0.3375
51	8.60	0.368	49	369.2	364.0	1.01	0.2512
52	9.40	0.456	48	475.5	460.7	1.03	0.3179
53	9.92	0.359	47	434.5	426.6	1.02	0.2944
54	9.00	0.353	47	361.7	358.3	1.01	0.2473
55	9.00	0.377	47	398.1	381.1	1.04	0.2630
56	7.20	0.357	46	483.5	483.4	1.00	0.3336
57	8.57	0.356	45	434.5	420.9	1.03	0.2905
58	7.20	0.355	44	489.2	483.4	1.01	0.3336
59	7.00	0.354	40	517.6	517.6	1.00	0.3572
60	9.70	0.349	40	386.7	386.7	1.00	0.2669
61	9.00	0.356	39	352.6	341.8	1.03	0.2359
62	9.50	0.452	33	517.6	492.5	1.05	0.3399
63	7.00	0.356	32	551.7	546.0	1.01	0.3768
64	10.00	0.336	23	563.1	531.2	1.06	0.3666
65	9.95	0.364	16	574.4	517.6	1.11	0.3572
66	8.95	0.348	16	529.0	517.6	1.02	0.3572
67	9.60	0.353	16	500.5	500.5	1.00	0.3454
68	9.10	0.350	12	585.8	580.1	1.01	0.4003
69	9.40	0.347	7	506.2	502.8	1.01	0.3470
70	9.30	0.355	5	557.4	541.5	1.03	0.3737
71	9.60	0.366	2	602.9	591.5	1.02	0.4082
72	9.80	0.337	0	532.3	530.1	1.00	0.3658
73	9.95	0.335	0	625.6	620.0	1.01	0.4279
74	9.20	0.355	0	602.9	580.1	1.04	0.4003

b - moisture content recorded by resistance type moisture meter.
c - RL is the radial-longitudinal system of crack initiation.

Test Data of Experiment No. 1

Double Cantilever Beam Specimen

Spec. no.	M.C. %	S.G.	Angle to RL degree	P_{max} N	P_Q N	P_{max}/P_Q	K_{IC} MPa$\sqrt{m}$
1	9.56	0.367	90	1059.7	981.2	1.08	0.397
2	9.79	0.392	90	1100.2	1047.8	1.05	0.424
3	9.51	0.373	90	1049.9	963.2	1.09	0.390
4	9.83	0.335	90	802.1	722.6	1.11	0.293
5	9.85	0.389	90	983.0	954.4	1.03	0.386
6	9.78	0.401	90	925.9	890.3	1.04	0.360
7	9.61	0.377	90	928.8	910.6	1.02	0.369
8	9.52	0.362	90	1040.8	1020.4	1.02	0.413
9	9.33	0.388	90	848.0	839.6	1.01	0.340
10	9.41	0.389	90	1021.5	954.7	1.07	0.387
11	9.21	0.374	90	1080.2	1038.4	1.04	0.420
12	8.78	0.368	90	852.3	796.5	1.07	0.322
13	9.14	0.332	90	1208.8	1140.4	1.06	0.462
14	9.26	0.387	90	1242.8	1230.5	1.01	0.498
15	9.03	0.396	90	826.3	802.2	1.03	0.325
16	8.98	0.332	90	1037.4	1007.2	1.03	0.408
17	9.75	0.327	90	1006.9	987.2	1.02	0.400

Test Data of Experiment 2

Effect of Crack-front width on K_{IC}

Spec. no.	Width mm	M.C. %	S.G.	P_{max} N	P_Q N	P_{max}/P_Q	K_{IC} MPa$\sqrt{m}$
1	7	8.98	0.335	69.5	66.7	1.04	0.2511
2	7	8.94	0.335	70.8	68.6	1.03	0.2585
3	7	9.21	0.335	70.0	68.6	1.02	0.2585
4	7	8.68	0.338	76.3	70.6	1.08	0.2659
5	7	8.83	0.338	69.4	66.7	1.04	0.2511
6	15	8.77	0.389	155.0	149.1	1.04	0.2619
7	15	8.46	0.379	127.4	122.6	1.04	0.2154
8	15	8.98	0.388	148.5	147.1	1.01	0.2585
9	15	9.02	0.367	118.8	117.7	1.01	0.2068
10	15	9.02	0.354	127.5	127.5	1.00	0.2240
11	15	8.76	0.378	121.2	117.7	1.03	0.2068
12	15	8.84	0.392	133.9	127.5	1.05	0.2240
13	21	9.24	0.377	178.7	173.6	1.03	0.2179
14	21	9.17	0.401	202.0	196.1	1.03	0.2462
15	21	9.09	0.410	208.0	205.9	1.01	0.2585
16	21	8.94	0.389	189.7	182.4	1.04	0.2289
17	21	9.01	0.397	216.2	204.0	1.06	0.2560
18	21	8.76	0.396	220.0	202.0	1.09	0.2535
19	29	8.49	0.377	207.9	196.1	1.06	0.1783
20	29	8.54	0.376	180.3	178.5	1.01	0.1622
21	29	8.78	0.377	220.1	215.7	1.02	0.1961
22	29	8.77	0.373	161.6	156.9	1.03	0.1426
23	29	8.92	0.373	226.3	219.7	1.03	0.1996
24	29	8.96	0.375	216.4	215.7	1.00	0.1961
25	29	8.88	0.372	209.9	207.9	1.01	0.1890
26	38	8.92	0.372	213.8	196.1	1.09	0.1353
27	38	8.92	0.324	186.3	179.4	1.04	0.1238
28	38	9.05	0.411	178.7	173.5	1.03	0.1197
29	38	9.18	0.408	279.5	269.7	1.04	0.1861
30	38	8.87	0.450	393.4	374.6	1.05	0.2585
31	38	9.10	0.330	251.0	235.3	1.07	0.1624
32	38	9.00	0.414	205.9	184.4	1.12	0.1272
33	38	9.80	0.374	289.3	284.4	1.02	0.1976
34	38	9.60	0.378	340.3	328.5	1.04	0.2267
35	38	9.80	0.369	344.3	334.3	1.03	0.2307

Test Data of Experiment No. 3

Effect of Crack-front Length on K_{IC}

Spec. no.	Board	M.C. %	S.G.	L mm	Angle to RL degree	P_{max} N	P_Q N	P_{max}/P_Q	K_{IC} MPa$\sqrt{m}$
1	A	8.50	0.41	75	90	538.1	511.5	1.05	0.2355
2	A	8.36	0.42	75	90	545.1	489.3	1.11	0.2252
3	A	8.49	0.42	100	90	635.2	622.7	1.02	0.2275
4	A	8.71	0.40	125	90	680.1	645.0	1.05	0.2014
5	A	8.65	0.43	125	90	803.4	778.4	1.03	0.2430
6	B	8.43	0.41	50	60	444.1	427.0	1.04	0.2947
7	B	9.19	0.41	50	60	416.6	389.2	1.06	0.2686
8	B	9.37	0.42	75	55	650.5	600.5	1.08	0.2764
9	B	9.35	0.42	75	58	694.9	667.2	1.04	0.3072
10	B	8.98	0.41	100	60	772.0	756.2	1.02	0.2762
11	B	8.96	0.41	125	65	841.4	822.9	1.03	0.2569
12	C	9.70	0.34	50	75	284.6	278.0	1.02	0.1918
13	C	9.69	0.34	50	75	303.2	300.2	1.01	0.2072
14	C	9.68	0.33	75	72	445.3	411.4	1.08	0.1894
15	C	9.75	0.32	100	68	674.0	645.0	1.04	0.2356
16	C	9.74	0.33	100	75	592.4	556.0	1.06	0.2031
17	C	9.54	0.34	125	79	581.2	578.2	1.01	0.1805
18	D	8.99	0.42	50	60	408.3	382.5	1.07	0.2640
19	D	8.98	0.41	100	60	695.5	689.4	1.01	0.2518
20	D	8.93	0.41	125	72	1063.9	1007.5	1.05	0.3145

Test Data of Experiment No. 4

Effect of Moisture Content on K_{IC}

Spec. no.	M.C. %	S.G.	Angle to RL degree	P_{max} N	P_Q N	P_{max}/P_Q	K_{IC} MPa$\sqrt{m}$
1	0.0	0.388	90	207.9	196.1	1.06	0.1353
2	0.0	0.357	90	280.4	269.7	1.04	0.1861
3	0.0	0.396	90	214.2	213.8	1.00	0.1475
4	0.0	0.403	70	205.6	204.0	1.01	0.1407
5	0.0	0.357	90	282.1	255.0	1.11	0.1759
6	0.0	0.394	90	274.4	262.8	1.05	0.1813
7	0.0	0.372	90	344.1	335.4	1.02	0.2314
8	0.0	0.356	90	337.9	326.5	1.04	0.2253
9	0.0	0.439	90	355.2	351.1	1.01	0.2422
10	0.0	0.410	90	225.8	219.7	1.03	0.1516
11	0.0	0.372	90	252.3	235.3	1.07	0.1724
12	0.0	0.366	90	322.1	313.8	1.02	0.2165
13	0.0	0.379	90	311.6	298.1	1.05	0.2057
14	0.0	0.387	90	206.9	196.1	1.05	0.1353
15	0.0	0.375	90	207.1	204.0	1.01	0.1407
16	0.0	0.371	90	186.9	179.4	1.04	0.1238
17	6.2	0.371	90	274.2	262.8	1.04	0.1813
18	6.1	0.365	90	231.9	219.7	1.06	0.1516
19	6.3	0.351	90	351.1	326.5	1.07	0.2253
20	6.1	0.344	90	252.7	240.3	1.05	0.1658
21	6.3	0.342	60	333.4	313.8	1.06	0.2165
22	6.1	0.340	90	302.1	298.1	1.01	0.2057
23	6.6	0.327	90	264.9	262.8	1.01	0.1813
24	6.8	0.334	90	260.1	255.0	1.02	0.1759
25	6.3	0.387	90	279.2	235.3	1.09	0.1624
26	6.1	0.312	90	330.7	313.8	1.05	0.2165
27	6.1	0.314	90	343.2	328.5	1.04	0.2267
28	6.7	0.386	90	220.6	213.8	1.03	0.1475
29	6.3	0.343	90	224.2	217.7	1.03	0.1502
30	6.5	0.317	90	378.9	362.8	1.05	0.2504
31	6.4	0.357	90	360.3	351.1	1.02	0.2422
32	6.7	0.369	90	359.2	335.4	1.07	0.2314

Test Data of Experiment No. 5

Mode II End-split Beam Specimen

Spec. no.	M.C. %	S.G.	Angle to RL degree	P_Q N	K_{IIC} MPa$\sqrt{m}$
1	13.3	0.376	0	13344	2.0522
2	13.5	0.388	7	12899	1.9837
3	13.7	0.378	12	14856	2.2847
4	13.9	0.360	18	12454	1.9153
5	11.3	0.473	32	16013	2.4626
6	13.3	0.387	38	15034	2.3121
7	14.0	0.370	39	13033	2.0043
8	12.6	0.378	43	13789	2.1206
9	13.8	0.375	45	18682	2.8731
10	11.7	0.380	46	17792	2.7362
11	14.5	0.539	48	19794	3.0441
12	13.9	0.360	55	18904	2.9072
13	13.7	0.381	60	12232	1.8812
14	14.5	0.423	64	19571	3.0098
15	12.8	0.324	75	12588	1.9359
16	13.3	0.349	88	13033	2.0043
17	12.9	0.347	90	14678	2.2573
18	13.5	0.398	90	12632	1.9427
19	12.5	0.384	90	12677	1.9496
20	13.5	0.349	90	14812	2.2779
21	12.9	0.313	90	12899	1.9837
22	13.5	0.345	90	13878	2.1343
23	12.0	0.310	90	15568	2.3942
24	12.6	0.314	90	15012	2.3087

Note : P_{max} is usually greater than $2P_Q$ since specimens are governed by the bending strength.

Test Data of Experiment No. 6

Mixed Mode Mid-cracked Beam

Phase 1[c] - Center point loading

Spec. no.	M.C. %	S.G.	Angle to RL degree	Crack angle degree	Load at	P_Q[b] N	K_{IQ} MPa$\sqrt{m}$	K_{IIQ} MPa$\sqrt{m}$
1	8.94	0.396	41	45	[a]center	4448	0.3360	0.8330
2	9.03	0.394	55	45	center	5560	0.4199	1.0413
3	9.02	0.374	65	45	center	5871	0.4435	1.0996
4	8.87	0.388	60	45	center	5894	0.4451	1.1038
5	8.96	0.401	90	45	center	4670	0.3527	0.8747
6	8.98	0.403	90	45	center	4448	0.3360	0.8330
7	9.23	0.416	90	45	center	3425	0.2587	0.6414
8	8.46	0.369	90	45	center	6227	0.4703	1.1662
9	8.79	0.388	90	45	center	3647	0.2755	0.6831
10	8.90	0.404	90	45	center	3514	0.2654	0.6581
11	8.37	0.399	90	45	center	3174	0.2397	0.5831
12	8.38	0.396	90	45	center	5338	0.4031	0.9996
13	8.42	0.393	90	45	center	4782	0.3612	0.8955
14	8.57	0.385	90	45	center	3336	0.2520	0.6248
15	8.69	0.344	90	45	center	3625	0.2738	0.6789
16	8.94	0.346	90	45	center	4003	0.3024	0.7497
17	9.00	0.384	90	45	center	4226	0.3192	0.7914
18	9.02	0.388	90	45	center	3892	0.2940	0.7289
19	8.89	0.374	90	45	center	5894	0.4451	1.1038
20	8.78	0.376	90	45	center	3781	0.2856	0.7081
21	8.98	0.392	90	45	center	3447	0.2603	0.6456
22	9.03	0.377	90	45	center	3505	0.2647	0.6564
23	8.65	0.354	90	45	center	3394	0.2563	0.6356
24	8.75	0.346	90	45	center	3336	0.2520	0.6248

a - Loading at the centerline, i.e., 450 mm from the support.

b - P_{max} is greater than 1.2 P_Q, beam strength governed by bending.

c - phase 1 is 45 degrees beam tests.

Test Data of Experiment No. 6 - Cont'd

Phase 1 - 45 deg. beam - Sixth point loading

Spec. no.	M.C. %	S.G.	Angle to RL degree	Crack angle degree	Load at	P_Q N	K_{IQ} MPa$\sqrt{m}$	K_{IIQ} MPa$\sqrt{m}$
1	8.44	0.375	11	45	6th	4670 4	0.3255	0.4768
2	8.64	0.386	40	45	6th	5115.2	0.3566	0.5222
3	8.76	0.398	51	45	6th	6004.8	0.4186	0.6130
4	9.04	0.401	58	45	6th	4781.6	0.3333	0.4882
5	8.56	0.375	73	45	6th	5560.0	0.3876	0.5676
6	8.94	0.336	87	45	6th	6227.2	0.4341	0.6357
7	8.48	0.384	90	45	6th	5782.4	0.4031	0.5903
8	8.52	0.386	90	45	6th	4448.0	0.3100	0.4541
9	8.79	0.383	90	45	6th	3647.4	0.2542	0.3724
10	9.12	0.396	90	45	6th	3558.4	0.2480	0.3633
11	9.08	0.399	90	45	6th	4670.4	0.3255	0.4768
12	9.12	0.391	90	45	6th	6004.8	0.4186	0.6130
13	9.26	0.405	90	45	6th	5115.2	0.3566	0.5222
14	8.96	0.386	90	45	6th	5560.0	0.3876	0.5676
15	8.94	0.377	90	45	6th	6227.2	0.4341	0.6357
16	9.04	0.389	90	45	6th	5560.0	0.3876	0.5676
17	9.02	0.403	90	45	6th	6449.6	0.4496	0.6585
18	8.59	0.380	90	45	6th	6672.0	0.4651	0.6812
20	8.54	0.377	90	45	6th	4448.0	0.3100	0.4541
21	9.34	0.411	90	45	6th	4448.0	0.3100	0.4541
22	9.33	0.408	90	45	6th	5449.0	0.3798	0.5563
23	9.31	0.412	90	45	6th	3447.6	0.2403	0.3519
24	9.16	0.402	90	45	6th	5115.3	0.3565	0.5222
25	9.22	0.398	90	45	6th	4782.0	0.3333	0.4882

Test Data of Experiment No. 6 - Cont'd

Phase 2 - 90 deg. beam - centerline loading

Spec. no.	M.C. %	S.G.	Angle to RL degree	Crack angle degree	P_Q N	K_{IQ} MPa$\sqrt{m}$	K_{IIQ} MPa$\sqrt{m}$
1	8.98	0.356	90	90	5393	0.3402	0.7246
2	8.73	0.398	90	90	4559	0.2876	0.6125
3	8.16	0.388	90	90	5627	0.3550	0.7560
4	8.48	0.359	90	90	6505	0.4104	0.8740
5	8.81	0.328	90	90	5338	0.3367	0.7172
6	9.04	0.396	90	90	4782	0.3017	0.6425
7	9.08	0.400	90	90	4559	0.2876	0.6125
8	8.48	0.377	90	90	3447	0.2175	0.4631
9	8.63	0.369	90	90	4537	0.2862	0.6096
10	8.71	0.399	90	90	6283	0.3937	0.8441
11	8.68	0.396	90	90	3781	0.2385	0.5080
12	8.70	0.394	90	90	5894	0.3718	0.7919
13	8.65	0.390	90	90	4337	0.2736	0.5827
14	8.68	0.388	90	90	3892	0.2455	0.5229
15	8.72	0.392	90	90	4782	0.3017	0.6425
16	8.71	0.392	90	90	4537	0.2862	0.6096

Note: Crack Initiation occured ±90 degrees to the initial crack simultaneously.

Test Data of Experiment No. 7

DCB under Mixed-mode Loading

Spec. no.	M.C. %	S.G.	Angle to RL degree	P_1 N	P_2 N	K_{IQ} MPa$\sqrt{m}$	K_{IIQ} MPa$\sqrt{m}$
1	8.42	0.379	90	1925	3825	0.4009	0.5761
2	8.73	0.386	90	1925	3336	0.4493	0.5024
3	8.71	0.384	90	1925	4448	0.3393	0.6699
4	8.76	0.379	90	1925	4003	0.3833	0.6029
5	9.26	0.359	90	1925	4448	0.3393	0.6699
6	8.16	0.403	90	1925	3670	0.4163	0.5526
7	8.96	0.396	90	1925	4003	0.3833	0.6029
8	8.94	0.394	90	1925	3558	0.4273	0.5359
9	8.89	0.382	90	1925	4114	0.3723	0.6196
10	8.75	0.374	90	1925	4448	0.3393	0.6699
11	8.96	0.369	90	2800	9341	0.2095	1.4067
12	8.94	0.346	90	2800	8229	0.3195	1.2393
13	9.07	0.358	90	2800	8674	0.2755	1.3062
14	9.01	0.398	90	2800	7784	0.3635	1.1723
15	8.92	0.374	90	2800	8006	0.3415	1.2058
16	8.96	0.368	90	2800	8562	0.2865	1.2895
17	8.46	0.348	90	--	--	--	--*
18	8.29	0.376	90	2800	8006	0.3415	1.2058
19	8.45	0.368	90	2800	8674	0.2755	1.3062
20	8.65	0.384	90	2800	9118	0.2315	1.3732

* Split occured in the specimen before testing.

Test Data of Experiment No. 8

Notched Beam Specimens

Spec. type	Spec. no.	M.C. %	S.G.	λ	Angle to RL degree	P_Q N	K_{IQ} $MPam^{2-\lambda}$	K_{IIQ} $MPam^{2-\lambda}$
A	1	8.84	0.382	1.6	90	4203	0.2676	0.4647
A	2	8.76	0.369	1.6	90	4559	0.2902	0.5041
A	3	8.42	0.384	1.6	90	2335	0.1487	0.2582
A	4	9.24	0.321	1.6	90	4114	0.2619	0.4549
A	5	9.80	0.402	1.6	90	5226	0.3327	0.5778
A	6	7.78	0.416	1.6	90	4504	0.2867	0.4980
A	7	8.12	0.332	1.6	90	4915	0.3129	0.5434
A	8	9.13	0.303	1.6	90	4114	0.2619	0.4549
B	1	8.41	0.342	1.6	90	4114	0.1776	0.9025
B	2	8.12	0.383	1.6	90	6338	0.2737	1.3904
B	3	8.56	0.369	1.6	90	5894	0.2545	1.2928
B	4	9.37	0.414	1.6	90	5115	0.2208	1.1221
B	5	10.01	0.311	1.6	90	6227	0.2689	1.3660
B	6	7.68	0.308	1.6	90	5226	0.2256	1.1465
B	7	8.08	0.324	1.6	90	5449	0.2352	1.1953
B	8	8.46	0.326	1.6	90	5560	0.2400	1.2197
C	1	8.11	0.414	1.7	90	8006	0.1940	0.6840
C	2	8.43	0.308	1.7	90	10342	0.2506	0.8835
C	3	8.56	0.388	1.7	90	9341	0.2263	0.7980
C	4	8.64	0.384	1.7	90	5338	0.1293	0.4560
C	5	7.13	0.369	1.7	90	8118	0.1967	0.6935
C	6	6.84	0.342	1.7	90	6116	0.1482	0.5225
C	7	8.42	0.324	1.7	90	10898	0.2640	0.9310
C	8	7.88	0.336	1.7	90	11898	0.2883	1.0165

APPENDIX III

Difference between Mode I Fracture Toughness of CTSs and DCB specimens.

A. Influence on K_{IC} of Assumed Elastic Properties

E_x (MPa)	Spec. type	K^*_{IC} (MPa$\sqrt{m}$)		
		$\frac{E_x}{E_y} = 10$	$\frac{E_x}{E_y} = 20$	$\frac{E_x}{E_y} = 30$
12500	DCB	0.0498	0.0403	0.0359
	CTS	0.0693	0.0688	0.0681
10000	DCB	0.0498	0.0403	0.0359
	CTS	0.0693	0.0688	0.0681
7500	DCB	0.0498	0.0403	0.0359
	CTS	0.0693	0.0688	0.0681

*$E_y/G = 1.0$ and $\nu_{xy} = 0.02$ were used in generating the chart.

As can be seen above, the variation of E_x has no influence on the fracture toughness providing the ratios $E_x:E_y$, $E_y:G$ and ν_{xy} are the same as those used in generating the chart. Thus, we can compute the ratio K_{ICTS}/K_{IDCB}, K_{IC} (DCB) and K_{IC} (CTS) for the three cases :

$\frac{E_x}{E_y}$	$\frac{K_{I(CTS)}}{K_{I(DCB)}}$	$K_{IC(DCB)}$ (MPa$\sqrt{m}$)	$K_{IC(CTS)}$ (MPa$\sqrt{m}$)
10	1.3909	0.4760	0.2059
20	1.7047	0.3855	0.2044
30	1.8970	0.3429	0.2023

The difference between the CTSs and DCB specimens is

significant for various ratios of E_x/E_y. This indicates that the difference in the mode I fracture toughness is not affected much by the assumed elastic properties.

B. T-test on the hypothesis that the two samples being compared are drawn from the same population.

The test is applied to the null hypothesis that the two samples being compared are drawn from the same population, and we calculate the probability of the difference of the two means having a value as large as, or greater than, observed.

Sample	Mean $\bar{K}_{IC}$ (MPa $\sqrt{m}$) $\bar{x}$	Standard deviation s	Sample size n
1. CTS	0.205	0.0510	33
2. DCB	0.387	0.0497	17

The pooled estimate of variance is

$$s_c^2 = \frac{n_1 s_1^2 + n_2 s_2^2}{n_1 + n_2} = \frac{33 \times 0.0510^2 + 17 \times 0.0497^2}{33 + 17} = 2.557 \times 10^{-3}$$

and

$$s_c = 0.0506 \text{ MPa}\sqrt{m}$$

The standard deviation of the difference of mean is thus :

$$S_d = s_c \sqrt{1/n_1 + 1/n_2}$$

$$= 0.0506 \sqrt{1/33 + 1/17}$$

$$= 0.01509$$

$$t = \frac{|\overline{x_1} - \overline{x_2}|}{S_d} = \frac{|0.205 - 0.387|}{0.01509} = 12.06$$

The number of degrees of freedom is 33 + 17 - 2 = 48, and from the t-distribution, it gives t = 2.0126 at the 95 percent level of confidence. Therefore, the null hypothesis can be rejected, and we conclude that the two samples are from different populations.

APPENDIX III

S.A.A. Australian Timber Engineering Code AS 1720-1975

Strength of Notched Beams

For a rectangular beam of depth D, notched on the tension edge as shown in Fig. 57, the nominal maximum bending stress $f_b = \frac{6M}{Bd_n^2}$ and nominal maximum shear stress $f_s = \frac{3V}{2Bd_n}$ calculated for the net section shall comply with the following interaction formula :

$$\frac{0.3f_b+0.7f_s}{C_3F_{sj}} \leqslant 1$$

where C_3 is a constant tabulated in table 11 and F_{sj} is the perimissible shear stress for joint details or the shear block strength for the species of interest.

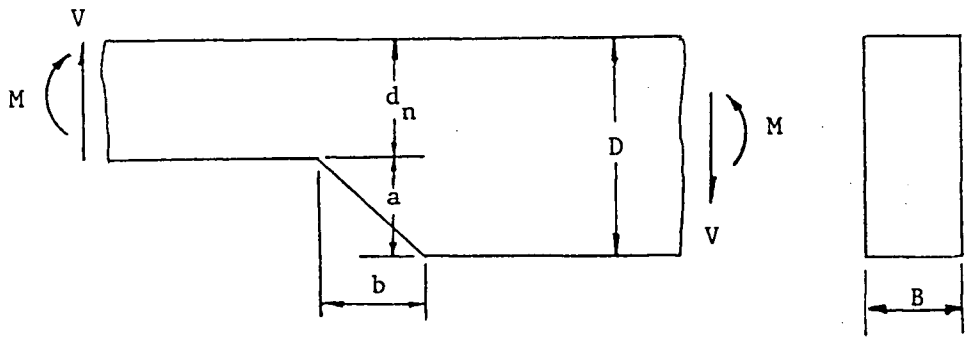

Figure 57 Notation for Notch

Table 11

Parameter C_3 for selected notch angles

notch slope	a ≥ 0.1 D	a < 0.1 D
b/a = 0	$3/D^{\frac{1}{2}}$	$1/a^{\frac{1}{2}}$
b/a = 2	$2.6/D^{\frac{1}{3}}$	$1.2/a^{\frac{1}{3}}$
b/a = 4	$2.2/D^{\frac{1}{4}}$	$1.3/a^{\frac{1}{4}}$